Journal of Computational Physics 566 (2026) 115242

Contents lists available at ScienceDirect

Journal of Computational Physics

journal homepage: www.elsevier.com/locate/jcp

# Fourth-order HyQMOM closures for multidimensional kinetic equations *

Spencer H. Bryngelson [a], Rodney O. Fox [b,*], Frédérique Laurent [c]

[a] School of Computational Science & Engineering, Georgia Institute of Technology, 756 W Peachtree St NW, Atlanta, GA, 30332, USA
[b] Department of Chemical and Biological Engineering, Iowa State University, 618 Bissell Road, Ames, IA, 50011-1098, USA
[c] EM2C & Fédération de Mathématiques de CentraleSupélec, CNRS, CentraleSupélec, Université Paris-Saclay, 3 rue Joliot-Curie, Gif-sur-Yvette, 91192, France

ARTICLE INFO

*Keywords:*
Kinetic equation
Quadrature-based moment methods
Hyperbolic conservation law
High-speed flows

ABSTRACT

The hyperbolic quadrature method of moments (HyQMOM) for closing a moment system of arbitrary even order found from a one-dimensional (1D) kinetic equation was introduced in our prior work (Fox & Laurent, SIAM J. Appl. Math., 82 (2022)). Here, fourth-order HyQMOM is extended to two-dimensional (2D) kinetic equations using up to 15 velocity moments and three-dimensional (3D) kinetic equations using up to 35 moments, i.e., including integer moments up to fourth order. Using the 2D 15-moment system, example calculations are carried out in a 2D spatial domain for problems involving impinging jets for various values of the Knudsen (Kn) and jet Mach (Ma) numbers. Due to the structure of the 2D HyQMOM closures for the fifth-order moments and the correction algorithm for moment realizability and hyperbolicity, a robust numerical algorithm for the moment system based on the HLL solver can be applied to simulate cases with arbitrary values of Kn and Ma. The extension to 3D kinetic equations requires up to twenty additional velocity moments, and can be derived and implemented numerically relatively straightforwardly. The main implementation difficulty in 3D is the formulation of the moment-correction algorithm using leading principal minors or moment projection. Nonetheless, the 3D moment systems are found to be hyperbolic under the same conditions as the 2D moment systems. Simulations of the 3D moment systems in 2D and 3D spatial domains demonstrate the robustness of the fourth-order HyQMOM closures for arbitrary Kn and Ma.

## 1. Introduction

The focus of this work is on moment methods for approximating solutions of the multidimensional kinetic equation for the velocity distribution function (VDF) with velocity vector $\mathbf{u} \in \mathbb{R}^d$ for $d = 2, 3$ [1–11]. We refer the reader to Rice et al. [10], Rice [11], Fox and Laurent [12], Laurent and Fox [13], Yilmaz et al. [14], Habscheid [15] for recent discussions of the relative merits and shortcomings of existing approximations; however, the main issues are loss of hyperbolicity for realizable moments, failure of the VDF reconstruction for realizable moments, and the high cost of VDF reconstruction, especially close to the boundary of moment space. In comparison, at least for $d = 1$, moment closures based on orthogonal polynomials suffer from none of these issues while providing accurate closures far from equilibrium [12–14,16,17]. Here, in particular, we extend the 1D hyperbolic quadrature method of moments (HyQ-

* Code available at https://github.com/comp-physics/HyQMOM.jl.

* Corresponding author.
*E-mail addresses:* shb@gatech.edu (S.H. Bryngelson), rofox@iastate.edu (R.O. Fox), frederique.laurent@centralesupelec.fr (F. Laurent).

https://doi.org/10.1016/j.jcp.2026.115242
Received 24 November 2025; Received in revised form 9 June 2026; Accepted 24 July 2026
Available online 28 July 2026

MOM) developed and validated in Fox and Laurent [12], Laurent and Fox [13] to handle 2D and 3D moment systems. Unlike earlier quadrature-based closures [18–20], HyQMOM does not use 1D Gaussian quadrature points to represent the VDF (or, in fact, any VDF reconstruction [21]). Instead, the 1D orthogonal polynomials associated with the VDF are used directly to define the moment needed to close the free-transport term [12,17]. (See Yilmaz et al. [14], Morin and McDonald [16], Boccelli et al. [22], Taunay and Mueller [23], Berger et al. [24], Bryngelson et al. [25], Charalampopoulos et al. [26], Huang et al. [27] for related work.) In other words, given the vector of velocity moments up to order $2n$ used to define the moment system, 1D HyQMOM provides a closure for the moment of order $2n+1$. As discussed in Section 2 below, the properties of the 1D orthogonal polynomials guarantee that the 1D HyQMOM closure yields a globally hyperbolic conservation law for arbitrary $n$ that generates solutions with realizable moments.

In the context of a multivariate VDF, avoiding the need for quadrature points to define the moment closure is a marked advantage since such points are not well defined nor easy to compute [28]. In contrast, multivariate orthogonal polynomials are well defined [29,30] and can be constructed from the moments of the VDF [29–31]. Thus, as in 1D HyQMOM, the unclosed moments of order $2n+1$ can be found from the known moments up to order $2n$ by using the orthogonality property of polynomials of different degrees, e.g., degrees $n$ and $n+1$. Specifically, the moments up to order $2n$ define the polynomials up to degree $n$, while the polynomials of degree $n+1$ depend on the moments of orders $2n+1$ and $2n+2$. The goal is then to define the polynomials of degree $n+1$ to achieve the desired properties of the characteristic polynomial for the moment system with arbitrary $n$. In 1D HyQMOM, the choice is unique and follows from the three-term recursion formula for the orthogonal polynomials [12,17]. In higher dimensions, a similar three-term formula (using matrices) also exists [29,30]; however, it is more difficult to manipulate since there are several multivariate polynomials for a given degree (e.g., in 2D there are $n+1$ polynomials of degree $n$ [28], see example in Appendix A).

In this work, we investigate a simplified closure starting from the multivariate polynomials for a tensor-product VDF [28]. As shown in Section 3.2, the resultant multivariate HyQMOM closure is nonlinear in the univariate moments, but linear in the cross moments. Moreover, the closure is exact for perfectly correlated variables, reducing to the 1D HyQMOM closure. However, because of this linearization, there is no guarantee that the solution to the moment system will be realizable after the free-transport step when the VDF is far from a tensor product [32]. Thus, unlike in Rice et al. [10], Rice [11] where only hyperbolicity is considered, an equally important part of our closure algorithm will be the detection and correction of non-realizable moments after the free-transport step. In 2/3D, the realizability constraints are formulated in terms of symmetric matrices $\Delta_k$ involving all moments up to order $2k$ [28–31,33]. The moment matrices for $k = 0, 1, \dots, 2n$ must be positive definite for the orthogonal polynomials up to degree $n$ to be well defined. In 1D, these matrices yield the Hankel determinants [34,35]. Here, the realizability and correction algorithms are derived for $n = 2$ based on Sylvester's criterion [36] and moment projection (Appendix B) for the 2D and 3D moment systems. In principle, the same method can be used for arbitrary $n$, but given the number of 3D moments of order $2n$, it may become computationally intractable for larger $n$. Thus, we focus on the properties of the fourth-order HyQMOM moment system in this work.

The remainder of this article is organized as follows. In Section 2 we provide a brief overview of 1D HyQMOM for the 1D VDF, including its relationship to the 1D orthogonal polynomials. In Section 3 we describe an extension of HyQMOM to a 2D VDF, which is based on the theory of multivariate orthogonal polynomials. The importance of 2D moment realizability is addressed, along with an algorithm for checking the realizability of moments up to fourth order. The 2D HyQMOM closures for the fifth-order moments are derived, and the hyperbolicity of the 2D moment system is investigated. In Section 4, numerical examples for the 2D moment system with 15 moments are provided to illustrate its behavior over a wide range of Knudsen (Kn) and jet Mach numbers (Ma). Next, in Section 5, the extension of HyQMOM to a 3D VDF is derived for 16, 26, and 35 moments up to fourth order [37–39]. It is demonstrated that the hyperbolicity of the 3D moment system is equivalent to that of the 2D system. The main challenge is thus to develop an algorithm to check the realizability of the 3D moment vector, which is again based on the theory of multivariate moment matrices. Using the 2D hyperbolic solver from Section 4, extended to 3D moments, Section 5 concludes with numerical examples illustrating the robustness of the 3D HyQMOM closures over a wide range of Kn and Ma. Lastly, in Section 6, we conclude with comments on the performance of the fourth-order HyQMOM, possible routes for improvement, and the feasibility of extending it to higher-order ($n > 2$) moments.

## 2. Overview of 1D HyQMOM

The 1D kinetic equation, including only free transport, for the VDF $f(t, x, u)$ is

$$\partial_t f + u \partial_x f = 0, \tag{1}$$

where $t \in \mathbb{R}^+$ is time, $x \in \mathbb{R}$ is space and $u \in \mathbb{R}$ is velocity. The $i$th-order velocity moments of $f$ is defined as $m_i = \int u^i f \, du$, and the 1D moment system for the set of moments $\mathbf{M}_{2n} := (m_0, m_1, \dots, m_{2n})^t$ with $n \in \mathbb{N}$ found from (1) is

$$\partial_t \mathbf{M}_{2n} + \partial_x \mathbf{F}(\mathbf{M}_{2n}) = \mathbf{0} \tag{2}$$

with flux vector $\mathbf{F}(\mathbf{M}_{2n}) := (m_1, m_2, \dots, m_{2n+1})^t$. HyQMOM provides a closure for the odd-order moment $m_{2n+1}$ given $\mathbf{M}_{2n}$ [12,13].

In general, except on the boundary of moment space, HyQMOM does not use a reconstructed VDF to define the flux closure. However, in 1D the generalized quadrature moment methods (GQMOM) [40] can be used with the moments $(\mathbf{M}_{2n}, m_{2n+1})$ to find an $N$-node Gaussian-quadrature approximation for any integer $N > n$. In doing so, GQMOM provides closures for all moments of order greater than $2n$, i.e., for $m_i$ with $i > 2n$ given $\mathbf{M}_{2n}$. For example, with $n = 1$, the Gaussian-GQMOM closure corresponds to Gaussian moments [40]. Furthermore, when needed for the evaluation of source terms, it is possible to approximate the VDF using the Grad-HyQMOM approximation in Appendix C.

### 2.1. 1D central and standardized moments

For $m_0 > 0$, the central moments are given by

$$c_k = \sum_{i=0}^{k} \binom{k}{i} (-\bar{u})^{k-i} \frac{m_i}{m_0} \tag{3}$$

with $\bar{u} = m_1/m_0$. By definition, $c_0 = 1$ and $c_1 = 0$. The central moment $c_2 \geq 0$ is the velocity variance. The HyQMOM closure can be expressed in terms of $c_{2n+1}$ or $m_{2n+1}$. Hereinafter, we assume that $c_2 > 0$ and work mainly with the standardized moments defined by

$$s_k = \frac{c_k}{c_2^{k/2}} = \langle \tilde{u}^k \rangle \quad \text{with} \quad \tilde{u} = \frac{u - \bar{u}}{c_2^{1/2}}. \tag{4}$$

By definition, $s_0 = 1$, $s_1 = 0$ and $s_2 = 1$ and $\mathbf{S}_{2n} = (s_0, \dots, s_{2n})$. The HyQMOM closure depends on the standardized moments $s_{2n+1}(s_3, \dots, s_{2n})$. In general, knowing $(m_0, \bar{u}, c_2, s_3, \dots, s_{2n+1})$ is equivalent to knowing $(\mathbf{M}_{2n}, m_{2n+1})$.

When Gaussian-GQMOM is applied with $(\mathbf{S}_{2n}, s_{2n+1})$ it provides closures for $s_i(s_3, \dots, s_{2n})$ for $i > 2n+1$. These closures can be computed using the inverse Chebyshev algorithm [40]. By construction, if $s_{2n}$ is strictly realizable, then so are $s_i$ for all $i \in \mathbb{N}$. The univariate VDF with these standardized moments will be denoted as $f_1$ such that

$$s_i = \int_{\mathbb{R}} \tilde{u}^i f_1(\tilde{u})\, \mathrm{d}\tilde{u}$$

are the standardized moments. In 2D cases, we will denote the univariate VDFs in each direction as $f_1$ and $f_2$. Hereinafter, for simplicity, we use the standardized VDF with moments $s_i$ unless stated otherwise.

### 2.2. 1D HyQMOM closure and its properties

Mathematical details on 1D HyQMOM can be found elsewhere [12,13]. Here we review the salient points.

#### 2.2.1. 1D HyQMOM closure for $s_{2n+1}$

For $k = 0, 1, \dots, n-1$; let $a_k$, $b_k$, and $b_n$ be the recurrence coefficients found from $\mathbf{S}_{2n}$ using the Chebyshev algorithm [41,42], and define two additional coefficients as

$$\alpha_n := \frac{1}{n} \sum_{k=0}^{n-1} a_k \quad \text{and} \quad \beta_n := \frac{2n+1}{n} b_n. \tag{5}$$

The HyQMOM closure for $s_{2n+1}$ is found by setting $a_n = \alpha_n$.

#### 2.2.2. Realizable moments

The 1D moment vector $\mathbf{S}_{2n}$ is realizable if and only if $b_k \geq 0$ for all $k = 0, 1, \dots, n$; and strictly realizable if $b_k > 0$ [35].

#### 2.2.3. Interior of moment space

The 1D moment vector $\mathbf{S}_{2n}$ is in the interior of moment space if and only if $b_k > 0$ for all $k = 0, 1, \dots, n$; i.e., if it is strictly realizable [35]. Hereinafter, we assume that $\mathbf{S}_{2n}$ is strictly realizable. In practice, this assumption can be verified by applying the Chebyshev algorithm [41].

The lower bound for $s_{2n}$ (i.e., the even-order moments) is found from $b_n = 0$. In contrast, for the truncated Hamburger moment problem [34], if $b_k > 0$ for all $k = 0, \dots, n$, the odd-order standardized moment $s_{2n+1}$ can take on any finite real value.

#### 2.2.4. Globally hyperbolic

A moment system is hyperbolic if all eigenvalues of the Jacobian matrix found from the flux vector $\mathbf{F}(\mathbf{M}_{2n})$ are real with a full set of eigenvectors. A moment system is globally hyperbolic if it is hyperbolic for every standardized moment vector $\mathbf{S}_{2n}$ in the interior of moment space.

### 2.3. Characteristic polynomial

Using the 1D HyQMOM closure in Section 2.2.1, the characteristic polynomial $P_{2n+1}$ for the Jacobian matrix found from $\mathbf{F}(\mathbf{M}_{2n})$ has the form [12]

$$P_{2n+1}(x) = Q_n(x) R_{n+1}(x). \tag{6}$$

Here, $Q_n$ is the orthogonal polynomial found from the three-term recurrence formula with $Q_{-1} = 0$ and $Q_0 = 1$:

$$Q_{n+1}(x) = (x - a_n) Q_n(x) - b_n Q_{n-1}(x) \tag{7}$$

where the recurrence coefficients are related to the standardized VDF $f_1$ by

$$a_n = \frac{\langle x Q_n^2 \rangle}{\langle Q_n^2 \rangle}, \quad b_n = \frac{\langle Q_n^2 \rangle}{\langle Q_{n-1}^2 \rangle}, \tag{8}$$

and $\langle(\cdot)\rangle = \int_{\mathbb{R}} (\cdot) f_1(x)\,\mathrm{d}x$ with $\langle Q_i Q_j\rangle = 0$ for $i \neq j$. The polynomial $R_{n+1}$ is defined by

$$R_{n+1}(x) = (x - \alpha_n)Q_n(x) - \beta_n Q_{n-1}(x). \tag{9}$$

If $b_n > 0$, the $n+1$ simple roots of $R_{n+1}$ separate and bound the $n$ roots of $Q_n$ so that the polynomial $P_{2n+1}$ has $2n+1$ simple roots. Thus, the moment system in (2) is globally hyperbolic for arbitrary $n$.

The coefficients of the polynomial $P_{2n+1}$ depend only on $\mathbf{S}_{2n}$ [12] (i.e., they do not depend on $\bar{u}$ and $c_2$). Thus, the $2n+1$ roots of $P_{2n+1}(x)$, denoted by $\hat{u}_k$, depend only on $\mathbf{S}_{2n}$. The characteristic polynomials for $n = 0, 1, 2$ are $P_1(x) = x$, $P_3(x) = x^3 - 3x$, and

$$P_5(x) = x^5 - \frac{5}{2}s_3 x^4 + \frac{1}{2}(1 + 9s_3^2 - 5s_4)x^3 + \frac{1}{2}s_3(1 - 6s_3^2 + 5s_4)x^2 - \frac{1}{2}(3 + 7s_3^2 - 5s_4)x - \frac{1}{2}s_3 \tag{10}$$

where realizability requires $b_2 = \langle Q_2^2\rangle = s_4 - s_3^2 - 1 \geq 0$. Due to orthogonality, $\langle P_5\rangle = 0$; hence, the HyQMOM closure for $s_5$ can be found from

$$0 = s_5 - \frac{5}{2}s_3 s_4 + \frac{1}{2}(1 + 9s_3^2 - 5s_4)s_3 + \frac{1}{2}s_3(1 - 6s_3^2 + 5s_4) - \frac{1}{2}s_3.$$

As described in Sections 3.2 and 5.4, the multivariate HyQMOM closure is found similarly.

#### 2.3.1. Roots

Let $\overline{P}_{2n+1}(u)$ be the monic polynomial defined by

$$\overline{P}_{2n+1}(u) = c_2^{(2n+1)/2} P_{2n+1}\left(\frac{u - \bar{u}}{c_2^{1/2}}\right) = c_2^{(2n+1)/2} P_{2n+1}(\tilde{u}). \tag{11}$$

The $2n+1$ roots of $\overline{P}_{2n+1}(u)$ and $P_{2n+1}(\tilde{u})$ are related by $u_k = \bar{u} + c_2^{1/2}\hat{u}_k$.

In summary, for any strictly realizable 1D moment vector with $2n+1$ components in the form of $\mathbf{M}_{2n}$, $a_n = \alpha_n$ from Section 2.2.1 provides the closure $m_{2n+1}$ that yields a globally hyperbolic moment system. In practice, using the inverse Chebyshev algorithm [12], $m_{2n+1}$ is found directly from $\mathbf{M}_{2n}$ without computing $\mathbf{S}_{2n}$.

## 3. 2D kinetic equation and selected moment systems

In this section, we discuss the 2D moment system, which extends the 1D system introduced in the previous section for $n = 1$ and 2. First, the requirements for 2D moments up to fourth order to be (strictly) realizable are described, leading to inequality constraints on the cross moments. Next, the methodology for finding HyQMOM closures for the cross moments is presented in Section 3.2. This method employs the 1D orthogonal polynomials written in terms of the 2D standardized moments denoted by $s_{ij}$ with $i, j \in \mathbb{N}$ (see (3) and (4) for definitions), e.g., $s_{11} = c_{11}/\sqrt{c_{20}c_{02}}$ where $c_{20}$ and $c_{02}$ are positive. The Hankel determinants in each direction are defined by $H_{20} = s_{40} - s_{30}^2 - 1 > 0$ and $H_{02} = s_{04} - s_{03}^2 - 1 > 0$. The primary focus for each selected moment set is to determine whether the closed moment system is globally hyperbolic and realizable after the free-transport step. Numerical examples for the 15-moment system are provided in Section 4 to illustrate the robustness of the 2D HyQMOM closure when combined with the moment realizability and hyperbolicity constraints derived in this section.

### 3.1. 2D moment realizability

Like the Hankel determinants $H_{2n}$ for 1D orthogonal polynomials [8], 2D orthogonal polynomials have realizability constraints based on matrix determinants (see example in Appendix A) [8,29–31]. In terms of the standardized moments, the first two are $|\Delta_1| > 0$ and $|\Delta_2| > 0$, where the symmetric moment matrices are

$$\Delta_1 = \begin{bmatrix} 1 & 0 & 0 \\ 0 & 1 & s_{11} \\ 0 & s_{11} & 1 \end{bmatrix} \quad \text{and} \quad \Delta_2 = \begin{bmatrix} & \Delta_1 & & 1 & s_{11} & 1 \\ & & & s_{30} & s_{21} & s_{12} \\ & & & s_{21} & s_{12} & s_{03} \\ 1 & s_{30} & s_{21} & s_{40} & s_{31} & s_{22} \\ s_{11} & s_{21} & s_{12} & s_{31} & s_{22} & s_{13} \\ 1 & s_{12} & s_{03} & s_{22} & s_{13} & s_{04} \end{bmatrix}, \tag{12}$$

and $s_{ij}$ are the 2D standardized integer moments. These matrices yield $|\Delta_1| = 1 - s_{11}^2 > 0$ so that $s_{11}^2 < 1$. (See Appendix D for the case with $|\Delta_1| = 0$.) Likewise, $|\Delta_2| = 0$ places bounds on the third- and fourth-order moments.

Expanding the determinant in block matrices, $|\Delta_2|$ can be expressed as $|\Delta_2| = |\Delta_1||\Delta_2^*|$ where

$$\Delta_2^* = \begin{bmatrix} s_{40} & s_{31} & s_{22} \\ s_{31} & s_{22} & s_{13} \\ s_{22} & s_{13} & s_{04} \end{bmatrix} - \mathbf{D} \quad \text{and} \quad \mathbf{D} = \frac{1}{|\Delta_1|}\begin{bmatrix} 1 & s_{30} & s_{21} \\ s_{11} & s_{21} & s_{12} \\ 1 & s_{12} & s_{03} \end{bmatrix}\begin{bmatrix} |\Delta_1| & 0 & 0 \\ 0 & 1 & -s_{11} \\ 0 & -s_{11} & 1 \end{bmatrix}\begin{bmatrix} 1 & s_{11} & 1 \\ s_{30} & s_{21} & s_{12} \\ s_{21} & s_{12} & s_{03} \end{bmatrix}, \tag{13}$$

from which it can be observed that $|\Delta_1| = 0$ implies $|\Delta_2| = 0$, but not vice versa. Hereinafter, the components of the symmetric matrix $\mathbf{D}$ will be denoted as $d_{ij}$. We will also use the fact that by permuting the indices, a condition on $s_{ij}$ provides the same condition for $s_{ji}$.

It is important to observe that $\mathbf{D}$ only depends on the moments up to third order, i.e., it does not depend on the fourth-order moments. Recall that the univariate moments are assumed to be realizable; hence, we are interested in the realizability constraints for the cross moments. We apply Sylvester's criterion [36] to the matrix $\Delta_2^*$ to generate sufficient conditions for $\Delta_2$ to be positive definite.

#### 3.1.1. Realizability constraint on third-order moments

For realizable moments, the matrix $\Delta_2^*$ must be non-negative. If the 2D standardized VDF corresponds to independent variables (i.e., $s_{ij} = s_{i0}s_{0j}$), then $|\Delta_2^*| = H_{20}H_{02}$. In general, the $3\times 3$ symmetric matrix $\Delta_2^*$ must be positive definite for realizable moments given that $H_{20}, H_{02} > 0$ for any given $(s_{30}, s_{03})$. A necessary condition is that the diagonal elements of $\Delta_2^*$ be positive. Using the first leading principal minor of $\Delta_2^*$, i.e., $(s_{40} - d_{11})$, to check for positive definiteness, we find the following inequalities:

$$H_{20}|\Delta_1| > (s_{21} - s_{11}s_{30})^2 \quad \text{and} \quad H_{02}|\Delta_1| > (s_{12} - s_{11}s_{03})^2. \tag{14}$$

The right-hand sides of these inequalities can be rewritten as quadratic equations with real roots, giving the realizability bounds for $s_{21}$ and $s_{12}$, respectively, i.e.,

$$\begin{aligned} -(H_{20}|\Delta_1|)^{1/2} &< s_{21} - s_{11}s_{30} < (H_{20}|\Delta_1|)^{1/2}, \\ -(H_{02}|\Delta_1|)^{1/2} &< s_{12} - s_{11}s_{03} < (H_{02}|\Delta_1|)^{1/2}, \end{aligned} \tag{15}$$

is necessary for $\Delta_2^*$ to be positive. The limit $|\Delta_1| = 0$ gives $s_{21} = s_{11}s_{30}$ and $s_{12} = s_{11}s_{03}$ as expected (see Appendix D). It is noteworthy that (15) puts bounds on the energy fluxes $q_1 = (c_{30} + c_{12})/2$ and $q_2 = (c_{21} + c_{03})/2$.

#### 3.1.2. Realizability constraint on fourth-order moments

A first set of constraints on $s_{22}$ can be found using the variables $X = \tilde{u}^2 - 1$ and $Y = \tilde{v}^2 - 1$, where $(\tilde{u}, \tilde{v})$ are the standardized 2D velocity components. For these variables, the determinant of the correlation matrix gives

$$(s_{22} - 1)^2 < (s_{40} - 1)(s_{04} - 1).$$

The right-hand side is positive, so the inequality yields

$$1 - \sqrt{(s_{40} - 1)(s_{04} - 1)} < s_{22} < 1 + \sqrt{(s_{40} - 1)(s_{04} - 1)} \tag{16}$$

where the lower limit applies when $(s_{40} - 1)(s_{04} - 1) < 1$. Likewise, setting $Z = \tilde{u}\tilde{v}$ such that $Z^2 = \tilde{u}^2\tilde{v}^2$, we find another lower limit: $s_{22} \geq s_{11}^2$. The larger of the two provides a lower bound for $s_{22}$.

The remaining two leading principal minors of $\Delta_2^*$ depend on the fourth-order cross moments $(s_{31}, s_{22}, s_{13})$ and must be positive as well. The second leading principal minor provides realizability bounds for $s_{31}$ and $s_{13}$ subject to the condition $s_{22} \geq d_{22}$. Using $s_{31}$ as an example, we have

$$\begin{vmatrix} s_{40} - d_{11} & s_{31} - d_{12} \\ s_{31} - d_{12} & s_{22} - d_{22} \end{vmatrix} = (s_{40} - d_{11})(s_{22} - d_{22}) - (s_{31} - d_{12})^2 > 0,$$

which provides a quadratic equation for $(s_{31} - d_{12})$ whose solution yields

$$\frac{s_{12}s_{21} + s_{21}s_{30} - s_{11}s_{21}^2 - s_{11}s_{12}s_{30} - G_{31}^{1/2}}{|\Delta_1|} < s_{31} - s_{11} < \frac{s_{12}s_{21} + s_{21}s_{30} - s_{11}s_{21}^2 - s_{11}s_{12}s_{30} + G_{31}^{1/2}}{|\Delta_1|}. \tag{17}$$

The discriminant $G_{31}$ depends on $s_{22}$ and is non-negative if

$$G_{31} = (|\Delta_1|(s_{22} - s_{11}^2) - s_{12}^2 + 2s_{11}s_{12}s_{21} - s_{21}^2)(|\Delta_1|H_{20} - (s_{21} - s_{11}s_{30})^2) \geq 0. \tag{18}$$

From (15), the second term in $G_{31}$ is non-negative (i.e., it is $s_{40} - d_{11}$), so this inequality requires the first term (which comes from $s_{22} - d_{22}$) to be positive:

$$s_{22} \geq s_{11}^2 + \frac{1}{|\Delta_1|}\begin{bmatrix} s_{21} \\ s_{12} \end{bmatrix}^t \begin{bmatrix} 1 & -s_{11} \\ -s_{11} & 1 \end{bmatrix} \begin{bmatrix} s_{21} \\ s_{12} \end{bmatrix}, \tag{19}$$

which, along with (16), sets another lower bound on $s_{22}$. Note also that (19) is invariant under permutation of the indices. The realizability bounds for $s_{31}$ are found from (17) and, by permuting the indices, those for $s_{13}$ as well. If (19) is satisfied, then $s_{22}$ can be held constant while adjusting $s_{31}$ and $s_{13}$ to satisfy (17).

The third leading principal minor of $\Delta_2^*$ is

$$\begin{vmatrix} s_{40} - d_{11} & s_{31} - d_{12} & s_{22} - d_{13} \\ s_{31} - d_{12} & s_{22} - d_{22} & s_{13} - d_{23} \\ s_{22} - d_{13} & s_{13} - d_{23} & s_{04} - d_{33} \end{vmatrix} = |\Delta_2^*| > 0,$$

and yields a third-order polynomial in $s_{22}$ with leading term $|\Delta_1|s_{22}^3$ and all coefficients are invariant under permutation. Thus, the three roots of the polynomial are also invariant under permutation. For independent Gaussian moments, the three roots are $(-1, 0, 3)$ and $s_{22} = 1$. The upper bound on $s_{22}$ is the largest root of this polynomial, and the left-hand side of the inequality (19) is near or below the second-largest root. In any case, (16) is a necessary (but not sufficient) condition for a positive element where equality holds when $|\Delta_1| = 0$ or $H_{20} = H_{02} = 0$.

To obtain accurate realizability bounds for $s_{22}$, the three real roots of the polynomial are found symbolically, and the middle ($R_2$) and largest ($R_3$) roots can be used to determine the lower and upper bounds:

$$\begin{aligned} s_{22,\min} &= \max\left(s_{11}^2, 1-\sqrt{(s_{40}-1)(s_{04}-1)}, R_2\right) \\ s_{22,\max} &= \min\left(1+\sqrt{(s_{40}-1)(s_{04}-1)}, R_3\right). \end{aligned} \tag{20}$$

In simulations, complex roots $R_2$ and $R_3$ are sometimes observed, in which case $s_{22}$ is left unchanged.[1] Otherwise, for a given non-realizable moment set with $H_{20}, H_{02}, |\Delta_1| > 0$, the inequalities (15), (17), and (20) can be used to bound the standardized cross moments $(s_{21}, s_{12}, s_{31}, s_{22}, s_{13})$ such that the moment set is realizable. Note that during this process, the univariate moments and $m_{11}$ remain unchanged.

#### 3.1.3. Realizability-correction algorithm

In the simulation code for 2D moment systems, the constraints derived above are enforced to ensure that the moments remain realizable after the spatial fluxes are applied. For the special case where $|\Delta_1| = 0$, the realizable standardized moments are determined as described in Appendix D. We must emphasize that the realizability-correction algorithm is an integral part of the 2D HyQMOM closure developed in this work. Without it, simulation of high-speed flows is not possible because the free-transport fluxes can generate non-realizable moments. Generally speaking, based on numerical experiments, low-speed flows satisfy the realizability constraints for arbitrary Kn, and hence the realizability-correction algorithm is not needed.

### 3.2. Higher-order HyQMOM moment closures for 2D velocity distributions

Our methodology for finding a 2D HyQMOM closure for the higher-order cross moments is based on the univariate orthogonal polynomials. (See Appendix A for an alternative approach using the multivariate orthogonal polynomials.) In 2D, let $\mathcal{U}_k(x)$ and $\mathcal{V}_k(y)$ be the orthogonal monomials of degree $k$ found from the univariate standardized moments in each direction. Note that there is a set of recurrence coefficients for each direction, e.g., for the $x$ direction $a_{x,k}$ and $b_{x,k}$. In the following, we include the direction only when needed to avoid confusion. For a given $n$ and 1D moments $\mathbf{M}_{2n}$, the coefficients up to $a_{n-1}$ and $b_n$ are known functions of the 1D standardized moments $\mathbf{S}_{2n}$ [12]. The 1D HyQMOM closure provides $a_n$, which gives us the closure for $s_{2n+1}$. Thus, using the recurrence formula, we have the following orthogonal polynomial of degree $n+1$:

$$\hat{Q}_{n+1}(x) = (x-a_n)Q_n(x) - b_n Q_{n-1}(x), \tag{21}$$

which depends only on the known moments $\mathbf{S}_{2n}$. For example, for $n=1$ we have $a_0 = a_1 = 0$ and $b_1 = 1$, so that $Q_0 = 1$, $Q_1 = x$ and $\hat{Q}_2 = x^2 - 1$ and $s_3 = \langle Q_1 Q_2 \rangle = 0$. Note that the polynomial $\hat{Q}_2 \neq Q_2 = x^2 - s_3 x - 1$ because $Q_2$ depends on $s_3$, which is not included in $\mathbf{S}_2$. However, they will be equal once the 1D HyQMOM closure $s_3 = 0$ is applied. Thus, for simplicity, we will use the same notation $Q_k$ for all polynomials of degree $k \geq n+1$, keeping in mind that the coefficients depend on $n$ through the known moments.

Continuing with $n=1$, the directional polynomials are $\mathcal{U}_0 = 1$, $\mathcal{U}_1 = x$ and $\mathcal{U}_2 = x^2 - 1$; and $\mathcal{V}_0 = 1$, $\mathcal{V}_1 = y$ and $\mathcal{V}_2 = y^2 - 1$. For the anisotropic Gaussian (AG) model [43], we require closures for $s_{21}$ and $s_{12}$, given that from 1D HyQMOM we have $s_{30} = s_{03} = 0$. These closures are found, respectively, using that $\langle \mathcal{U}_2 \mathcal{V}_1 \rangle = 0$ and $\langle \mathcal{U}_1 \mathcal{V}_2 \rangle = 0$, which yields $s_{21} = s_{12} = 0$. For larger $n$, the closure for the unknown cross moment $s_{ij}$ is found from

$$\langle \mathcal{U}_i \mathcal{V}_j \rangle = 0 \quad \text{for } i+j \geq 2n+1 \text{ with } i,j > 0, \tag{22}$$

and 1D HyQMOM is used for $i=0$ or $j=0$. Notice that for $n>1$, we must define $(Q_{n+2}, \dots, Q_{2n})$ in terms of the known 1D moments $\mathbf{S}_{2n}$ where $Q_{n+1}$ follows from (21). In practice, we must find closures for the coefficients $(a_{n+1}, \dots, a_{2n-1})$ and $(b_{n+1}, \dots, b_{2n-1})$ with $b_k > 0$. Such polynomials could be defined using GQMOM [40], but other definitions may be needed to ensure global hyperbolicity. Indeed, the main constraint for choosing these coefficients is that the resulting moment system must be globally hyperbolic [12].

Here, consistent with 1D HyQMOM, we assume that for $k > n$, $a_k = a_n$ and $b_k = \beta_k b_n$ where the $\beta_k > 0$ are rational numbers and independent of the directions.[2] As in GQMOM, we use $b_n$ to define $b_k$ so that the system degenerates correctly at the boundary of moment space where $b_n = 0$. These assumptions leave $n-1$ degrees of freedom for choosing the $\beta_k$. Thus far, only a few cases have been explored. Below, we consider special cases with $n=1$ and $n=2$. In Section 3.4 we begin with cases using a subset of the moments in $\mathbf{S}_{2n}$, i.e., only the pure moments $s_{k0}$ and $s_{0k}$ for which closures are needed for $s_{k1}$ and $s_{1k}$. Such unknown moments are found from $\langle \mathcal{U}_i \mathcal{V}_j \rangle = 0$.

Using (21) for the $\mathcal{U}_k$ results in

$$\langle \mathcal{U}_{i+1} \mathcal{V}_1 \rangle = \langle x \mathcal{U}_i \mathcal{V}_1 \rangle - a_{x,i} \langle \mathcal{U}_i \mathcal{V}_1 \rangle - b_{x,i} \langle \mathcal{U}_{i-1} \mathcal{V}_1 \rangle \quad \text{for } i \geq 1. \tag{23}$$

Then, since none of the cross moments are known, we have $\langle \mathcal{U}_i \mathcal{V}_1 \rangle = 0$ for $i \geq 0$ and thus the closure reduces to $\langle x \mathcal{U}_i(x) \mathcal{V}_1(y) \rangle = \langle xy \mathcal{U}_i(x) \rangle = 0$.[3] This result does not depend on the choice of $\beta_k$, and reduces to $s_{i1} = s_{1i} = 0$. Likewise, in Section 3.5, we consider the extended AG model, where all second-order moments are known, i.e., the cross moment $s_{11}$ can be nonzero. In this case, the closures found from (23) depend on $s_{11}$ as seen in (32).

[1] The smallest root is negative, so no value of $s_{22}$ exists that makes $\Delta_2$ positive.

[2] We could also let $\beta_n$ be a free parameter as in HyQMOM [12]. However, only $\beta_n = 1$ yields the correct behavior when $s_{11}^2 = 1$.

[3] Since $\mathcal{U}_i$ is a polynomial of degree $i$, setting $i = 0$ yields $s_{11} = 0$. This pattern continues for all $i$.

In summary, the closures found from (22) are exact only for the case where the 2D VDF is separable. Indeed, for a 2D tensor-product VDF, the 2D orthogonal polynomials of degree $n$ are $Q_{i,n-i}(x,y) = \mathcal{U}_i(x)\mathcal{V}_{n-i}(y)$ for $i \in (0,\dots,n)$ where $Q_{0,0} = 1$ and $[Q_{1,0}(x,y)\, Q_{0,1}(x,y)]^t = [x\ y]^t$, etc. [28,29,31]. Since polynomials with different degrees are orthogonal, $\langle \mathcal{U}_i \mathcal{V}_j \rangle = 0$ for $i \neq j$ is exact for a tensor-product VDF (e.g, the Maxwellian). The same theory holds in 3D [29,30]. In general, the 2D VDF will not be separable, and (22) can generate non-realizable cross moments when used to close the free-transport flux for the moment system (e.g., with large-Mach-number flows). One possible solution is to use the 2D orthogonal polynomials directly (see Appendix A); however, the resulting closures are more complicated to analyze. Instead, here we will use (22) along with the realizability corrections derived in Section 3.1 to define the 2D HyQMOM closures. We shall see that the proposed closures are nonlinear in the univariate standardized moments but linear in the standardized cross moments. If the 2D orthogonal polynomials were used, then the closures would be nonlinear in all the standardized moments.

### 3.3. 2D kinetic equation

Consider the 2D VDF $f(t,\mathbf{x},\mathbf{u})$ defined for $(t,\mathbf{x},\mathbf{u}) \in \mathbb{R}^+ \times \mathbb{R}^2 \times \mathbb{R}^2$. This VDF is non-negative and its moments with respect to the velocity vector $\mathbf{u} = (u_1\ u_2)^t$ are finite. The kinetic equation for the 2D VDF, including only free transport, is

$$\partial_t f + \mathbf{u} \cdot \partial_{\mathbf{x}} f = 0 \tag{24}$$

with initial condition $f(0,\mathbf{x},\mathbf{u}) = f_0(\mathbf{x},\mathbf{u})$.

If collisions are included using the BGK model [44,45], then there will be an additional term on the right-hand side that depends on the Knudsen number (Kn). However, since this term will be closed when working with the moments, for clarity, we do not include it in the discussion below. The velocity vector can be written in terms of the Cartesian direction vectors $\mathbf{e}_i$ for $i \in 1,2$. For example, in 2D, $\mathbf{u} = u_1\mathbf{e}_1 + u_2\mathbf{e}_2$ and (24) becomes

$$\partial_t f + \mathbf{e}_i \cdot \partial_{\mathbf{x}}(u_i f) = 0 \tag{25}$$

where repeated Roman indices imply summation.

In this section, we seek to approximate a selected set of 2D moments of increasing order using a moment system found from (24). Selected moment systems based on specific assumptions and their closures are formulated in 2D for clarity, but can easily be extended to three dimensions [2]. In 2D, the integer moments are denoted by

$$m_{ij} = \int_{\mathbb{R}^2} u_1^i u_2^j f \,\mathrm{d}u_1\,\mathrm{d}u_2 \tag{26}$$

for $i+j \in (0,1,\dots,2n)$ for a given integer $n \geq 1$. For clarity, in this work, we consider only $n=1$ and $n=2$. The extension to 3D integer moments $m_{ijk}$ is straightforward for each case. However, in general, a well-posed extension to include moments up to a given order $l = i+j+k > 4$ is an open problem. We begin with a 2D moment system where the joint VDF has a tensor-product form, and then extend the analysis up to the moment system with all fourth-order moments.

### 3.4. Independent moment system

For independent moments, we have $m_{ij}m_{00} = m_{i0}m_{0j}$ so that the cross moments do not provide additional information. In this case, the VDF has a tensor-product form $f(\mathbf{u}) = f_1(u_1)f_2(u_2)$. Note that $f_1$ and $f_2$ need not be the same distributions.

#### 3.4.1. $n = 1$

For this case, the 2D moment system has five moments up to second order (denoted by $m_{i0}$ and $m_{0i}$ with $i \in (0,\dots,2)$). The kinetic equation for free transport yields

$$\partial_t \begin{bmatrix} m_{00} & m_{01} & m_{02} \\ m_{10} & & \\ m_{20} & & \end{bmatrix} + \partial_{x_1} \begin{bmatrix} m_{10} & \bar{u}_1 m_{01} & \bar{u}_1 m_{02} \\ m_{20} & & \\ m_{30} & & \end{bmatrix} + \partial_{x_2} \begin{bmatrix} m_{01} & m_{02} & m_{03} \\ \bar{u}_2 m_{10} & & \\ \bar{u}_2 m_{20} & & \end{bmatrix} = \mathbf{0} \tag{27}$$

with mean velocities $\bar{u}_1 = m_{10}/m_{00}$ and $\bar{u}_2 = m_{01}/m_{00}$ and 1D HyQMOM closures

$$m_{30} = m_{00}\bar{u}_1(\bar{u}_1^2 + 3c_{20}), \quad m_{03} = m_{00}\bar{u}_2(\bar{u}_2^2 + 3c_{02}) \tag{28}$$

where $c_{20}$ and $c_{02}$ are the second-order central moments. For isotropic moments, $c_{20} = c_{02}$ and the system reduces to the Euler equations.[4] Otherwise, the system is globally hyperbolic with an anisotropic pressure tensor due to $c_{20} \neq c_{02}$.

[4] The total energy is $\frac{1}{2}(m_{20} + m_{02})$ and the pressure is $\frac{1}{2}m_{00}(c_{20} + c_{02})$. Similar variables can be defined using the even-order moments with larger $n$.

#### 3.4.2. $n = 2$

For this case, the moment system has nine moments up to fourth order (denoted by $m_{i0}$ and $m_{0i}$ with $i \in (0, \dots, 4)$). The moment system is

$$\partial_t \begin{bmatrix} m_{00} & m_{01} & m_{02} & m_{03} & m_{04} \\ m_{10} & & & & \\ m_{20} & & & & \\ m_{30} & & & & \\ m_{40} & & & & \end{bmatrix} + \partial_{x_1} \begin{bmatrix} m_{10} & \bar{u}_1 m_{01} & \bar{u}_1 m_{02} & \bar{u}_1 m_{03} & \bar{u}_1 m_{04} \\ m_{20} & & & & \\ m_{30} & & & & \\ m_{40} & & & & \\ m_{50} & & & & \end{bmatrix} + \partial_{x_2} \begin{bmatrix} m_{01} & m_{02} & m_{03} & m_{04} & m_{05} \\ \bar{u}_2 m_{10} & & & & \\ \bar{u}_2 m_{20} & & & & \\ \bar{u}_2 m_{30} & & & & \\ \bar{u}_2 m_{40} & & & & \end{bmatrix} = \mathbf{0}. \tag{29}$$

The Jacobian matrix can be written in terms of two block-diagonal matrices. One is the identity matrix of size four multiplied by $\bar{u}_i$, and the other is the 1D HyQMOM Jacobian. Thus, the system is globally hyperbolic. The same pattern continues for $n > 2$ and arbitrary dimensions. Like the Euler equation, this model ignores correlations between velocity components, but can capture particle trajectory crossing (see Appendix D).

### 3.5. Anisotropic gaussian system

For the AG system [2,43], the 2D moment system includes the second-order cross-moment $m_{11}$.

#### 3.5.1. $n = 1$

For the AG model [46], the 2D moment system with six moments is

$$\partial_t \begin{bmatrix} m_{00} & m_{01} & m_{02} \\ m_{10} & m_{11} & \\ m_{20} & & \end{bmatrix} + \partial_{x_1} \begin{bmatrix} m_{10} & m_{11} & m_{12} \\ m_{20} & m_{21} & \\ m_{30} & & \end{bmatrix} + \partial_{x_2} \begin{bmatrix} m_{01} & m_{02} & m_{03} \\ m_{11} & m_{12} & \\ m_{21} & & \end{bmatrix} = \mathbf{0}, \tag{30}$$

which requires closures for the third-order moments. In terms of the central moments, the closures are $c_{30} = c_{21} = c_{12} = c_{03} = 0$. This moment system is globally hyperbolic for arbitrary dimensions [46]. While the AG model accounts for correlations between the velocity components, it cannot represent a bi-modal VDF (i.e., particle trajectory crossing). The latter requires at least $n = 2$ (see Appendix D).

### 3.6. 2D 10-moment extended AG closure

For this model, the moment system for free transport is

$$\partial_t \begin{bmatrix} m_{00} & m_{01} & m_{02} & m_{03} & m_{04} \\ m_{10} & m_{11} & & & \\ m_{20} & & & & \\ m_{30} & & & & \\ m_{40} & & & & \end{bmatrix} + \partial_{x_1} \begin{bmatrix} m_{10} & m_{11} & m_{12} & m_{13} & m_{14} \\ m_{20} & m_{21} & & & \\ m_{30} & & & & \\ m_{40} & & & & \\ m_{50} & & & & \end{bmatrix} + \partial_{x_2} \begin{bmatrix} m_{01} & m_{02} & m_{03} & m_{04} & m_{05} \\ m_{11} & m_{12} & & & \\ m_{21} & & & & \\ m_{31} & & & & \\ m_{41} & & & & \end{bmatrix} = \mathbf{0}, \tag{31}$$

which requires closures for the third- and fourth-order cross moments, e.g., $m_{21}$ and $m_{12}$, as well as the fifth-order pure moments. This 10-moment system suffices for simulating 2D high-speed crossing jets.

The closures are most easily written in terms of the standardized moments (see (3) and (4) for definitions, e.g., $s_{11} = c_{11}/\sqrt{c_{20}c_{02}}$). The closures for the standardized cross moments are

$$s_{21} = s_{30}s_{11},\ s_{12} = s_{03}s_{11}, \quad s_{31} = s_{40}s_{11},\ s_{13} = s_{04}s_{11}, \quad s_{41} = s_{50}s_{11},\ s_{14} = s_{05}s_{11}; \tag{32}$$

and the fifth-order pure moments are closed with 1D HyQMOM:

$$s_{50} = \frac{1}{2}s_{30}(5s_{40} - 3s_{30}^2 - 1),\ s_{05} = \frac{1}{2}s_{03}(5s_{04} - 3s_{03}^2 - 1). \tag{33}$$

Notice that when $s_{11} = 0$ (uncorrelated) and $s_{11} = \pm 1$ (perfectly correlated), the closures in (32) are exact.[5] Unlike for the second-order moment AG model, we do not assume that the moments $s_{30}$ and $s_{03}$ are zero. Compared to the independent 9-moment system in Section 3.4, here we do not assume $s_{11} = 0$ so that $s_{11}$ can take any value in the interval $[-1, 1]$. Nevertheless, as shown below, if $s_{11} = 0$ then the two models have nearly the same characteristic wave speeds.[6] The closures in (32) and 1D HyQMOM can be easily extended to $n > 2$.

Arranging the ten variables as

$$X = [m_{00}, m_{10}, m_{20}, m_{30}, m_{40}, m_{01}, m_{11}, m_{02}, m_{03}, m_{04}],$$

the Jacobian for direction $x_1$ is lower-block-diagonal with three diagonal blocks. The first $5 \times 5$ block comes from 1D HyQMOM with characteristic polynomial $Q_2(x)R_3(x)$ [12].[7] The second $2 \times 2$ block has characteristic polynomial $Q_2(x)$. The third $3 \times 3$ block has a characteristic polynomial $S_3$ defined by

$$S_3(y) = (y - a_2)Q_2(y) - \frac{3}{2} b_2 Q_1(y) \tag{34}$$

where $y = x/s_{11}$ and $a_2 = s_{03}/2$ and $b_2 = s_{04} - s_{03}^2 - 1$.[8] In summary, the characteristic polynomial has the form

$$P_{10}(x) = Q_2^2(x) R_3(x) S_3(y).$$

Thus, the ten eigenvalues of the system in (31) are real-valued, and the repeated eigenvalues from $Q_2$ have independent eigenvectors; therefore, the system is globally hyperbolic.

Numerical tests suggest that the model does not produce non-realizable moments, even when initialized with $s_{11} = \pm 1$. Moreover, without collisions, such moments remain perfectly correlated. Also notice that on the boundary of moment space where $b_2 = 0$, we have $S_3 \equiv R_3$ so that all eigenvalues are found from $Q_2 = 0$ and $x = a_2$,[9] i.e.,

$$P_{10}(x) = Q_2^3(x) Q_2(y)(x - s_{30}/2)(x - s_{11}s_{03}/2).$$

In general, the eigenvalues with the largest magnitude will come from the roots of $R_3$ or $S_3$, which depend on $(s_{30}, s_{40})$ and $(s_{11}, s_{03}, s_{04})$, respectively. However, since the zeros of $S_3$ are scaled by $s_{11}$, $R_3$ will likely determine the fastest wave speeds in most applications.

### 3.7. Third-order anisotropic model with $n = 2$

For this case, the 2D moment system with twelve moments includes the third-order cross moments $m_{21}$ and $m_{12}$. The 2D moment system for free transport is

$$\partial_t \begin{bmatrix} m_{00} & m_{01} & m_{02} & m_{03} & m_{04} \\ m_{10} & m_{11} & m_{12} & & \\ m_{20} & m_{21} & & & \\ m_{30} & & & & \\ m_{40} & & & & \end{bmatrix} + \partial_{x_1} \begin{bmatrix} m_{10} & m_{11} & m_{12} & m_{13} & m_{14} \\ m_{20} & m_{21} & m_{22} & & \\ m_{30} & m_{31} & & & \\ m_{40} & & & & \\ m_{50} & & & & \end{bmatrix} + \partial_{x_2} \begin{bmatrix} m_{01} & m_{02} & m_{03} & m_{04} & m_{05} \\ m_{11} & m_{12} & m_{13} & & \\ m_{21} & m_{22} & & & \\ m_{31} & & & & \\ m_{41} & & & & \end{bmatrix} = \mathbf{0}, \tag{35}$$

which requires closures for the fourth-order cross moments, e.g., $m_{31}$ and $m_{22}$, as well as some fifth-order moments. The closures are most easily written in terms of the standardized moments.

For this case, we require closures for $(s_{31}, s_{22}, s_{41})$, which are found, respectively, from $\langle \mathcal{U}_3 \mathcal{V}_1 \rangle = 0$, $\langle \mathcal{U}_2 \mathcal{V}_2 \rangle = 0$ and $\langle \mathcal{U}_4 \mathcal{V}_1 \rangle = 0$. (The closures for $(s_{13}, s_{14})$ are found by permuting the indices.) The polynomials $\mathcal{U}_2$ and $\mathcal{V}_2$ are known in closed form, e.g., $\mathcal{U}_2 = x^2 - s_{30}x - 1$, hence the closure for $s_{22}$ has no free parameters. Using (21), we have

$$\mathcal{U}_3(x) = (x - a_{x,2})\mathcal{U}_2(x) - b_{x,2}\mathcal{U}_1(x), \quad \mathcal{U}_4(x) = (x - a_{x,2})\mathcal{U}_3(x) - \beta_3 b_{x,2}\mathcal{U}_2(x), \tag{36}$$

with $a_{x,2} = s_{30}/2$ and $b_{x,2} = s_{40} - s_{30}^2 - 1$. The resulting closures for $s_{31}$ and $s_{41}$ are found, respectively, from

$$\langle xy\mathcal{U}_2 \rangle = a_{x,2}\langle y\mathcal{U}_2 \rangle + b_{x,2}s_{11}, \quad \langle xy\mathcal{U}_3 \rangle = a_{x,2}\langle y\mathcal{U}_3 \rangle + \beta_3 b_{x,2}\langle y\mathcal{U}_2 \rangle. \tag{37}$$

Notice that the closure for $s_{41}$ depends on $\beta_3$.

[5] When $s_{11} = \pm 1$, the moments are related by $s_{30} = s_{11}s_{03}$ and $s_{40} = s_{04}$. In general, the conditional mean of $Y$ given $X$ is $\langle Y|X \rangle = s_{11}X$. Thus, the conditional part of the moments is $\langle \langle Y|X \rangle^j \rangle = s_{11}^j s_{j0}$. Perfect correlation of standardized variables implies $Y = s_{11}X$ so that $\langle Y^j \rangle = s_{0j} = s_{11}^j s_{j0}$ and $\langle X^i Y^j \rangle = s_{ij} = s_{11}^j s_{i+j0}$ when $s_{11} = \pm 1$.

[6] Since there are ten eigenvalues instead of nine, one eigenvalue splits into two with equal magnitudes. The eight other eigenvalues are the same.

[7] $R_3(x) = (x - a_2)Q_2(x) - \frac{5}{2} b_2 Q_1(x)$ with $a_2 = s_{30}/2$ and $b_2 = s_{40} - s_{30}^2 - 1$.

[8] When $s_{11} = 0$, the three eigenvalues are null. Otherwise, they are scaled by $s_{11}$.

[9] The zeros of $Q_2(x)$ and $Q_2(y)$ are real but depend on different moments unless $s_{11} = \pm 1$.

Here, we set $\beta_3 = 3/2$ to obtain simple expressions for the eigenvalues of the $4\times4$ matrix $S_4$ described below. The closures for the standardized cross moments are then[10]

$$\begin{aligned}
s_{31} &= \frac{3}{2}s_{30}(s_{21} - s_{30}s_{11}) + s_{40}s_{11}, \; s_{13} = \frac{3}{2}s_{03}(s_{12} - s_{03}s_{11}) + s_{04}s_{11},\\
s_{22} &= 1 - s_{30}s_{03}s_{11} + s_{30}s_{12} + s_{03}s_{21},\\
s_{41} &= \frac{1}{4}(10s_{40} - 3s_{30}^2 - 6)s_{21} - \frac{1}{4}(3s_{30}^2 - 4)s_{30}s_{11}, \; s_{14} = \frac{1}{4}(10s_{04} - 3s_{03}^2 - 6)s_{12} - \frac{1}{4}(3s_{03}^2 - 4)s_{03}s_{11}a
\end{aligned} \tag{38}$$

and the fifth-order pure moments are closed with (33). In the limit $s_{21} = s_{30}s_{11}$ and $s_{12} = s_{03}s_{11}$, the closures reduce to the 10-moment closure, e.g, $s_{41} = s_{50}s_{11}$. This limit includes the boundary of moment space where $s_{22} = s_{40} = s_{04}$. Also notice that $\langle y\mathcal{U}_2\rangle = s_{21} - s_{30}s_{11}$ and thus that the closure for $s_{41}$ does not depend on $\beta_3$ when $b_{x,2} = 0$ or $s_{21} = s_{30}s_{11}$. Remarkably, in the limit $s_{21} = s_{30}s_{11}$ we find $s_{41} = s_{50}s_{11}$ where $s_{50}$ comes from 1D HyQMOM.

Arranging the twelve variables as

$$X = [m_{00}, m_{10}, m_{20}, m_{30}, m_{40}, m_{01}, m_{11}, m_{21}, m_{02}, m_{12}, m_{03}, m_{04}],$$

the Jacobian for direction $x_1$ is lower-block-diagonal with three diagonal blocks. The first $5\times5$ block comes from 1D HyQMOM with characteristic polynomial $Q_2(x)R_3(x)$ [12]. The second $3\times3$ block has characteristic polynomial $Q_3(x)$ based on $(s_{30}, s_{40})$.

The third $4\times4$ block has a characteristic polynomial $S_4$ that does not depend on $s_{40}$. Thus, if it obeys a 3-term recursion formula, it depends on $b_{y,2}$ and not $b_{x,2}$. Setting $s_{21} = s_{30}s_{11}$, $S_4$ reduces to two $2\times2$ blocks. The first block yields another characteristic polynomial $Q_2(x)$ and the second has real-valued roots that do not depend on $s_{04}$:

$$\frac{1}{2}s_{30} \pm \frac{1}{2}\sqrt{s_{30}^2 + 4}, \quad 2s_{12} - \frac{3}{2}s_{03}s_{11} \pm \frac{1}{2}\sqrt{4s_{11}^2 + s_{12}^2}.$$

In general, the four roots of $S_4$ depend on $(s_{11}, s_{30}, s_{21}, s_{12}, s_{03}, s_{04})$. However, on the boundary of moment space where $s_{04} = 1 + s_{03}^2$, setting $s_{12} = s_{03}s_{11}$ we find the following four roots of $S_4$:

$$\frac{1}{2}s_{30} \pm \frac{1}{2}\sqrt{s_{30}^2 + 4 + s_{03}(s_{21} - s_{30}s_{11})}, \quad \frac{1}{2}s_{03}s_{11} \pm \frac{1}{2}s_{11}\sqrt{s_{03}^2 + 4}.$$

Notice that the first two roots are the same when $s_{21} = s_{30}s_{11}$, and the latter must satisfy (15).

Further work is needed to check for global hyperbolicity. Still, all four roots are real-valued near the anisotropic Gaussian VDF, i.e., $(\pm1, \pm s_{11})$ and near the boundary of moment space.[11]

### 3.8. Fourth-order anisotropic model with $n = 2$

The case with $n = 2$ and known fourth-order moments is relatively unexplored [2]. The 2D 15-moment system for free transport is

$$\partial_t \begin{bmatrix} m_{00} & m_{01} & m_{02} & m_{03} & m_{04} \\ m_{10} & m_{11} & m_{12} & m_{13} & \\ m_{20} & m_{21} & m_{22} & & \\ m_{30} & m_{31} & & & \\ m_{40} & & & & \end{bmatrix} + \partial_{x_1} \begin{bmatrix} m_{10} & m_{11} & m_{12} & m_{13} & m_{14} \\ m_{20} & m_{21} & m_{22} & m_{23} & \\ m_{30} & m_{31} & m_{32} & & \\ m_{40} & m_{41} & & & \\ m_{50} & & & & \end{bmatrix} + \partial_{x_2} \begin{bmatrix} m_{01} & m_{02} & m_{03} & m_{04} & m_{05} \\ m_{11} & m_{12} & m_{13} & m_{14} & \\ m_{21} & m_{22} & m_{23} & & \\ m_{31} & m_{32} & & & \\ m_{41} & & & & \end{bmatrix} = \mathbf{0}. \tag{39}$$

Compared to the third-order case, the same orthogonal polynomials are used (with $\beta_3 = 3/2$), but now the moments $(s_{31}, s_{22}, s_{13})$ are known. Thus, the closures for $s_{41}$ and $s_{32}$ are

$$\begin{aligned}
s_{41} &= -\frac{1}{4}s_{30}(8s_{40} - 9s_{30}^2 - 4)s_{11} + \frac{1}{4}(10s_{40} - 15s_{30}^2 - 6)s_{21} + 2s_{30}s_{31},\\
s_{32} &= \frac{1}{2}(2s_{40} - 3s_{30}^2)(s_{12} - s_{03}s_{11}) + \frac{1}{2}s_{03}(2s_{31} - 3s_{30}s_{21}) + \frac{1}{2}s_{30}(3s_{22} - 1),
\end{aligned} \tag{40}$$

and $(s_{23}, s_{14})$ are found by permuting the indices. As in the previous cases, these closures reduce to the exact expressions for independent variables (e.g., $s_{32} = s_{30}$), and for $s_{11} = \pm1$ (e.g., $s_{32} = s_{50}$). Furthermore, this is true for any choice for $\beta_3$, which appears in $(s_{41}, s_{14})$. However, the value of $\beta_3$ will modify the eigenvalues/eigenvectors of the Jacobian for partially correlated moments.

Arranging the fifteen variables as

$$X = [m_{00}, m_{10}, m_{20}, m_{30}, m_{40}, m_{01}, m_{11}, m_{21}, m_{31}, m_{02}, m_{12}, m_{22}, m_{03}, m_{13}, m_{04}],$$

[10] This closure for $s_{22}$ is not exact in the limit $s_{11}^2 = 1$. An alternative is $s_{22} = 1 + |s_{11}|\sqrt{(s_{40} - 1)(s_{04} - 1)}$.

[11] On the boundary of moment space, the 1D VDF consists of two delta functions. While one 1D VDF can be on the boundary and the other can be continuous, it is more likely that the 2D VDF will consist of two delta functions. In this case, $s_{30} = s_{11}s_{03}$, $s_{21} = s_{30}$, and $s_{12} = s_{03}$.

the Jacobian for direction $x_1$ is lower-block-diagonal with three diagonal blocks. The first $5 \times 5$ block comes from 1D HyQMOM with characteristic polynomial $Q_2(x)R_3(x)$ [12]. The second $4 \times 4$ block has characteristic polynomial $Q_4 = (x - a_2)Q_3 - \frac{3}{2}b_2Q_2$ based on $(s_{30}, s_{40})$. The third $6 \times 6$ block involves the third- and fourth-order moments in both directions, as well as the cross moments. Except for the term

$$s_{31} - s_{11}s_{40} + \frac{3}{2}s_{30}(s_{11}s_{30} - s_{21}) \tag{41}$$

appearing in row 3/column 4, this matrix decomposes into two $3 \times 3$ blocks. When (41) is null, the first matrix is $Q_3$ based on $(s_{30}, s_{40})$, and the second has real eigenvalues for uncorrelated variables. While further work is required to determine the full range of hyperbolicity of the $6 \times 6$ block, complex eigenvalues have been observed in simulations with a large Mach number. In the simulation code, when the eigenvalues are complex, we can recover hyperbolicity by setting the standardized moments as follows:

$$s_{21} = s_{11}s_{30},\ s_{12} = s_{11}s_{03},\ s_{31} = s_{11}s_{40},\ s_{13} = s_{11}s_{04},\ s_{22} > \frac{1}{3} + \frac{5}{6}s_{03}s_{11}s_{30}, \tag{42}$$

for which the six eigenvalues are real and distinct. The four equalities eliminate (41) and decouple the two $3 \times 3$ blocks, while the inequality on $s_{22}$ ensures that the remaining three eigenvalues are real-valued. A simple alternative for maintaining global hyperbolicity is to use the modified closures in (B.1).

Numerical tests using 1D Riemann problems have been carried out for the 15-moment system. Remarkably, even when the fields are initialized as bi-variate Gaussian with $s_{11} = \pm 1$, all moments remain realizable for any value of Kn. Tests with fully 2D spatial cases are also promising, but (without enforcing the realizability constraints) non-realizable moments with $|\Delta_2^*| < 0$ and complex eigenvalues are observed for high-Mach-number crossing jets. Thus, to eliminate these issues, we use (42) point-wise to enforce global hyperbolicity and the realizability constraints in Section 3.1 and Appendix D after updating the moments due to the free-transport fluxes.

### 3.9. Fourth-order, 13-moment system

As discussed above, the Jacobian matrix for the 15-moment system simplifies considerably for a particular choice of $s_{31}$ and $s_{13}$ (see (41)). Using 2D HyQMOM to fix these two fourth-order moments and (40) yields the following closures:

$$\begin{aligned}
&s_{31} = s_{11}s_{40} + \frac{3}{2}s_{30}(s_{21} - s_{11}s_{30}),\ s_{13} = s_{11}s_{04} + \frac{3}{2}s_{03}(s_{12} - s_{11}s_{03}),\\
&s_{32} = \frac{1}{2}(2s_{40} - 3s_{30}^2)s_{12} + \frac{3}{2}s_{30}s_{22} - \frac{1}{2}s_{30},\ s_{23} = \frac{1}{2}(2s_{04} - 3s_{03}^2)s_{21} + \frac{3}{2}s_{03}s_{22} - \frac{1}{2}s_{03},\\
&s_{41} = \frac{1}{4}s_{30}(4 - 3s_{30}^2)s_{11} + \frac{1}{4}(10s_{40} - 3s_{30}^2 - 6)s_{21},\ s_{14} = \frac{1}{4}s_{03}(4 - 3s_{03}^2)s_{11} + \frac{1}{4}(10s_{04} - 3s_{03}^2 - 6)s_{12}.
\end{aligned} \tag{43}$$

In the limit $s_{11}^2 = 1$ (i.e., $|\Delta_1| = 0$), the closures for the fifth-order moments reduce to the HyQMOM closures for $s_{50}$ and $s_{05}$. Thus, simulations initialized as bi-variate Gaussian with $s_{11} = \pm 1$ should be robust in the 1D (perfectly correlated) limit.

These observations suggest that the 13-moment system keeping only fourth-order moments with even indices:

$$\partial_t \begin{bmatrix} m_{00} & m_{01} & m_{02} & m_{03} & m_{04} \\ m_{10} & m_{11} & m_{12} & & \\ m_{20} & m_{21} & m_{22} & & \\ m_{30} & & & & \\ m_{40} & & & & \end{bmatrix} + \partial_{x_1} \begin{bmatrix} m_{10} & m_{11} & m_{12} & m_{13} & m_{14} \\ m_{20} & m_{21} & m_{22} & & \\ m_{30} & m_{31} & m_{32} & & \\ m_{40} & & & & \\ m_{50} & & & & \end{bmatrix} + \partial_{x_2} \begin{bmatrix} m_{01} & m_{02} & m_{03} & m_{04} & m_{05} \\ m_{11} & m_{12} & m_{13} & & \\ m_{21} & m_{22} & m_{23} & & \\ m_{31} & & & & \\ m_{41} & & & & \end{bmatrix} = \mathbf{0} \tag{44}$$

with moment vector

$$X = [m_{00}, m_{10}, m_{20}, m_{30}, m_{40}, m_{01}, m_{11}, m_{21}, m_{02}, m_{12}, m_{22}, m_{03}, m_{04}]$$

may be more robust than the full 15-moment system. The moment closures for spatial fluxes use (43), and the $13 \times 13$ Jacobian matrix in each spatial direction is lower-block diagonal with four diagonal blocks of sizes 5, 3, 3, and 2. In the $x_1$-direction, the roots of the two blocks of size three are found from $Q_3(x) = 0$, i.e., they are real-valued and repeated but have independent eigenvectors, while the block of size 2 has two standardized eigenvalues:

$$\lambda_{1,2} = 2s_{12} - \frac{3}{2}s_{03}s_{11} \pm \frac{(4s_{11}^2 + s_{12}^2)^{1/2}}{2}, \tag{45}$$

which are always real-valued. The 13-moment system is thus globally hyperbolic. Although it is theoretically possible for the eigenvalues in (45) to have larger magnitude than the roots of $R_3$ from 1D HyQMOM, such behavior is likely to be rare (e.g., only with large Ma), and hence the roots of $R_3$ will usually determine the fastest wave speeds.

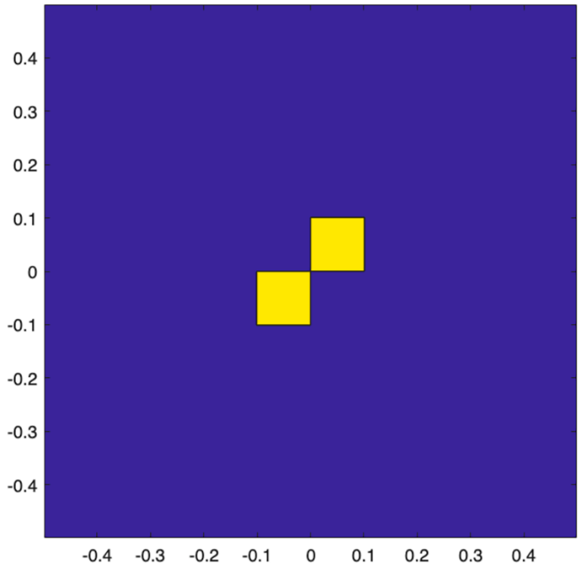


**Fig. 1.** Initial conditions in the 2D computational domain. Unless stated otherwise, the dimensionless density $m_{00} = 1$ on the two central squares and 0.1 elsewhere. The other velocity moments are joint Gaussian with unit variances, and the correlation coefficient $s_{11}$ is either 0 or $\pm 1$. In the low-density region, the dimensionless mean velocity is found from $m_{10} = m_{01} = 0$, while in the high-density squares $m_{01} = m_{10} = \pm \mathrm{Ma}/\sqrt{2}$ where in the lower square it is positive and in the upper square it is negative. Setting $\mathrm{Ma} = 0$ results in a pressure-driven flow; otherwise, impinging/crossing jets correspond to large Ma.

In summary, while the closures developed in this section appear promising, in practice, the 13- and 15-moment systems with the correction step are robust, especially for low-speed flows. For cases with dilute high-speed (relative to fluctuating velocity) crossing jets[12], the 10-moment system in Section 3.6 suffices for capturing the relevant physics. For the 13- and 15-moment systems, the correction steps described in Appendix D are essential to avoid unrealizable moments for high-speed crossing jets (i.e., negative $\Delta_2^*$, etc.). In the next section, we focus on numerical examples using the 15-moment system with high Mach numbers.

## 4. Some 2D numerical examples for the 15-moment system

In this section, we present 2D numerical examples using the fourth-order, 15-moment system in Section 3.8 and include the BGK model for elastic collisions [45]. Our main interest is to test the robustness of the moment-correction algorithm for extremely non-equilibrium conditions (e.g., hypersonic crossing jets). Indeed, for low-speed cases, the moment-correction algorithm is not needed as the moments remain realizable for all values of the Knudsen number. Consistent with Rice et al. [10], for 1D spatial domains the 2D HyQMOM closure was found to be robust for Riemann problems involving a pressure jump for arbitrary Kn. Here "Riemann problem" denotes the genuine one-dimensional initial-value problem with a single isolated discontinuity; the two-dimensional impinging-/crossing-jet configurations considered below contain several piecewise-constant states and are referred to as two-state initial-value problems. Remarkably, this is true when the initial VDF has $s_{11}^2 = 1$ (i.e., perfectly correlated variables), which is not the case for the other moment systems with $n = 2$ where $|\Delta_1|$ can become negative. In general, if $s_{11} \neq 0$ then both mean-velocity components are non-zero. Thus, it is of interest to test the 2D HyQMOM closure in a 2D spatial domain with strongly non-equilibrium initial conditions. Moreover, in the 1D domain, if $s_{11} = 0$ for the initial conditions, then it remains zero. Generally speaking, this will not be the case in 2D domains where the flow generates a non-zero $s_{11}$ due to the spatial flux.

### 4.1. 2D test case

The 2D problem on a double-square domain (see Fig. 1) is initialized with two high-density square regions in the center ($m_{00} = 1$) surrounded by a low-density region ($m_{00} = 0.1$ or 0.01). As in a classical 1D shock tube with initial zero mean velocity [47], the initial pressure ratio defines a shock Mach number $\mathrm{Ma}_s$, which is held constant for all cases. Explicitly, $\mathrm{Ma}_s$ is the Mach number of the shock generated by the initial pressure (equivalently, for the isothermal initial state, density) discontinuity through the standard shock-tube relation; it is set by the pressure ratio alone and is distinct from the jet Mach number Ma defined below, which is set by the imposed mean velocity $U$. The two Mach numbers are independent control parameters. It is worth noting that the diagonal spatial symmetries of the initial distribution must be preserved for all subsequent times. The center density normalizes the density $N_0$ such that Kn

[12] i.e., high-Kn and high-Ma flows.

defines the dimensionless collision time scale in the BGK model for elastic collision [45], i.e.,

$$\frac{\partial \mathbf{M}_{2n}}{\partial t} = \frac{\mathbf{G}_{2n} - \mathbf{M}_{2n}}{\tau_c} \qquad \text{with} \qquad \tau_c = \frac{\mathrm{Kn}}{2m_{00}\sqrt{\Theta}}$$

where $\Theta = (c_{20} + c_{02})/2$ is the dimensionless "temperature" and $\mathbf{G}_{2n}$ are the Maxwellian moments with the same $(m_{00}, \bar{\mathbf{u}}, \Theta)$. Thus, at time zero, the collision time scale in the center squares is $\tau_c = \mathrm{Kn}/2$, implying that Kn is inversely proportional to $N_0$, i.e., increasing Kn corresponds to decreasing $N_0$ at a fixed temperature.

The initial rms velocity $u'$ is used to normalize the velocity, and is uniform at time zero such that $\Theta_0 = 1$. To produce impinging/crossing jets, the mean velocity $U$ in the center squares is set equal and opposite, and the jet Mach number is defined by $\mathrm{Ma} = U/u'$.[13] These initial conditions were chosen because they generate trajectory crossing for large Ma and Kn, as well as non-zero energy fluxes. The initial VDF is jointly Gaussian with zero mean velocity and unit variances. The initial value of $s_{11}$ controls the covariance. Here (and in the Supplementary Material), we show results for $s_{11} = 0$ and $s_{11} = \pm 1$, but any intermediate value also works. Since the collisions force $s_{11}$ to zero, only the highest Kn is used with initial condition $s_{11} = \pm 1$.

In this work, we are mainly interested in whether the closure is robust for all Kn and Ma, leaving aside the question of accuracy. Indeed, it is known that with $\mathrm{Ma} = 0$ but large $\mathrm{Ma}_s$, 1D HyQMOM with $n = 2$ is accurate only for relatively small Kn, i.e., one must increase $n$ to get accurate results for increasing Kn [10,12,13,15,16]. Nonetheless, for large Ma, 1D HyQMOM can accurately capture jet crossing with $n = 2$, and the same is true with 2D HyQMOM, as shown below. In contrast, for low-speed flows with small $\mathrm{Ma}_s$, the HyQMOM closures are robust and globally hyperbolic without realizability corrections. Indeed, the eigenvalues for the moment system are nearly constant for such flows, independent of Kn.[14] Similar results were reported for such cases in Rice et al. [10] using a third-order orthogonal-polynomial-based closure.

### 4.2. Hyperbolic solver

The numerical solutions reported below used the HLL solver [47,50] for spatial transport from Fox and Laurent [12] (i.e., first order in space and time). However, we expect the results would be similar using other hyperbolic solvers as done in Rice et al. [10]. The minimum/maximum eigenvalues needed for the HLL fluxes are found from the three roots of the orthogonal polynomial $R_3$ and the six eigenvalues of the $6 \times 6$ block discussed in Section 3.8. For low-speed flows, the roots of $R_3$ suffice, but for high-speed flows, there are small regions where the HLL fluxes use the six eigenvalues. In any case, the eigenvalues are well defined for any set of realizable moments. In a 1D domain, it is possible to use a large number of grid cells to test convergence. However, for large Ma in 2D, we are limited by computational cost to a uniform mesh with at most $1024 \times 1024$ cells.[15] Future work along the lines of Fan et al. [51] is needed to refine the hyperbolic solver to achieve higher-order spatial convergence with guaranteed moment realizability. The BGK collisions are treated with operator splitting and a semi-implicit scheme [12]. In the figures below and in the Supplementary Material, contour plots of the principal moments are shown at a dimensionless time chosen to avoid waves leaving the domain. These plots include the Hankel determinants for the 1D moments $H_{20}$ and $H_{02}$, and $|\Delta_1|$ and $|\Delta_2^*|$ defined in (12). As they should, all contour plots exhibit the same diagonal spatial symmetries as the initial distribution in Fig. 1. As discussed in Section 4.3, when a realizability correction is needed, it occurs at isolated points that are clearly evident in the contour plots of the fourth-order moments (e.g., with density ratio 0.01, $\mathrm{Ma} = 100$, $\mathrm{Kn} = 1000$ in the Supplementary Material). Likewise, hyperbolicity corrections appear as isolated points in the contour plots of the flux eigenvalues. For example, high-speed crossing jets without realizability corrections have a contour plot for $|\Delta_2^*|$ with local negative regions that grow quickly. With realizability corrections, such regions remain positive. In general, controlling hyperbolicity is necessary for the robustness of the HLL solver, while small regions with non-realizable fourth-order moments can be tolerated by the solver.

### 4.3. Grid convergence, correction activity, and rotational invariance

In this section, we quantify the accuracy of the method under mesh refinement, the activity and magnitude of the moment-correction algorithm, and the rotational invariance of the closure. All computations below use the open-source solver, which reproduces the reference implementation to machine precision (maximum absolute difference $2 \times 10^{-15}$ over all moments). Similar to the bubble problem in Rice et al. [10], we use a smooth, rotationally symmetric initial condition – an isothermal Gaussian density profile $\rho(r) = \rho_\infty + \Delta\rho \exp(-r^2/2w^2)$ with zero mean velocity. The shock Mach number $\mathrm{Ma}_s$ is fixed by the density ratio $(\rho_\infty + \Delta\rho)/\rho_\infty$. For the density ratio (i.e., 2) used in Rice et al. [10], moment- and hyperbolicity corrections are never required due to the low-speed nature of the flow. However, for $\mathrm{Ma} = 0$ and $\mathrm{Kn} = \infty$, corrections are required starting at a density ratio around 200. Data for $\mathrm{Kn} = 1$ are discussed below.

---

13 Impinging jets correspond to small Kn, while crossing jets correspond to large Kn. For pure trajectory crossing, there are no collisions. Cases with a large Tsien parameter, KnMa [48], are the most difficult to capture with moment methods.

14 If the initial VDF is non-Gaussian everywhere, then for $\mathrm{Kn} \to \infty$ the eigenvalues will correspond to the zeros of the characteristic polynomial $P_5$. As $\mathrm{Kn} \to 0$, the eigenvalues converge to the roots of Hermite polynomials [49]. In any case, low-Ma cases are straightforward to treat with HyQMOM because moment realizability is not an issue.

15 With the projection method in Appendix B, cases up to $2048 \times 2048$ are tractable on a laptop with sufficient memory. In any case, the hyperbolic solver is highly scalable.

**Table 1**
Observed order of accuracy $p$ (density, $L^1$) for the bubble problem, by Knudsen number. The rate approaches the design first order under refinement and is independent of Kn.

| | 256 → 512 | 512 → 1024 |
|---|---|---|
| Kn = 0.01 | 0.96 | 0.98 |
| Kn = 0.1 | 0.96 | 0.98 |
| Kn = 1.0 | 0.96 | 0.99 |

**Table 2**
Correction activity versus Mach number (crossing jets, $256^2$, density ratio 0.01, Kn = 1): fraction of cells corrected for hyperbolicity and mean correction magnitude $\|\Delta M\|$.

| Ma | hyperbolicity-corrected fraction | mean $\|\Delta M\|$ |
|---|---|---|
| 0 | $8 \times 10^{-5}$ | $8 \times 10^{-6}$ |
| 2 | $9 \times 10^{-4}$ | $4 \times 10^{-4}$ |
| 4 | $1.4 \times 10^{-3}$ | $2 \times 10^{-3}$ |

**Table 3**
Activity of the realizability/hyperbolicity correction for the bubble problem with Ma = 0 and Kn = 1, versus the initial density ratio. “Cells corrected” is the fraction of cell updates in which the correction is active; max $\|\Delta M\|$ is the largest moment change applied; the conservation error is the relative drift of total mass. The corrected-cell fraction is mesh independent (19.8% at $256^2$ vs. 19.6% at $512^2$ for ratio 100).

| density ratio | cells corrected | max $\|\Delta M\|$ | conservation error |
|---|---|---|---|
| 2 | 0% | 0.04 | $2 \times 10^{-16}$ |
| 50 | 20% | 1.5 | $1 \times 10^{-15}$ |
| 100 | 23% | 1.8 | $7 \times 10^{-16}$ |
| 150 | 25% | 1.6 | $5 \times 10^{-12}$ |
| 200 | 26% | 2.2 | $2 \times 10^{-11}$ |

*4.3.1. Grid convergence*

We refine the mesh through $128^2$, $256^2$, $512^2$, and $1024^2$, and Table 1 reports the observed order of accuracy $p = \log_2(e_h/e_{h/2})$. The discretization converges at its design first order, with $p \to 1$ under refinement, uniformly across Knudsen numbers spanning the continuum, transition, and rarefied regimes.

*4.3.2. Rotational invariance*

For the rotationally symmetric bubble problem from Rice et al. [10], the residual angular variation of the density remains below 0.05%, uniformly in Kn. The moment closure thus preserves rotational symmetry to within a small, quantified bound. This result is consistent with those reported in Rice et al. [10] for a third-order moment closure.

*4.3.3. Activity of the correction algorithm*

The realizability/hyperbolicity correction acts as a local safeguard whose footprint scales with Ma. For crossing jets with increasing Ma, Table 2 reports the fraction of cells receiving a hyperbolicity correction and the mean magnitude $\|\Delta M\|$ of the moment change. At low speed the hyperbolicity correction is essentially never triggered and the realizability adjustment is negligible in magnitude. Both grow monotonically and controllably with Ma, consistent with activation near strong shocks. For small Kn neither correction is needed (cf. Section 6). For the bubble problem in Rice et al. [10] with Ma = 0 and Kn = 1, Table 3 reports similar information for increasing $\mathrm{Ma}_s$. As noted above, larger $\mathrm{Ma}_s$ leads to a stronger shock, which can active the hyperbolicity correction at isolated regions in the domain.

*4.3.4. Local conservation*

The correction algorithm modifies only the standardized moments and leaves the conserved hydrodynamic moments – density, momentum, and energy – unchanged at each cell to machine precision ($\sim 10^{-15}$ per correction). In most cases, the univariate standardized moments are also unchanged. Thus, for every Kn and Ma examined below, no conservation error is introduced by the correction algorithm.

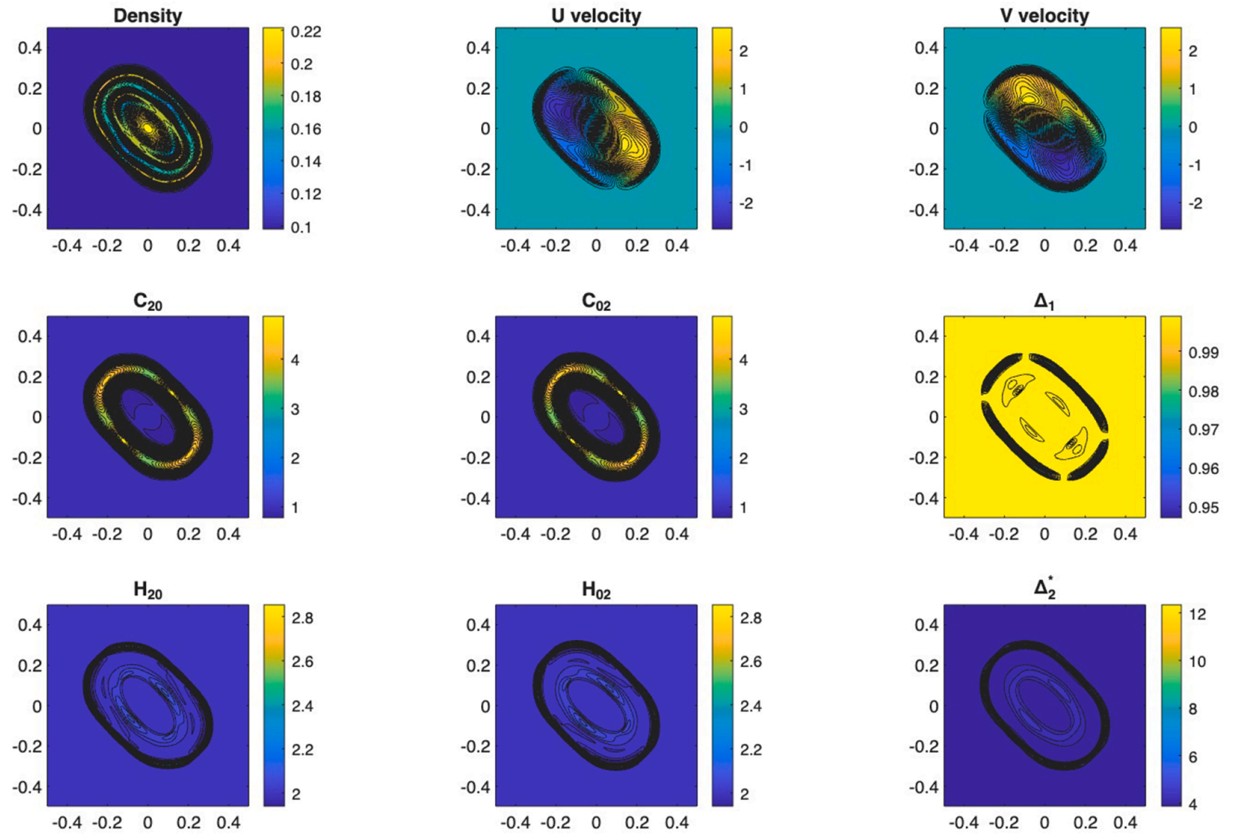


**Fig. 2.** Ma = 4, Kn = 0.001, $t = 0.05$. Low-order moments and Hankel determinants.

### 4.4. Example results for 2D test case

For Ma = 0, no issues with hyperbolicity were observed for the considered density ratios. The HLL solver ran with CFL = 0.5, and in all cases, the largest and smallest eigenvalues came from $R_3$. The perfectly correlated cases exhibited small overshoots for $s_{11}^2$ (i.e., negative $|\Delta_2|$), but no remedial corrections were needed to correct the moments. In the 1D cases, such overshoots decrease on finer meshes and are therefore most likely due to the numerical algorithm rather than the closure. In summary, for low-speed flows, the 15-moment, 2D HyQMOM closure is remarkably robust from a numerical perspective and requires neither realizability nor hyperbolicity corrections. It should therefore serve as a good starting point for simulating non-equilibrium flows at small to moderate Mach and arbitrary Knudsen numbers.

Next, we consider a supersonic case with Ma = 4 and vary Kn between 0.001 and 1. Runs with Kn = 1000 are similar to those with Kn = 1. For each Kn, four sets of contour plots are presented at $t = 0.06$ in the Supplementary Material. Using Kn = 0.001 as an example, in Fig. 2 the lower-order moments and Hankel determinants are shown. In Fig. 3 the third- and fourth-order standardized moments are shown. In Fig. 4 the eigenvalues (top row), Cholesky diagonal elements (middle row), and roots of the third-degree polynomial found from $\Delta_2^*$ are shown. The first two rows must be positive for the cross moments to be realizable. In Fig. 5, the six eigenvalues for the $6 \times 6$ flux Jacobian are shown in the top and middle rows, and the bottom row shows the difference between two pairs of eigenvalues. These differences must be positive for real, distinct eigenvalues and a hyperbolic system. Note that the hyperbolicity and realizability plots are used to demonstrate that the constraints on the moments are correctly implemented after the spatial fluxes. Without these constraints, the code with Ma > 1 (or $\mathrm{Ma}_s > 1$) may not be robust.

From the density plots, we see in Fig. 6 that Kn = 0.1 corresponds approximately to the crossover from impinging (Kn < 0.1) to crossing (Kn > 0.1) jets. In other words, for Kn ≥ 1, the collisions are negligible compared to free transport. From 1D HyQMOM, we know that the accurate representation of free transport requires higher-order velocity moments than fourth order.[16] However, the results for larger Ma and Kn demonstrate that the simulation algorithm produces realizable moments even if they are not accurate. Indeed, without the correction algorithms described in Appendix D, the high-Ma cases can only be run with small Ma Kn (i.e., near the AG/Euler limit).

[16] The pure crossing jet discussed in Appendix D is an exception because it depends only on moments up to third order.

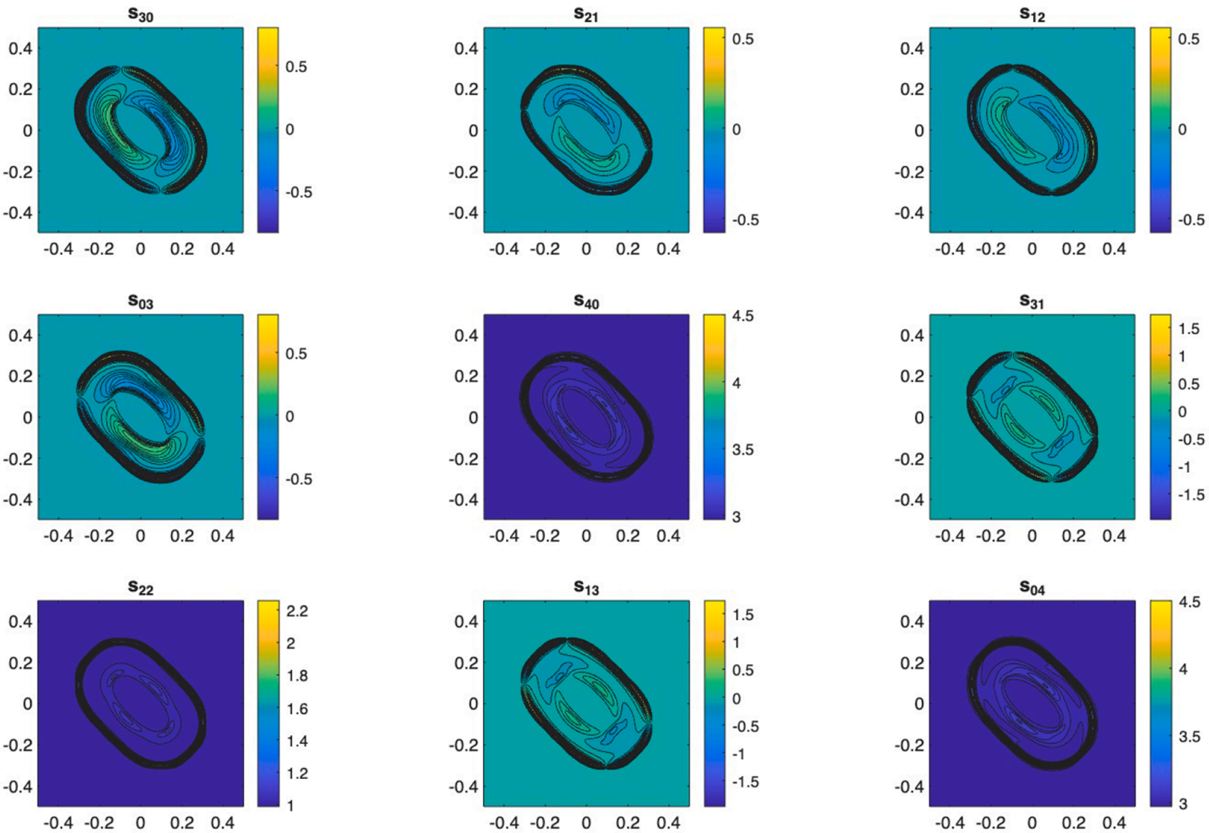


**Fig. 3.** Ma = 4, Kn = 0.001, $t = 0.05$. Standardized moments.

Example results for hypersonic crossing jets with outer-to-inner density ($m_{00}$) ratio 0.01, Ma = 100, and Kn = 1 on a $200 \times 200$ mesh are shown at $t = 0.002$ in Fig. 7 and in the Supplementary Material. Note that the shock Mach number associated with the density ratio (i.e., when Ma = 0) is meaningfully larger than in the previous cases. From the minimum/maximum eigenvalues $\lambda_1$ and $\lambda_6$, we observe that the maximum wave speed is larger than 500. As seen in Boccelli et al. [22], it is worth noting that the density is moving relatively slowly compared to the third- and fourth-order standardized moments, which vary rapidly at the edges of the crossing jets. For comparison, results for impinging jets with Ma = 100 and Kn = 0.001 are shown at $t = 0.002$ in the Supplementary Material. From the standardized moments in Fig. 8, it can be seen that outside the denser center region, the moment system is far from Maxwellian due to the high Ma and small density ratio. In general, for small Kn neither moment-realizability nor hyperbolicity corrections are needed for this Ma. Note that, compared to Kn = 1, the waves travel faster for Kn = 0.001.

## 5. Extension of HyQMOM to 3D moment systems

In the previous sections, we considered moments for a 2D VDF with phase space $\mathbf{u} \in \mathbb{R}^2$, deriving realizability constraints for the fifteen moments up to fourth order. Here, the 3D VDF has phase space $\mathbf{u} \in \mathbb{R}^3$, so we begin in Section 5.1 by deriving the realizability constraints for the 35 3D moments $\mathbf{M}_4$ up to fourth order [38], which are meaningfully more complex than in 2D. With the 3D realizability constraints in hand, we then consider the hyperbolicity of the 3D HyQMOM closure for such moments in Section 5.4. The numerical implementation for the hyperbolic moment system found from the 3D kinetic equation is very similar to the 2D moment system in Section 4. As in the 2D case, local moment-realizability and hyperbolicity corrections are only needed for highly non-equilibrium flows.

### 5.1. 3D moment realizability

The first step is to check and correct the realizability of the three 2D moment sets ($s_{ij0}, s_{i0k}, s_{0jk}$) using the procedure in Section 3.1, which is necessary but not sufficient for realizable 3D moments. At the same time, we treat the edges as described in Section 5.1.1.[17] Thus, hereinafter, we assume that the three 2D moments sets are realizable and that $H_{200}, H_{020}, H_{002} > 0$. As in 2D, another set of

[17] Non-realizable points near edges and corners are usually due to non-realizable 2D second-order moments.

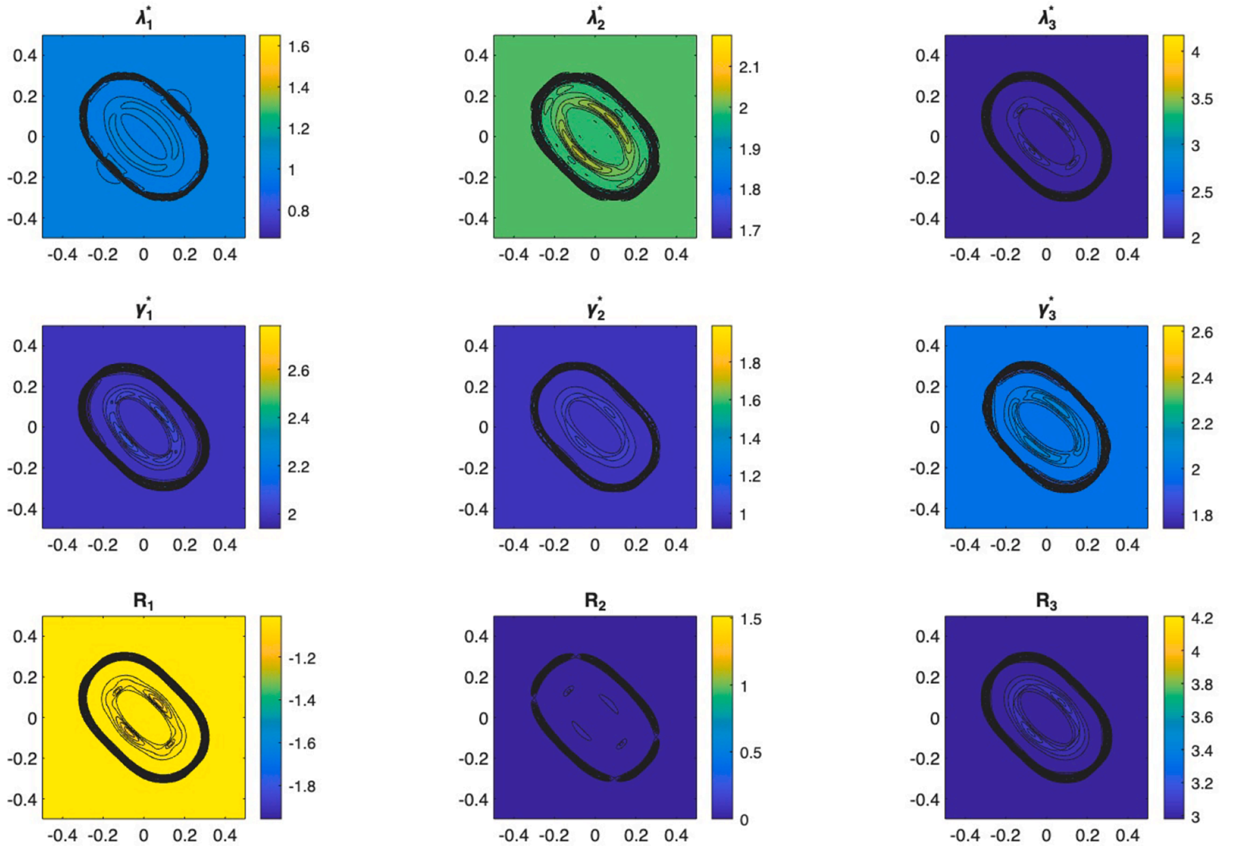


**Fig. 4.** Ma = 4, Kn = 0.001, $t = 0.05$. Realizability of $\Delta_2^*$. Top row: eigenvalues. Middle row: Cholesky diagonal elements. Bottom row: roots of the polynomial.

constraints on $s_{220}$ can be found using the variables $X = \tilde{u}^2 - 1$, $Y = \tilde{v}^2 - 1$ and $Z = \tilde{u}\tilde{v}$ where $(\tilde{u}, \tilde{v})$ are the standardized 2D velocity components. From these variables, the bounds on $s_{220}$ are

$$\max\left(s_{110}^2, 1 - \sqrt{(s_{400} - 1)(s_{040} - 1)}\right) < s_{220} < 1 + \sqrt{(s_{400} - 1)(s_{040} - 1)}\,. \tag{46}$$

Analogous constraints are found for $s_{202}$ and $s_{022}$ by permuting the indices. As discussed below, (46) is less restrictive than the bounds found from the leading principal minors of the 3D moment matrices.

The 3D orthogonal polynomials have realizability constraints based on non-negative, symmetric, moment matrices [29,30]. In terms of the standardized moments $s_{ijk}$ up to fourth order, the two matrices are

$$\Delta_1 = \begin{bmatrix} 1 & 0 & 0 & 0 \\ 0 & 1 & s_{110} & s_{101} \\ 0 & s_{110} & 1 & s_{011} \\ 0 & s_{101} & s_{011} & 1 \end{bmatrix}, \quad \Delta_2 = \begin{bmatrix} 1 & 0 & 0 & 0 & 1 & s_{110} & s_{101} & 1 & s_{011} & 1 \\ 0 & 1 & s_{110} & s_{101} & s_{300} & s_{210} & s_{201} & s_{120} & s_{111} & s_{102} \\ 0 & s_{110} & 1 & s_{011} & s_{210} & s_{120} & s_{111} & s_{030} & s_{021} & s_{012} \\ 0 & s_{101} & s_{011} & 1 & s_{201} & s_{111} & s_{102} & s_{021} & s_{012} & s_{003} \\ 1 & s_{300} & s_{210} & s_{201} & s_{400} & s_{310} & s_{301} & s_{220} & s_{211} & s_{202} \\ s_{110} & s_{210} & s_{120} & s_{111} & s_{310} & s_{220} & s_{211} & s_{130} & s_{121} & s_{112} \\ s_{101} & s_{201} & s_{111} & s_{102} & s_{301} & s_{211} & s_{202} & s_{121} & s_{112} & s_{103} \\ 1 & s_{120} & s_{030} & s_{021} & s_{220} & s_{130} & s_{121} & s_{040} & s_{031} & s_{022} \\ s_{011} & s_{111} & s_{021} & s_{012} & s_{211} & s_{121} & s_{112} & s_{031} & s_{022} & s_{013} \\ 1 & s_{102} & s_{012} & s_{003} & s_{202} & s_{112} & s_{103} & s_{022} & s_{013} & s_{004} \end{bmatrix}. \tag{47}$$

For realizable moments in the interior of moment space, these matrices must be positive definite [30]. Also, by permuting the indices, different matrices will be found that have the same eigenvalues. Thus, it suffices to work with one set of indices to find formulas that can be applied to the other permutations. For example, there are three possible permutations of $s_{110}$ and six of $s_{210}$.

#### *5.1.1. Realizability constraints for second-order cross moments*

In strongly non-equilibrium cases, the second-order moments can become non-realizable. This is true not only for HyQMOM, but also for second-order moment closures [32], such as the AG model [43,46]. From the leading principal minors, non-negative $\Delta_1$

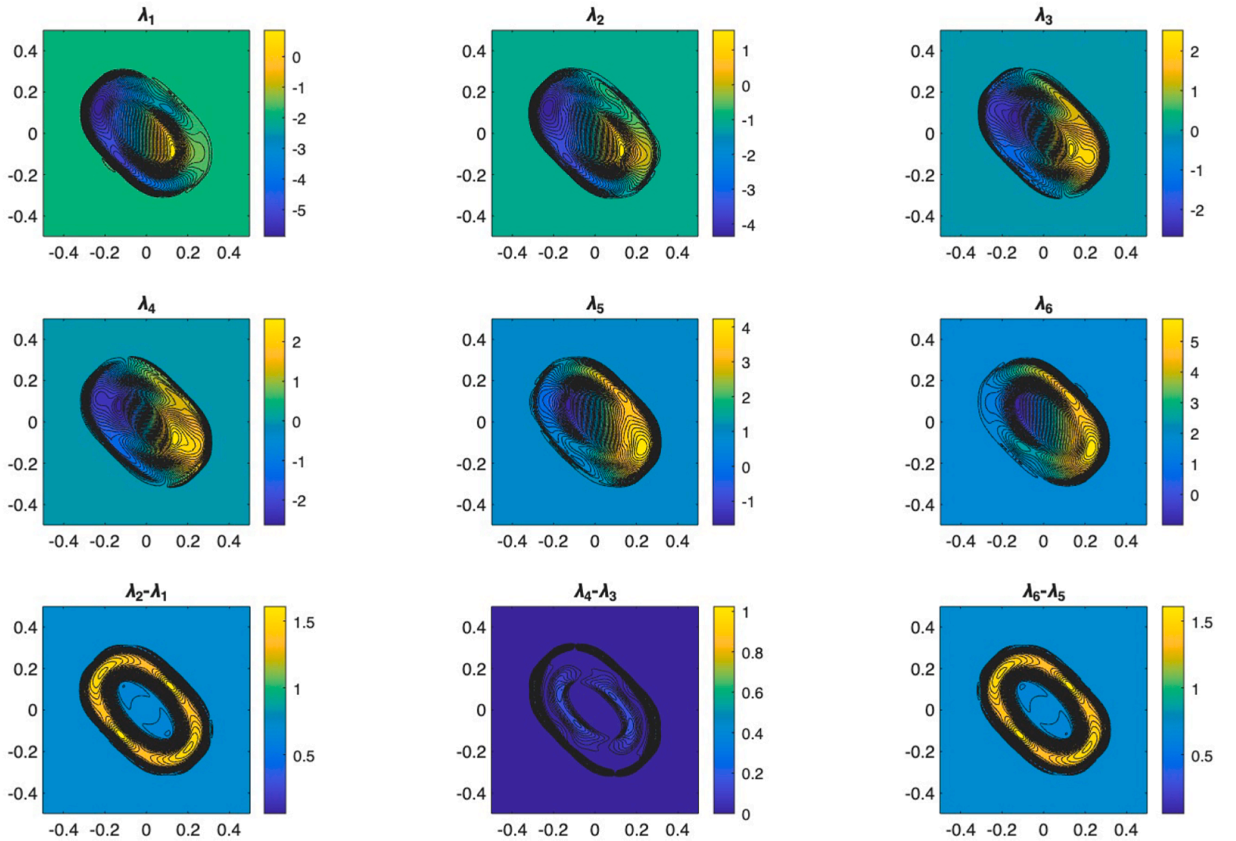


**Fig. 5.** Ma = 4, Kn = 0.001, $t = 0.05$. Flux eigenvalues for hyperbolicity.

requires

$$s_{110}^2, s_{101}^2, s_{011}^2 \le 1, \tag{48}$$

and

$$1 + 2s_{110}s_{101}s_{011} - (s_{110}^2 + s_{101}^2 + s_{011}^2) \ge 0, \tag{49}$$

where equality in (49) defines the boundary of second-order moment space. For example, if $s_{011} = 0$ in (49), then $s_{110}^2 + s_{101}^2 = 1$ on the boundary; or if $s_{011} = 1$, then $s_{110} = s_{101}$. Note that (48) is the same as for the 2D system (i.e., it is assumed to be satisfied). Thus, (49) is an additional requirement for the 3D second-order cross moments to be realizable. As shown in Fig. 9, the boundary of moment space can be found using the following formulas:

$$\begin{aligned} s_{011} - s_{110}s_{101} &= aR_{110}R_{101}, \\ s_{101} - s_{110}s_{011} &= bR_{110}R_{011}, \\ s_{110} - s_{011}s_{101} &= cR_{101}R_{011}, \end{aligned} \tag{50}$$

where

$$R_{110} = (1 - s_{110}^2)^{1/2}, \; R_{101} = (1 - s_{101}^2)^{1/2}, \; R_{011} = (1 - s_{011}^2)^{1/2}, \tag{51}$$

and $a, b, c = \pm 1$ with $abc = -1$.[18] Note that in simulations, the case where one of the 2D moments $(s_{110}, s_{101}, s_{011})$ is non-realizable has already been treated, so the coefficients in (51) are real-valued. The four vectors $(a, b, c) = (-1, -1, -1), (-1, 1, 1), (1, -1, 1), (1, 1, -1)$ define the four faces and are normal to the boundary at the center of each face (intersection of red sphere and blue surface in Fig. 9).

For a 3D crossing jet, there are exactly four possible cases (see Appendix D):

$$(s_{110}, s_{101}, s_{011}) = (1, 1, 1), (1, -1, -1), (-1, -1, 1), (-1, 1, -1).$$

Thus, a 3D crossing jet corresponds to one of the four corners in Fig. 9 where three edges intersect. On the boundary of moment space, other special cases can be identified. For example, $s_{110}s_{101}s_{011} \ge -1/8$ must hold when $s_{110}^2 + s_{101}^2 + s_{011}^2 \ge 3/5$ (see red sphere

[18] Since $a^2 = 1$, etc., we have $ab = -c$, $bc = -a$ and $ab = -c$.

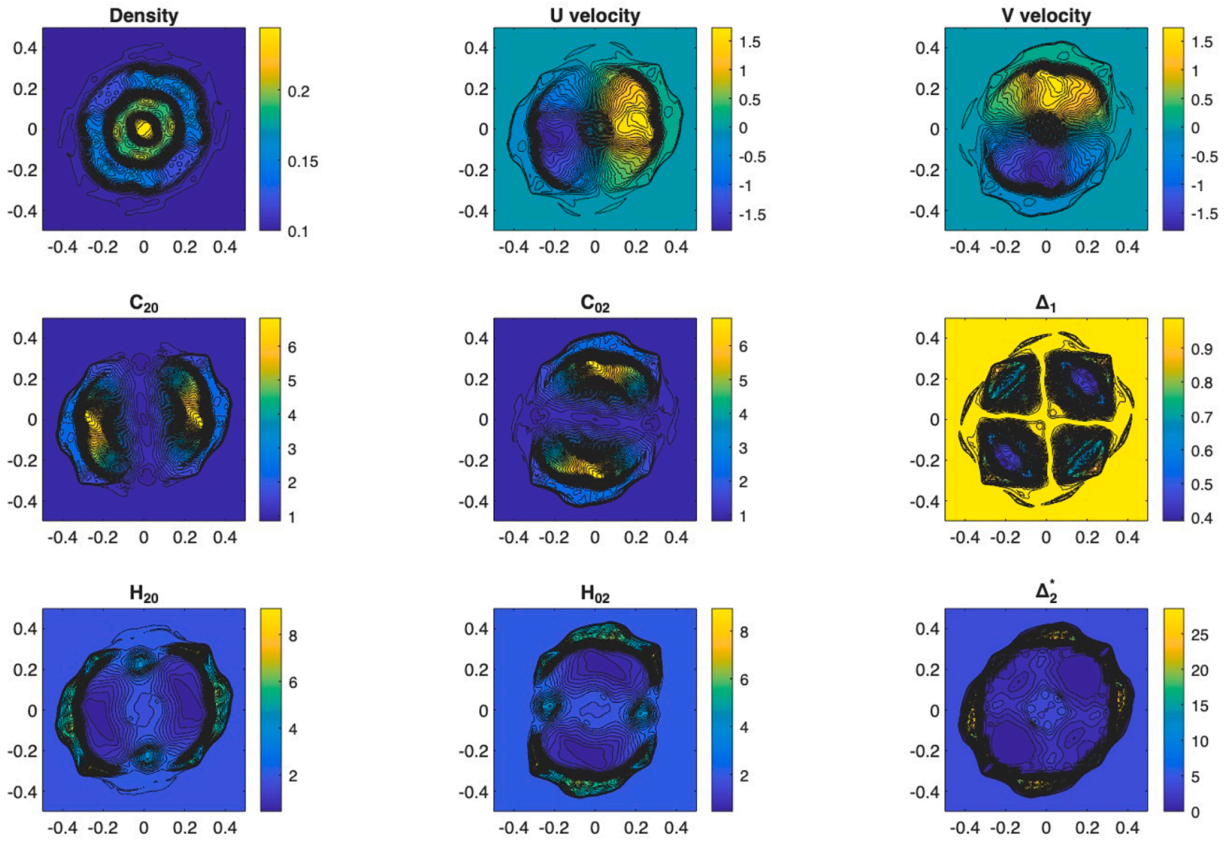


**Fig. 6.** Ma = 4, Kn = 0.1, $t = 0.05$. Low-order moments and Hankel determinants.

in Fig. 9). From (49) it is obvious that $s_{110}s_{101}s_{011} \geq 0$ when $s^2_{110} + s^2_{101} + s^2_{011} \geq 1$ and that the unit sphere touches the boundary at points where a correlation coefficient is null (e.g., $s_{110} = 0$). Thus, between the unit sphere and the sphere with radius $\sqrt{3/4}$, we have $s_{110}s_{101}s_{011} \leq 0$. Furthermore, on the boundary of second-order moment space, the 3D standardized VDF $f(\tilde{u}, \tilde{v}, \tilde{w})$ is confined to a planar surface in velocity phase space defined by

$$S_1(\tilde{u}, \tilde{v}, \tilde{w}) = aR_{011}\tilde{u} + bR_{101}\tilde{v} + cR_{110}\tilde{w} = 0 \tag{52}$$

where the coefficients are determined from $\langle \tilde{u}S_1 \rangle = \langle \tilde{v}S_1 \rangle = \langle \tilde{w}S_1 \rangle = 0$.

On this surface, only two of the three coefficients in (51) are free, with the third found from (50). Moreover, on the six edges, one of the coefficients is zero, and the other two are positive and equal. For example, if $R_{011} = 0$ then $R_{101} = R_{110}$ and $b\tilde{v} + c\tilde{w} = 0$ from (52). Furthermore, in the four corners, all coefficients are null and $a\tilde{u} + b\tilde{v} = 0$, $a\tilde{u} + c\tilde{w} = 0$, $b\tilde{v} + c\tilde{w} = 0$. Note that for the corners and edges $(a, b, c) = (s_{011}, s_{101}, s_{110})$. Otherwise, given the second-order moments, on a face, the values of $(a, b, c)$ are found from (50).

For robust simulations, it will be necessary to determine whether the second-order cross moments are realizable, i.e., inside the boundary shown in Fig. 9, and to correct them if they are not. This is accomplished by defining a realizability surface in second-order moment space:

$$S_2(s_{110}, s_{101}, s_{011}) = 1 + 2s_{110}s_{101}s_{011} - (s^2_{110} + s^2_{101} + s^2_{011}). \tag{53}$$

If $S_2 \geq 0$, then the second-order moments are realizable. Otherwise, if $S_2 < 0$ we correct the moments by finding the largest scale factor $0 < \alpha < 1$ such that $S_2(\alpha s_{110}, \alpha s_{101}, \alpha s_{011}) = 0$ (i.e., a point on the surface in Fig. 9), and replace the moments $(s_{110}, s_{101}, s_{011})$ with the scaled moments $(\alpha s_{110}, \alpha s_{101}, \alpha s_{011})$ for which $S_2 = 0$. Recall that at this point the 2D second-order moments have already been corrected, e.g., $s^2_{110} \leq 1$. This implies that the rescaled moments will correspond to one of the four faces.

In summary, when $S_2 > 0$, the realizability of the third- and fourth-order moments is checked and corrected as described below in Section 5.1.2. Otherwise, when $S_2 \leq 0$, their values are found starting from (52). We will consider separately the procedure used for corners, edges, and faces.

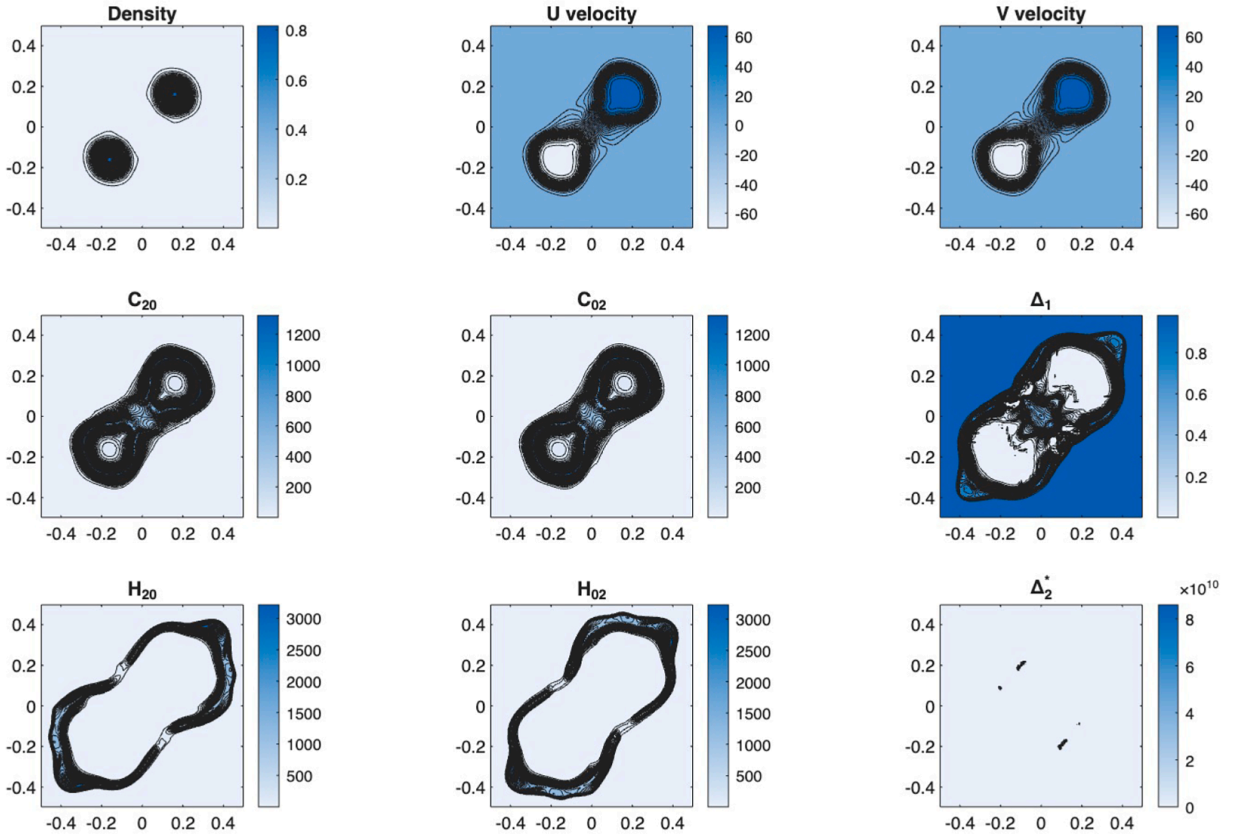


**Fig. 7.** Crossing jets with Ma = 100 and Kn = 1000 at $t = 0.003$. Low-order moments and Hankel determinants.

*Corners.* The standardized VDF at the corners reduces to a univariate VDF, e.g., $f(\tilde{u},\tilde{v},\tilde{w}) = f(\tilde{u})\delta(a\tilde{u}+b\tilde{v})\delta(a\tilde{u}+c\tilde{w})$, such that the moments can be written as

$$s_{ijk} = (-1)^{j+k} c^j b^k \int \tilde{u}^{i+j+k} f(\tilde{u}) d\tilde{u} = (-1)^{j+k} s_{110}^j s_{101}^k s_{i+j+k\,00} \tag{54}$$

where $s_{110}, s_{101} = \pm 1$ in the corners. Thus, all of the cross moments can be expressed in terms of univariate moments in one direction. The correction algorithm proceeds as in the 2D case, and is implemented when $R_{011} = R_{101} = R_{110} = 0$. In simulations, non-realizable points near corners almost always occur (albeit almost never) with non-realizable 2D moments.[19] Thus, corners are handled simultaneously with the correction of the 2D moment sets.

*Edges.* The standardized VDF along the edges depends on which of $R_{011}, R_{101}, R_{110}$ is null. Using $R_{011} = 0$ as an example, the VDF is $f(\tilde{u},\tilde{v},\tilde{w}) = f(\tilde{u},\tilde{v})\delta(\tilde{w}-a\tilde{v}) = f(\tilde{u},\tilde{w})\delta(\tilde{v}-a\tilde{w})$ along two edges, and the moments are

$$s_{ijk} = a^k \int \tilde{u}^i \tilde{v}^{j+k} f(\tilde{u},\tilde{v}) d\tilde{u} d\tilde{v} = s_{011}^k s_{i\,j+k\,0} \quad \text{or} \quad s_{ijk} = s_{011}^j s_{i\,0\,k+j} \tag{55}$$

where $s_{011} = \pm 1$. Thus, along the two edges where $R_{011} = 0$, all moments must be corrected given the realizable 2D moments $s_{i\,j+k\,0}$ or $s_{i\,0\,j+k}$. Here we choose $s_{i\,j+k\,0}$ if $R_{110} > R_{101}$ and $s_{i\,0\,j+k}$ otherwise. The correction procedure for $R_{101} = 0$ or $R_{110} = 0$ is analogous. As shown next, edges are a special case of faces. In simulations, non-realizable points near edges almost always occur with non-realizable 2D moments, e.g., $s_{011}^2 > 1$. Thus, edges are handled simultaneously with the 2D moment sets, using (55) to reset the moments in the other directions.

*Faces.* Using (52) to express $\tilde{w}$ in terms of $(\tilde{u},\tilde{v})$, the moments on the faces where the coefficients are all positive ($0 < R_{011}, R_{101}, R_{110}$) can be written as

$$s_{ijk} = (cR_{110})^{-k} \int \tilde{u}^i \tilde{v}^j (-aR_{011}\tilde{u} - bR_{101}\tilde{v})^k f(\tilde{u},\tilde{v}) d\tilde{u} d\tilde{v} = \sum_{l=0}^{k} \binom{k}{l} \gamma_1^l \gamma_2^{k-l} s_{i+l\,j+k-l\,0} \tag{56}$$

[19] In fact, during simulations, non-realizable points at corners are rare compared to edges.

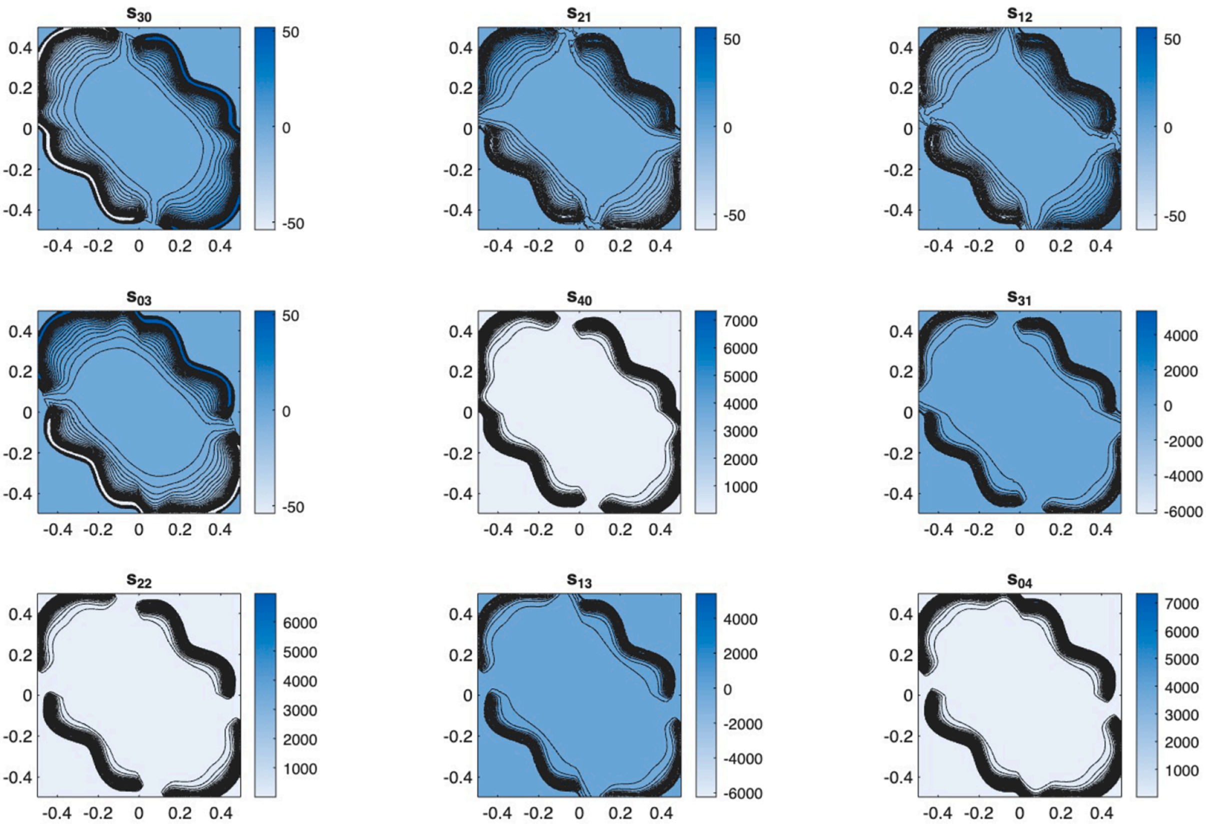


**Fig. 8.** Impinging jets with Ma = 100 and Kn = 0.001 at $t = 0.002$. Standardized moments.

where $\gamma_1 = (s_{101} - s_{110}s_{011})/(1 - s_{110}^2)$ and $\gamma_2 = (s_{011} - s_{110}s_{101})/(1 - s_{110}^2)$. Thus, for example, $s_{111} = \gamma_1 s_{210} + \gamma_2 s_{120}$ and $s_{211} = \gamma_1 s_{310} + \gamma_2 s_{220}$. Two other forms exist by expressing $\tilde{v}$ in terms of $(\tilde{u}, \tilde{w})$:

$$s_{ijk} = (bR_{101})^{-j} \int \tilde{u}^i (-aR_{011}\tilde{u} - cR_{110}\tilde{w})^j \tilde{w}^k f(\tilde{u}, \tilde{w}) d\tilde{u} d\tilde{w} = \sum_{l=0}^{j} \binom{j}{l} \gamma_3^l \gamma_4^{j-l} s_{i+l\,0\,k+j-l} \tag{57}$$

where $\gamma_3 = (s_{110} - s_{101}s_{011})/(1 - s_{101}^2)$ and $\gamma_4 = (s_{011} - s_{110}s_{101})/(1 - s_{101}^2)$; and $\tilde{u}$ in terms of $(\tilde{v}, \tilde{w})$:

$$s_{ijk} = (aR_{011})^{-i} \int (-bR_{101}\tilde{v} - cR_{110}\tilde{w})^i \tilde{v}^j \tilde{w}^k f(\tilde{v}, \tilde{w}) d\tilde{v} d\tilde{w} = \sum_{l=0}^{i} \binom{i}{l} \gamma_5^l \gamma_6^{i-l} s_{0\,j+l\,k+i-l} \tag{58}$$

where $\gamma_5 = (s_{101} - s_{110}s_{011})(1 - s_{011}^2)$ and $\gamma_6 = (s_{110} - s_{101}s_{011})(1 - s_{011}^2)$. Recall that only two of the three second-order cross moments are independent when $S_2 = 0$, and the 2D moments appearing on the right-hand sides are realizable. In fully 3D simulations, most non-realizable points will correspond to faces.

In the correction procedure with $3 \le i + j + k \le 4$, we use the largest coefficient to choose between the three formulas. For example, if $R_{110}$ is largest, then (56) is used; or if $R_{101}$ is largest, then (57) is used; otherwise we use (58). Note that with this algorithm, faces and edges can be treated together without worrying about dividing by zero. However, as mentioned earlier, points near edges are handled together with the 2D moments. At the four points where $s_{110}^2 = s_{101}^2 = s_{011}^2 = 1/4$, we use the arithmetic averages to fix the moments.[20]

In summary, whenever any one of the second-order moments is found to be non-realizable, all of the higher-order moments are corrected according to whether the point is on a corner, edge, or face. Otherwise, if all of the second-order moments are realizable, then we proceed to check the third- and fourth-order moments as described next.

[20] Unlike the 2D case where $s_{101} = s_{011} = 0$, such points never occur in a simulation with finite-precision algorithms.

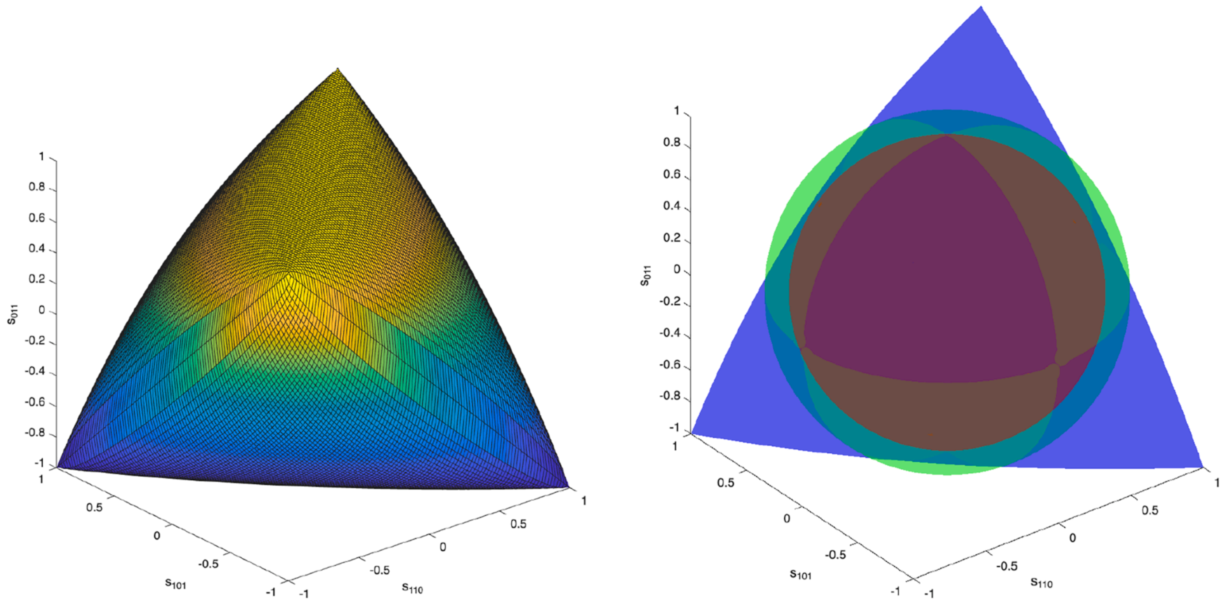


**Fig. 9.** Boundary of moment space for $s_{110}$, $s_{101}$, and $s_{011}$ where $|\Delta_1| = 0$. It has the form of a "puffy" regular tetrahedron centered at the origin. Left: complete surface. Right: a sphere of radius $\sqrt{3/4}$ (red) touches the boundary (blue) at one point on each face (e.g., 1/2,-1/2,1/2). Outside the unit sphere (green), $0 \le s_{110}s_{101}s_{011}$ on the boundary. Crossing jets (i.e., the VDF is two delta functions) correspond to one of the four extreme corner points where $s_{110}s_{101}s_{011} = 1$. On the six edges connecting the corners where one of the cross moments equals $\pm 1$, the VDF is positive on a 1D line in 3D phase space. Elsewhere on the four faces between the edges, the VDF is positive on a 2D surface in 3D phase space. (For interpretation of the references to colour in this figure legend, the reader is referred to the web version of this article.)

### 5.1.2. Realizability of third- and fourth-order moments

Hereinafter, we assume that $\Delta_1$ is positive definite and rewrite $\Delta_2$ using block matrices:

$$\Delta_2 = \begin{bmatrix} \Delta_1 & \mathbf{B}^t \\ \mathbf{B} & \mathbf{C} \end{bmatrix} \text{ where } \mathbf{B} = \begin{bmatrix} 1 & s_{300} & s_{210} & s_{201} \\ s_{110} & s_{210} & s_{120} & s_{111} \\ s_{101} & s_{201} & s_{111} & s_{102} \\ 1 & s_{120} & s_{030} & s_{021} \\ s_{011} & s_{111} & s_{021} & s_{012} \\ 1 & s_{102} & s_{012} & s_{003} \end{bmatrix} \text{ and } \mathbf{C} = \begin{bmatrix} s_{400} & s_{310} & s_{301} & s_{220} & s_{211} & s_{202} \\ s_{310} & s_{220} & s_{211} & s_{130} & s_{121} & s_{112} \\ s_{301} & s_{211} & s_{202} & s_{121} & s_{112} & s_{103} \\ s_{220} & s_{130} & s_{121} & s_{040} & s_{031} & s_{022} \\ s_{211} & s_{121} & s_{112} & s_{031} & s_{022} & s_{013} \\ s_{202} & s_{112} & s_{103} & s_{022} & s_{013} & s_{004} \end{bmatrix}.$$

Expanding the determinant in block matrices, $|\Delta_2|$ can be expressed as $|\Delta_2| = |\Delta_1||\Delta_2^*|$ where

$$\Delta_2^* = \mathbf{C} - \mathbf{D} \quad \text{and} \quad \mathbf{D} = \mathbf{B}\Delta_1^{-1}\mathbf{B}^t. \tag{59}$$

As in 2D, the symmetric matrix $\mathbf{D}$ with components $d_{ij}$ depends only on moments up to third order, while the symmetric matrix $\mathbf{C}$ depends only on the fourth-order standardized moments. For moments with one of the indices equal to zero, the number of occurrences of a cross moment in $\mathbf{C}$ will determine the degree of the polynomial that must be solved to determine its bounds. For example, $(s_{310}, s_{301}, s_{130}, s_{103}, s_{031}, s_{013})$ each appear twice, while $(s_{220}, s_{202}, s_{022})$ each appear three times. On the other hand, $(s_{211}, s_{121}, s_{112})$ each appear four times, but can be limited using a second-order polynomial.

If the $6 \times 6$ symmetric matrix $\Delta_2^*$ is positive definite for realizable univariate moments, then the 15 third- and fourth-order cross moments are realizable. As seen for the second-order cross moments in Section 5.1.1, the 2D constraints for realizability provide nine necessary conditions for the realizability of the 2D cross moments. In principle, the six leading principal minors of $\Delta_2^*$ can be used to find these constraints (i.e., Sylvester's criterion [36]). However, the 3D formulas are significantly more difficult to analyze symbolically and implement numerically compared to the 2D system.[21]

In summary, we assume that the univariate moments are strictly realizable (i.e., $H_{200}, H_{020}, H_{002} > 0$), as are the second-order cross moments (i.e., $|\Delta_1| > 0$), and seek constraints on the third- and fourth-order cross moments using (59). This will mainly be done by enforcing the six leading principal minors of $\Delta_2^*$ to be positive for the six permutations of $\Delta_2^*$. In our 3D test cases, correction of the second-order moments was never required.

[21] The simplest 3D case occurs when the third direction is independent of the first two, such that $s_{ijk} = s_{ij0}s_{00k}$, in which case the 2D realizability constraints are sufficient.

#### 5.1.3. Realizability constraint for $(s_{210}, s_{201})$

The first leading principal minor $(s_{400} - d_{11}) > 0$ provides limits for the pair of third-order cross moments $(s_{210}, s_{201})$:

$$\begin{bmatrix} s_{210} - s_{110}s_{300} \\ s_{201} - s_{101}s_{300} \end{bmatrix}^t \begin{bmatrix} 1 - s_{101}^2 & s_{101}s_{110} - s_{011} \\ s_{101}s_{110} - s_{011} & 1 - s_{110}^2 \end{bmatrix} \begin{bmatrix} s_{210} - s_{110}s_{300} \\ s_{201} - s_{101}s_{300} \end{bmatrix} < H_{200}|\Delta_1|, \tag{60}$$

provided that $|\Delta_1| > 0$ (i.e., the coefficient matrix in (60) is positive definite). Note that the left-hand side can be written as $\mathbf{V}^t\mathbf{V}$ with column vector $\mathbf{V} = \mathbf{R}[s_{210} - s_{110}s_{300}, s_{201} - s_{101}s_{300}]^t$ where $\mathbf{R}$ is the square root of the coefficient matrix.

If the inequality in (60) is not satisfied and $\mathbf{V}^t\mathbf{V} > 0$,[22] then it is possible to scale the left-hand side using a factor $0 < \alpha < 1$ such that $\alpha\mathbf{V}$ is inside the boundary of moments space, and hence to correct $(s_{210}, s_{201})$ to be realizable. In this manner, six of the seven third-order cross moments (i.e., except $s_{111}$) can be made realizable. The limits for $(s_{120}, s_{021})$ and $(s_{012}, s_{102})$ follow by permuting the indices. When the third direction is independent of the first two directions, i.e., $s_{101} = 0$, $s_{011} = 0$, and $s_{201} = 0$, the limits on $s_{210}$ are the same as in 2D.[23] Otherwise, (60) defines a rotated ellipse in $(s_{210} - s_{110}s_{300}, s_{201} - s_{101}s_{300})$-moment space. As seen in 2D, the 3D energy flux, e.g., $q_1 = (c_{300} + c_{120} + c_{102})/2$, is limited by (60).

A necessary condition for $\Delta_2^*$ to be positive is that the six diagonal elements must all be positive. Thus, when the first element of $\Delta_2^*$ approaches zero (e.g., $(s_{400} - d_{11}) \to 0$), some of the fourth-order cross moments must approach limiting values. These values can be found by setting the elements of the first row/column of $\Delta_2^*$ to zero. Note that the six permutations yield the same limits. In the moment-correction algorithm, if any of the diagonal elements are zero, then, except for $(s_{220}, s_{202}, s_{022})$, the fourth-order moments are set to their limiting values. For example, if the first diagonal element is zero (or negative) the moments $(s_{310}, s_{301}, s_{211})$ are fixed.[24] This procedure is applied to each of the diagonal elements. If all diagonal elements are zero, then all of the fourth-order moments will be determined. Otherwise, the remaining fourth-order moments are corrected as described below, without changing the fixed values found when the diagonal elements are zero.

#### 5.1.4. Realizability constraints for $s_{111}$

Finding the value of $s_{111}$ on the corners and edges of the surface in Fig. 9 is straightforward due to the linear dependence between the standardized velocities. For example, at the corner $(1, 1, 1)$, we find $s_{111} = s_{300} = s_{030} = s_{003}$; and along the edge connecting $(1, 1, 1)$ and $(-1, -1, 1)$ we find $s_{111} = s_{120} = s_{102}$. On the faces, we have $|\Delta_1| = 0$ but finding the exact value of $s_{111}$ is complicated (see (56)–(58)). Thus, consistent with the edges, we limit $s_{111}$ by

$$\min\left(A_{110}, A_{101}, A_{011}\right) \le s_{111} \le \max\left(A_{110}, A_{101}, A_{011}\right) \tag{61}$$

where $A_{110} = \gamma_1 s_{210} + \gamma_2 s_{120}$, $A_{101} = \gamma_3 s_{201} + \gamma_4 s_{102}$ and $A_{011} = \gamma_5 s_{021} + \gamma_6 s_{012}$ with the $\gamma_i$ defined in Section 5.1.1. Another possibility, given in Appendix E, is to treat $(s_{310}, s_{111})$ together, even though they have different orders. With all of the third-order moments constrained, the matrix $\mathbf{D}$ in (59) is fixed when searching for the constraints on the fourth-order moments.

#### 5.1.5. Realizability constraint on $s_{310}$

Continuing with the second leading principal minor:

$$\begin{vmatrix} s_{400} - d_{11} & s_{310} - d_{12} \\ s_{310} - d_{12} & s_{220} - d_{22} \end{vmatrix} = (s_{400} - d_{11})(s_{220} - d_{22}) - (s_{310} - d_{12})^2 > 0,$$

the quadratic equation for $X = (s_{310} - d_{12})$ will have real-valued roots under the following conditions:

$$G_{310} = (s_{220} - d_{22})(s_{400} - d_{11}) = G_{310,a}G_{310,b} \quad \text{with} \quad G_{310,a}, G_{310,b} \ge 0 \tag{62}$$

where

$$G_{310,a} = s_{220} - s_{110}^2 - \frac{1}{|\Delta_1|}\begin{bmatrix} s_{210} \\ s_{120} \\ s_{111} \end{bmatrix}^t \begin{bmatrix} 1 - s_{011}^2 & s_{011}s_{101} - s_{110} & s_{011}s_{110} - s_{101} \\ s_{011}s_{101} - s_{110} & 1 - s_{101}^2 & s_{101}s_{110} - s_{011} \\ s_{011}s_{110} - s_{101} & s_{101}s_{110} - s_{011} & 1 - s_{110}^2 \end{bmatrix} \begin{bmatrix} s_{210} \\ s_{120} \\ s_{111} \end{bmatrix}, \tag{63}$$

with the determinant of the (positive) coefficient matrix equal to $|\Delta_1|^2 > 0$; and

$$G_{310,b} = H_{200} - \frac{1}{|\Delta_1|}\begin{bmatrix} s_{210} - s_{110}s_{300} \\ s_{201} - s_{101}s_{300} \end{bmatrix}^t \begin{bmatrix} 1 - s_{101}^2 & s_{101}s_{110} - s_{011} \\ s_{101}s_{110} - s_{011} & 1 - s_{110}^2 \end{bmatrix} \begin{bmatrix} s_{210} - s_{110}s_{300} \\ s_{201} - s_{101}s_{300} \end{bmatrix}, \tag{64}$$

which is always positive due to (60). The constraint $G_{310,a} \ge 0$ places a lower bound on $s_{220}$:

$$s_{220} \ge d_{22} = s_{110}^2 + \frac{1}{|\Delta_1|}\begin{bmatrix} s_{210} \\ s_{120} \\ s_{111} \end{bmatrix}^t \begin{bmatrix} 1 - s_{011}^2 & s_{011}s_{101} - s_{110} & s_{011}s_{110} - s_{101} \\ s_{011}s_{101} - s_{110} & 1 - s_{101}^2 & s_{101}s_{110} - s_{011} \\ s_{011}s_{110} - s_{101} & s_{101}s_{110} - s_{011} & 1 - s_{110}^2 \end{bmatrix} \begin{bmatrix} s_{210} \\ s_{120} \\ s_{111} \end{bmatrix} \ge 0. \tag{65}$$

[22] If $\mathbf{V}^t\mathbf{V} = 0$ (i.e., for $(s_{102}, s_{012})$ in 2D), we set $\mathbf{V} = 0$.

[23] Recall that uncorrelated is not equivalent to independent. For example, in 3D cases, the spatial fluxes can keep $s_{101} = s_{011} = 0$, but $s_{102}$ and $s_{012}$ are non-zero, i.e., the third direction is uncorrelated but not independent of the first and second directions.

[24] Notice that because $d_{12} \ge d_{22}$, forcing $s_{220} = d_{12}$ provides a larger lower bound than the diagonal element $s_{220} = d_{22}$. For example, the Maxwellian gives $d_{12} = 1$ and $d_{22} = 0$. The same is true for $s_{202}$ and $s_{022}$ found from the other permutations.

Similarly, by permuting the indices, $G_{301,a} \geq 0$ and $G_{031,a} \geq 0$ give lower bounds for $s_{202}$ and $s_{022}$, respectively. Note also that $G_{130,a} \geq 0$ yields the same constraint on $s_{220}$ as $G_{310,a} \geq 0$, i.e., $G_{310} = G_{130}$, so that no additional constraints are obtained from the same pair. These constraints on $(s_{220}, s_{202}, s_{022})$ can all be applied before checking $s_{310}$ and its six permutations. As in the 2D case, we can anticipate that $(s_{220}, s_{202}, s_{022})$ will have additional constraints (e.g., an upper limit).[25]

Using the results above, the realizability constraint for $s_{310}$ is

$$d_{12} - G_{310}^{1/2} < s_{310} < d_{12} + G_{310}^{1/2}, \tag{66}$$

where $d_{12} = s_{110} + b_{310}/|\Delta_1|$ with

$$\begin{aligned} b_{310} &= (1 - s_{110}^2)s_{201}s_{111} + (1 - s_{101}^2)s_{210}s_{120} + (1 - s_{011}^2)s_{210}s_{300} + (s_{011}s_{101} - s_{110})(s_{120}s_{300} + s_{210}^2) \\ &\quad + (s_{101}s_{110} - s_{011})(s_{120}s_{201} + s_{210}s_{111}) + (s_{011}s_{110} - s_{101})(s_{111}s_{300} + s_{201}s_{210}). \end{aligned} \tag{67}$$

In summary, there are two possible cases: if $s_{220}$ satisfies (65), then $G_{310} > 0$ and $s_{310}$ must satisfy (66); otherwise, $s_{220}$ is fixed such that $G_{310} = 0$ and $s_{310} = d_{12}$. This is repeated for the six permutations.

### 5.1.6. *Realizability constraint for* $s_{211}$

With the known $(s_{310}, s_{301})$ from Section 5.1.5, the third leading principal minor

$$\begin{vmatrix} s_{400} - d_{11} & s_{310} - d_{12} & s_{301} - d_{13} \\ s_{310} - d_{12} & s_{220} - d_{22} & s_{211} - d_{23} \\ s_{301} - d_{13} & s_{211} - d_{23} & s_{202} - d_{33} \end{vmatrix} > 0 \tag{68}$$

depends on the fourth-order moments $(s_{220}, s_{202})$. The realizability constraint is quadratic in terms of $X = (s_{211} - d_{23})$:

$$\begin{aligned} &(s_{400} - d_{11})X^2 - 2(s_{301} - d_{13})(s_{310} - d_{12})X + (s_{202} - d_{33})(s_{310} - d_{12})^2 + (s_{220} - d_{22})(s_{301} - d_{13})^2 \\ &\quad - (s_{400} - d_{11})(s_{220} - d_{22})(s_{202} - d_{33}) = 0 \end{aligned}$$

where from Section 5.1.3 we have $(s_{400} - d_{11}) > 0$. From the discriminant, the two roots are real-valued if $G_{211} = G_{211,a}G_{211,b} \geq 0$ where

$$G_{211,a} = (s_{400} - d_{11})(s_{220} - d_{22}) - (s_{301} - d_{13})^2 \quad \text{and} \quad G_{211,b} = (s_{400} - d_{11})(s_{202} - d_{33}) - (s_{310} - d_{12})^2.$$

A sufficient condition is $G_{211,a}, G_{211,b} \geq 0$, yielding the following constraints:[26]

$$s_{220} \geq d_{22} + \frac{(s_{301} - d_{13})^2}{s_{400} - d_{11}} \quad \text{and} \quad s_{202} \geq d_{33} + \frac{(s_{310} - d_{12})^2}{s_{400} - d_{11}},$$

which can be compared to (65). Also, under a permutation of the second and third indices, the constraints are the same,[27] so that $G_{211}$ is invariant.

When permuting the indices in $G_{211}$, the conditions $G_{121} = G_{121,a}G_{121,b} \geq 0$ and $G_{112} = G_{112,a}G_{112,b} \geq 0$ must also hold. For the first and second indices, we have

$$G_{121,a} = (s_{040} - d_{44})(s_{220} - d_{22}) - (s_{031} - d_{45})^2 \quad \text{and} \quad G_{121,b} = (s_{040} - d_{44})(s_{022} - d_{55}) - (s_{130} - d_{24})^2,$$

and for the first and third, we have

$$G_{112,a} = (s_{004} - d_{66})(s_{022} - d_{55}) - (s_{103} - d_{36})^2 \quad \text{and} \quad G_{112,b} = (s_{004} - d_{66})(s_{202} - d_{33}) - (s_{310} - d_{12})^2.$$

Thus, using $G_{211,a}, G_{121,a} \geq 0$, the lower bound on $s_{220}$ must satisfy[28]

$$s_{220} \geq d_{22} + \max\left(\frac{(s_{301} - d_{13})^2}{s_{400} - d_{11}}, \frac{(s_{031} - d_{45})^2}{s_{040} - d_{44}}\right), \tag{69}$$

and those for $s_{202}$ and $s_{022}$ follow by permuting the indices. As noted for $s_{310}$, these constraints on $(s_{220}, s_{202}, s_{022})$ can be computed first. Note that the minimum $s_{220}$ found from (65) is smaller than from (69). Nevertheless, in the correction algorithm, we limit $s_{310}$ using (66) with the stricter bounds found with (65).

Using the above results for the lower bounds on $(s_{220}, s_{202})$, the realizability constraint for $s_{211}$ is

$$d_{23} + \frac{b_{211} - G_{211}^{1/2}}{s_{400} - d_{11}} < s_{211} < d_{23} + \frac{b_{211} + G_{211}^{1/2}}{s_{400} - d_{11}}, \tag{70}$$

with $b_{211} = (s_{301} - d_{13})(s_{310} - d_{12})$, and those for $s_{121}$ and $s_{112}$ follow by permuting the indices. As done for $s_{310}$, the lower bound from (69) is used to find $s_{211}$, even though a larger lower bound may be needed to satisfy the remaining leading principal minors.[29]

---

25 Another lower limit is $s_{220} \geq d_{14}$, etc., for the other permutations. In general, this lower limit is larger than $s_{220} \geq d_{22}$ such that $G_{310,a} \geq 0$.

26 In general, the diagonal elements must satisfy $(s_{220} - d_{22}) > 0$ and $(s_{202} - d_{33}) > 0$.

27 By permuting the second and third indices, $d_{12} \leftrightarrows d_{13}$.

28 By permuting the first and second indices, $d_{11} \leftrightarrows d_{44}$.

29 The alternative would be to recompute $(s_{310}, s_{031})$, and $s_{220}$ from (69), iterating to convergence. In any case, $s_{220}$ must satisfy the largest lower bound found from all leading principal minors.

#### 5.1.7. More realizability constraints for $(s_{220}, s_{202}, s_{022})$

As done in Section 3.1, here we now assume that all moments except possibly $(s_{220}, s_{202}, s_{022})$ are realizable, and look for constraints for these three moments using the remaining leading principal minors of $\Delta_2^*$. Recall that the 2D algorithm has already been applied to find necessary bounds for these moments. Thus, in many cases, no further corrections may be required.

During this process, we fix the values of all other cross moments, e.g., $s_{310}$ and $s_{211}$. To simplify the notation, we denote the components of $\Delta_2^*$ by $e_{ij}$ and define

$$(X, Y, Z) = (e_{14}, e_{16}, e_{46}) = (s_{220} - d_{14}, s_{202} - d_{16}, s_{022} - d_{46}) \geq 0$$

and

$$(e_X, e_Y, e_Z) = (e_{22} - e_{14}, e_{33} - e_{16}, e_{55} - e_{46}) = (d_{14} - d_{22}, d_{16} - d_{33}, d_{46} - d_{55}) \geq 0.$$

With this notation, the fourth leading principal minor becomes

$$D_1 = \begin{vmatrix} e_{11} & e_{12} & e_{13} & X \\ e_{12} & X + e_X & e_{23} & e_{24} \\ e_{13} & e_{23} & Y + e_Y & e_{34} \\ X & e_{24} & e_{34} & e_{44} \end{vmatrix} = \begin{vmatrix} e_{11} & e_{12} & e_{13} \\ e_{12} & X + e_X & e_{23} \\ e_{13} & e_{23} & Y + e_Y \end{vmatrix} D_1^* > 0,$$

and is a third-degree polynomial in $X$ and linear in $Y$. The first determinant on the right-hand side is positive due to (68), so that we must have $D_1^* > 0$ where

$$D_1^*(X, Y) = e_{44} - \begin{bmatrix} X \\ e_{24} \\ e_{34} \end{bmatrix}^t \begin{bmatrix} e_{11} & e_{12} & e_{13} \\ e_{12} & X + e_X & e_{23} \\ e_{13} & e_{23} & Y + e_Y \end{bmatrix}^{-1} \begin{bmatrix} X \\ e_{24} \\ e_{34} \end{bmatrix},$$

and the inverse matrix and $e_{44} = s_{040} - d_{44}$ are positive. The realizability condition is then found from $D_1^* = 0$, which is a third-degree polynomial in $X$ for fixed $Y$. By permuting the indices pairwise, a total of six polynomials can be found, all of which must be positive. For example, $(ijk) \to (jik)$ gives $D_1^*(X, Y) \to D_1^*(Y, X)$, $(ijk) \to (kji)$ gives $D_1^*(X, Y) \to D_1^*(Z, Y)$, and $(ijk) \to (ikj)$ gives $D_1^*(X, Y) \to D_1^*(X, Z)$.

As seen in 2D, the roots of the third-degree polynomials will give upper and lower bounds for $D_1^* \geq 0$. However, in 3D, the roots depend on a second variable. For example, $D_1^*(X, Y) = 0$ and $D_1^*(X, Z) = 0$ will give two sets of three real-valued roots[30] such that $R_{X,2}(Y) < X < R_{X,3}(Y))$ and $R_{X,2}(Z) < X < R_{X,3}(Z))$ defines the realizability ranges for $X$:

$$\max(0, R_{X,2}(Y), R_{X,2}(Z)) < X < \min(R_{X,3}(Y), R_{X,3}(Z)). \tag{71}$$

Analogous constraints apply to $Y$ and $Z$. Obviously, one must check for degenerate cases where (71) cannot be satisfied for any $X > 0$, or a polynomial has only one or no positive real-valued root. For the numerical examples in Section 5.5, having a positive fourth leading principal minor suffices for realizable fourth-order moments.

The fifth leading principal minor

$$D_2 = \begin{vmatrix} e_{11} & e_{12} & e_{13} & X & e_{15} \\ e_{12} & X + e_X & e_{23} & e_{24} & e_{25} \\ e_{13} & e_{23} & Y + e_Y & e_{34} & e_{35} \\ X & e_{24} & e_{34} & e_{44} & e_{45} \\ e_{15} & e_{25} & e_{35} & e_{45} & Z + e_Z \end{vmatrix} = D_1 D_2^* > 0$$

is a third-degree polynomial in $X$ and linear in $Y$ and $Z$. Assuming that $D_1 > 0$, we must have $D_2^* > 0$ where

$$D_2^*(X, Y, Z) = Z + e_Z - \begin{bmatrix} e_{15} \\ e_{25} \\ e_{35} \\ e_{45} \end{bmatrix}^t \begin{bmatrix} e_{11} & e_{12} & e_{13} & X \\ e_{12} & X + e_X & e_{23} & e_{24} \\ e_{13} & e_{23} & Y + e_Y & e_{34} \\ X & e_{24} & e_{34} & e_{44} \end{bmatrix}^{-1} \begin{bmatrix} e_{15} \\ e_{25} \\ e_{35} \\ e_{45} \end{bmatrix}.$$

As the inverse matrix is positive, this gives a lower bound for $Z$, in particular when $X = Y = 0$. Pairwise permutations give lower bounds on $X$ and $Y$. For example, $(ijk) \to (jik)$ gives $D_2^*(X, Y, Z) \to D_2^*(X, Z, Y)$ and provides a lower bound for $Y$. Also, a second lower bound for $Z$ is found from $(ijk) \to (ikj)$, which gives $D_2^*(X, Y, Z) \to D_2^*(Y, X, Z)$, so we must use the larger of the two. When permuting the indices, only three independent minors are found, corresponding to third-degree polynomials in $X$, $Y$, and $Z$, respectively.

The determinant $|\Delta_2^*|$ provides another constraint on the realizability limits for $(X, Y, Z)$:

$$D_3 = \begin{vmatrix} e_{11} & e_{12} & e_{13} & X & e_{15} & Y \\ e_{12} & X + e_X & e_{23} & e_{24} & e_{25} & e_{26} \\ e_{13} & e_{23} & Y + e_Y & e_{34} & e_{35} & e_{36} \\ X & e_{24} & e_{34} & e_{44} & e_{45} & Z \\ e_{15} & e_{25} & e_{35} & e_{45} & Z + e_Z & e_{56} \\ Y & e_{26} & e_{36} & Z & e_{56} & e_{66} \end{vmatrix} = D_2 D_3^* > 0.$$

[30] The roots are assumed to be ordered such that $R_1 \leq R_2 \leq R_3$. If two of the roots are complex for a given $Y$ or $Z$, then no realizable $X$ exists.

Since $D_2 > 0$, we must have $D_3^* > 0$ where

$$D_3^*(X,Y,Z) = e_{66} - \begin{bmatrix} Y \\ e_{26} \\ e_{36} \\ Z \\ e_{56} \end{bmatrix}^t \begin{bmatrix} e_{11} & e_{12} & e_{13} & X & e_{15} \\ e_{12} & X + e_X & e_{23} & e_{24} & e_{25} \\ e_{13} & e_{23} & Y + e_Y & e_{34} & e_{35} \\ X & e_{24} & e_{34} & e_{44} & e_{45} \\ e_{15} & e_{25} & e_{35} & e_{45} & Z + e_Z \end{bmatrix}^{-1} \begin{bmatrix} Y \\ e_{26} \\ e_{36} \\ Z \\ e_{56} \end{bmatrix}$$

and the inverse matrix and $e_{66}$ are positive. This constraint is a third-degree multivariate polynomial in the three variables $(X, Y, Z)$, and is the same for every permutation of the indices. At this point, we have (several) upper/lower bounds for each variable.[31] If these bounds satisfy $D_3^*(X, Y, Z) > 0$, then no further work is required. Otherwise, the realizability limits for $(X, Y, Z)$ must be tightened until $D_3^*(X, Y, Z) > 0$. As in 2D, changes in $(X, Y, Z)$ may affect the bounds on the other fourth-order moments. Thus, an iterative process is employed to ensure all fourth-order moments are realizable for a fixed set of second- and third-order moments.

In summary, for high-speed flows, an essential part of the 3D HyQMOM closure is the realizability-correction algorithm, which checks and corrects the moments to ensure they are realizable. This algorithm takes in the full moment vector $\mathbf{M}_4$ and outputs the realizable moments, overwriting the original moment vector. The algorithm can be applied at any step. Still, the correction is mainly used before computing the eigenvalues of the hyperbolic fluxes and after the moments are updated due to free transport. For low-speed flows, realizability checks are not needed, as all moments in $\mathbf{M}_4$ remain realizable for arbitrary Kn. Alternatively, in Appendix B, a more intrusive but computationally faster method for realizability corrections based on projection is discussed. Such a method is especially attractive for 3D cases with 35 moments because no iterations are required to achieve realizability.

### 5.2. 3D 16-moment extended AG closure

Analogous to the 2D case in Section 3.6, the simplest moment system for simulating 3D high-speed crossing jets uses the following 16 moments:

$$X = \begin{bmatrix} m_{000} & m_{010} & m_{020} & m_{030} & m_{040} & m_{001} & m_{002} & m_{003} & m_{004} & m_{011} \\ m_{100} & m_{110} & & & & m_{101} & & & & \\ m_{200} & & & & & & & & & \\ m_{300} & & & & & & & & & \\ m_{400} & & & & & & & & & \end{bmatrix}, \tag{72}$$

and requires closures for 22 moments:

$$[m_{500}\ m_{410}\ m_{401}\ m_{310}\ m_{301}\ m_{210}\ m_{201}\ m_{140}\ m_{130}\ m_{120}\ m_{111}\ m_{104}\ m_{103}\ m_{102}\ m_{050}\ m_{041}\ m_{031}\ m_{021}\ m_{014}\ m_{013}\ m_{012}\ m_{005}].$$

In terms of the standardized moments, the closures for moments with one or two zero indices are found from the 2D case in Section 3.6. The only moment with three non-zero indices is $m_{111}$, which is closed using

$$s_{111} = \frac{1}{3}(s_{110}s_{101}s_{300} + s_{110}s_{011}s_{030} + s_{101}s_{011}s_{003}). \tag{73}$$

As in the 2D case, the 16-moment system is globally hyperbolic, and the third- and fourth-order moments are always realizable. Nonetheless, for high-speed flows, the second-order moment-correction scheme described in Section 5.1.1 must be used after the transport step to keep $(s_{110}, s_{101}, s_{011})$ realizable (i.e., $S_2 \geq 0$).

In summary, the 16-moment extended AG system is numerically robust for all-speed flows. For low-speed flows, the closures for the third-order moments (e.g., the energy flux) may be too simple for some applications; however, they provide an easy non-zero extension of the AG closure.

### 5.3. 3D fourth-order, 26-moment system

In 3D, the even-index fourth-order moment system corresponding to Section 3.9 uses the following 26 moments:[32]

$$X = \begin{bmatrix} m_{000} & m_{010} & m_{020} & m_{030} & m_{040} & m_{001} & m_{002} & m_{003} & m_{004} & m_{011} & m_{021} & m_{012} & m_{022} \\ m_{100} & m_{110} & m_{120} & & & m_{101} & m_{102} & & & m_{111} & & & \\ m_{200} & m_{210} & m_{220} & & & m_{201} & m_{202} & & & & & & \\ m_{300} & & & & & & & & & & & & \\ m_{400} & & & & & & & & & & & & \end{bmatrix}. \tag{74}$$

[31] As in (20), we use the largest of the lower bounds and the smallest of the upper bounds.

[32] The ordering of the columns is selected to make the Jacobian of the flux in the $x_1$ direction block diagonal.

The remaining nine fourth-order moments with odd indices are closed using

$$s_{211} = s_{011} + s_{300}s_{111}, \quad s_{310} = s_{110}s_{400} + \frac{3}{2}s_{300}(s_{210} - s_{110}s_{300}), \tag{75}$$

and their permutations. The fifth-order moments needed for the fluxes are found as in Section 5.4, but simplified using (75). Like the 2D 13-moment system, the 3D 26-moment system is globally hyperbolic, and therefore no hyperbolicity corrections are required in the numerical algorithm. Moreover, because nine of the fourth-order moments are fixed, checking the remaining moments for realizability is somewhat simpler with the 26-moment system.

### 5.4. 3D fourth-order, 35-moment system

The full 35-moment system includes all fourth-order moments (i.e., $m_{310}$, $m_{211}$ and their permutations):

$$X = \begin{bmatrix} m_{000} & m_{010} & m_{020} & m_{030} & m_{040} & m_{001} & m_{002} & m_{003} & m_{004} & m_{011} & m_{021} & m_{031} & m_{012} & m_{013} & m_{022} \\ m_{100} & m_{110} & m_{120} & m_{130} & & m_{101} & m_{102} & m_{103} & & m_{111} & m_{121} & & m_{112} & & \\ m_{200} & m_{210} & m_{220} & & & m_{201} & m_{202} & & & m_{211} & & & & & \\ m_{300} & m_{310} & & & & m_{301} & & & & & & & & & \\ m_{400} & & & & & & & & & & & & & & \end{bmatrix}, \tag{76}$$

and requires closures for the 21 fifth-order moments:[33]

$$[m_{500}\ m_{410}\ m_{320}\ m_{230}\ m_{140}\ m_{401}\ m_{302}\ m_{203}\ m_{104}\ m_{311}\ m_{221}\ m_{131}\ m_{212}\ m_{113}\ m_{122}\ m_{050}\ m_{041}\ m_{032}\ m_{023}\ m_{014}\ m_{005}].$$

The HyQMOM closures for the ten fifth-order moments with indices containing zero are found by permuting the indices for the 2D closures. For the seven moment indices not including zero, there are two – $m_{311}$ and $m_{221}$ – that are found using the orthogonal polynomials, and the others are found by permuting the indices.

As in 2D, the 3D HyQMOM closures are most cleanly written in terms of the standardized moments:

$$\begin{aligned} s_{311} &= \frac{3}{2}s_{300}s_{211} + \frac{1}{2}(2s_{400} - 3s_{300}^2)s_{111} - \frac{1}{2}s_{300}s_{011}, \\ s_{221} &= s_{300}(s_{121} - s_{101}) + s_{030}(s_{211} - s_{011}) + s_{201} + s_{021} - s_{300}s_{030}s_{111}. \end{aligned} \tag{77}$$

Notice that the first nine columns in (76) involve 2D moments and therefore the Jacobian corresponding to their fluxes will be the same as for the 2D case in Section 3.8. Thus, one needs only to consider the last six columns involving 3D cross moments, which appear linearly in (77). Starting with the column $(m_{011}, m_{111}, m_{211})^t$ with flux $(m_{111}, m_{211}, m_{311})^t$, the diagonal block from the flux Jacobian for direction $x_1$ in terms of the standardized moments is

$$\begin{bmatrix} 0 & 1 & 0 \\ 0 & 0 & 1 \\ -s_{300}/2 & (2s_{400} - 3s_{300}^2)/2 & 3s_{300}/2 \end{bmatrix},$$

whose standardized eigenvalues are the roots of $\mathcal{U}_3(x) = 0$. For the column $(m_{021}, m_{121})^t$ with flux $(m_{121}, m_{221})^t$, the diagonal block is

$$\begin{bmatrix} 0 & 1 \\ 1 & s_{300} \end{bmatrix},$$

whose standardized eigenvalues are the roots of $\mathcal{U}_2(x) = 0$. Likewise, the column $(m_{012}, m_{112})^t$ with flux $(m_{112}, m_{212})^t$ generates standardized eigenvalues that are the roots of $\mathcal{U}_2(x) = 0$. The column $m_{031}$ with flux $m_{131}$ generates a zero root, as do $m_{013}$ and $m_{022}$. Thus, all eigenvalues for the fluxes involving cross moments are real-valued.

In summary, the 35-moment system is hyperbolic if the corresponding 2D moment systems are hyperbolic. In numerical simulations, the latter is assured using the hyperbolicity-correction algorithm developed in Section 3.8. For low-speed flows, the system is always hyperbolic, and the minimum/maximum eigenvalues are found from $R_3$, i.e., from the univariate moments.

### 5.5. Some 2D numerical examples for the 35-moment system

In this section, we employ the same numerical algorithm as in Section 4, but extend it to the 35-moment system in the 2D spatial domain depicted in Fig. 1. For low-speed flows, extending the HLL solver from 15 to 35 variables is straightforward, and neither moment-realizability nor hyperbolicity corrections are needed. For high-speed flows, the main challenge comes in implementing the moment-realizability correction algorithm from Section 5.1.[34] In the 2D spatial domain, only $s_{110}$ can differ meaningfully from zero. Thus, we are restricted to testing only a small part of the second-order realizability domain shown in Fig. 9 (i.e., non-realizable moments arise only near the two edges with $s_{110} = \pm 1$). As in Section 4, we vary the two parameters Ma and Kn over wide ranges to test the robustness of the numerical algorithm for moment-realizability corrections. Example results are shown in Figs. 10 and 11 for Ma = 10 and Kn = 1 at $t = 0.004$, and for several other values of Ma and Kn in the Supplementary Material.

[33] The first fifteen moments correspond to the columns of $X$, and the other six are needed for transport in the other two directions.

[34] This difficult issue can be circumvented by using the projection method in Appendix B.

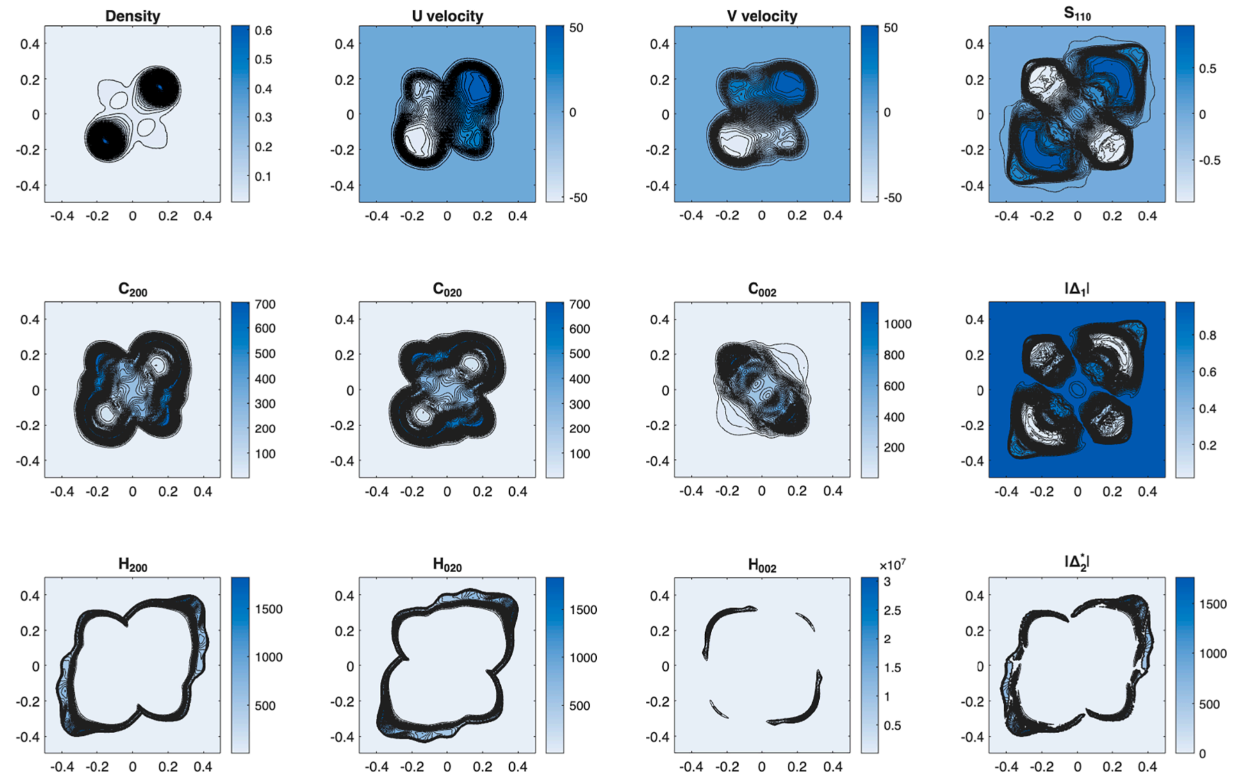


**Fig. 10.** Impinging jets with $\mathrm{Ma} = 70$ and $\mathrm{Kn} = 1$ at $t = 0.004$. Contour plots of lower-order moments. Regions where $|\Delta_1| \approx 0$ correspond to edges with $s_{110} = \pm 1$.

Cases with large Ma and $\mathrm{Kn} = 1$ exhibit complex behavior (more so than without collisions). For example, the weak collisions result in mass moving perpendicular to the mean velocity with a highly non-equilibrium VDF. This can be observed in the density and velocity fields in Fig. 10. The large, non-Maxwellian values of $H_{002}$ and $s_{004}$, as well as the large value of $c_{002}$ as compared to $c_{200}$,[35] are characteristic of weakly collisional crossing jets. The ability of the correction algorithm to ensure realizability is confirmed by the contour plots for the determinants $|\Delta_1|$ and $|\Delta_2^*|$. Indeed, without realizability corrections after transport, locally the third- and fourth-order moments become quickly non-physical once the jets begin to cross. Lastly, it can be observed that the contour plots retain the symmetry of the initial conditions, even under extremely non-equilibrium conditions.

### 5.6. 3D numerical examples for the 35-moment system

We solve the fourth-order, 35-moment HyQMOM system for 3D free transport with BGK collisions on uniform Cartesian meshes over a cubic domain. The hyperbolic solver used to solve these equations is parallelized via an MPI pencil decomposition and conducted in Julia. Spatial discretization is finite-volume with HLL numerical fluxes; fifth-order fluxes in each coordinate use the one-dimensional HyQMOM closure, while cross-moment fluxes employ the multivariate HyQMOM closures derived above. The configuration is discretized in a uniformly spaced $100^3$ 3D grid. Time integration is explicit and subject to a CFL stability constraint, and collisions are incorporated by operator splitting with a BGK relaxation term. After each transport update, a realizability/hyperbolicity enforcement pass ensures positivity of the multivariate moment matrices ($\Delta_1$, $\Delta_2^*$) and real, distinct eigenvalues in the $6 \times 6$ cross-moment block, applying minimal, local corrections only when necessary (typically at high Ma). This framework yields robust wave-speed bounds drawn from both the 1D characteristic polynomial and the cross-moment block, and is applied uniformly in all three spatial directions.

The 3D test problems consist of symmetric crossing jet configurations initialized as two equal-density cubic jets embedded in a uniform, quiescent background. The background density is lower than the jet density, the temperature is uniform, and initial cross-correlations are set to zero. Each jet occupies a small cubic subregion (a fixed fraction of the domain length in each direction), displaced symmetrically from the domain center, and carries a diagonal velocity directed along opposite space diagonals so that the jets approach and interact near the domain center; the diagonal speed is chosen to achieve a prescribed jet Mach number. We explore a broad range of Mach and Knudsen numbers on uniform meshes, monitoring standardized and central moments, as well as realizability

[35] In the weakly collisional regime, the relative values of $c_{002}$ and $c_{200}$ may be sensitive to the collision model (e.g., BGK versus hard-sphere model).

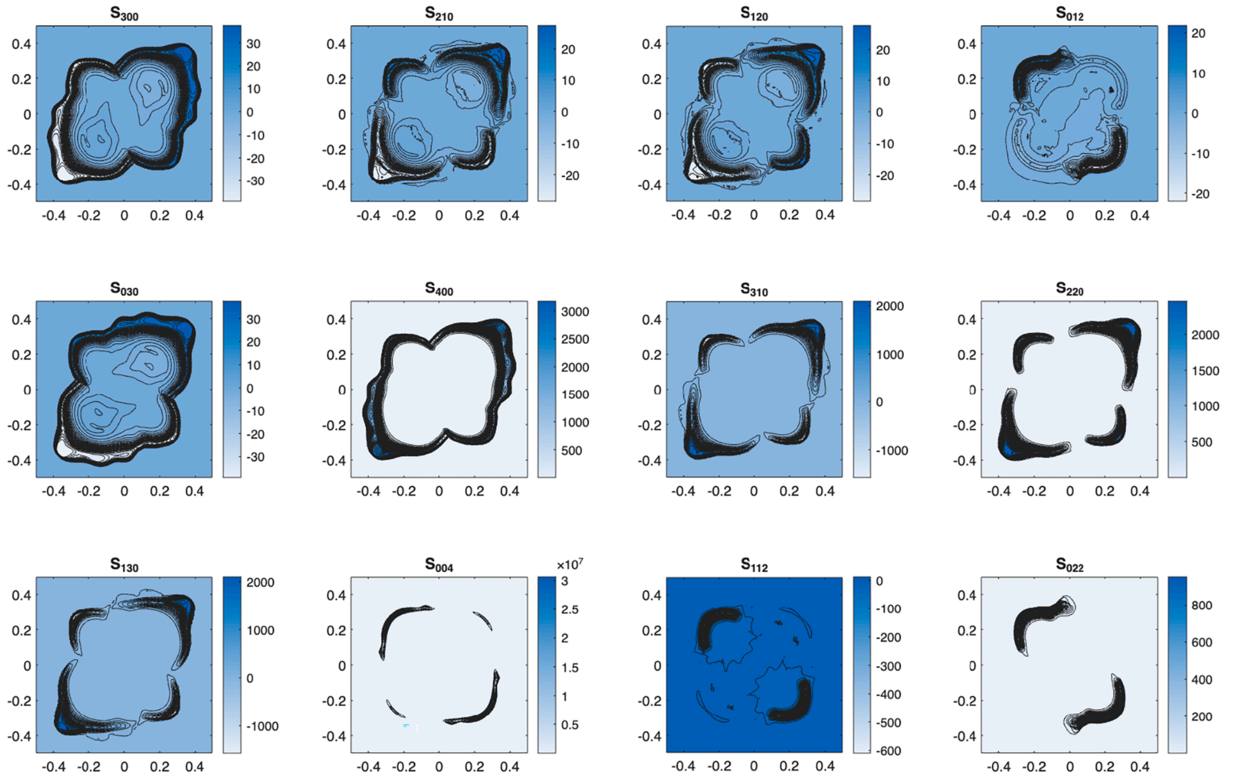


**Fig. 11.** Impinging jets with Ma = 70 and Kn = 1 at $t = 0.004$. Contour plots of standardized moments. The perpendicular-oriented high values of $s_{004}$, $s_{022}$, etc. will correspond to toroidal surfaces in 3D jets.

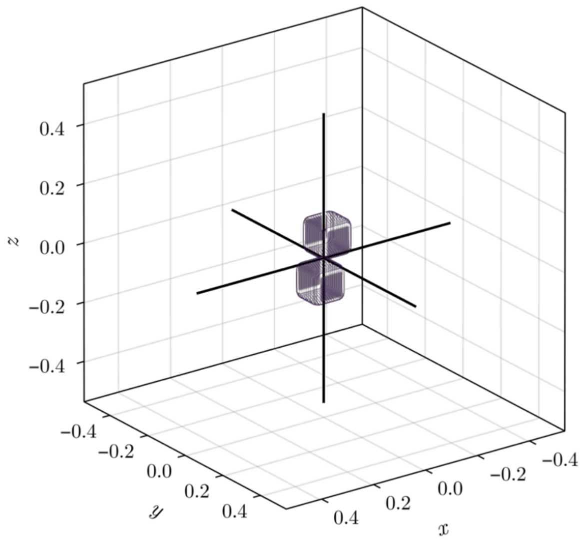


**Fig. 12.** Initial condition for density with 3D jets. Inside the two cubes $\rho = 1$, while outside $\rho = 0.01$. For Ma = 3, the velocity of the cubes is pointed towards the center (i.e., direction vectors (−1,−1,1) and (1,1,−1)) and null otherwise. All other initial conditions are the same as in 2D.

diagnostics. The closures, realizability constraints, and hyperbolicity conditions used here are exactly those developed in the preceding sections (with details for 3D moment matrices and bounds in Sections 5.1 to 5.4 and Appendix D), and the implementation follows these specifications without further modeling assumptions.

For the fully 3D simulation, we employ the initial conditions shown in Fig. 12, which are identical to those in 2D but with two cubic high-density regions positioned off-axis. The initial velocities (magnitude Ma) are fixed such that the cubes cross at the center of the computational domain for large Kn. For this configuration, the second-order moments can approach the faces and corners of

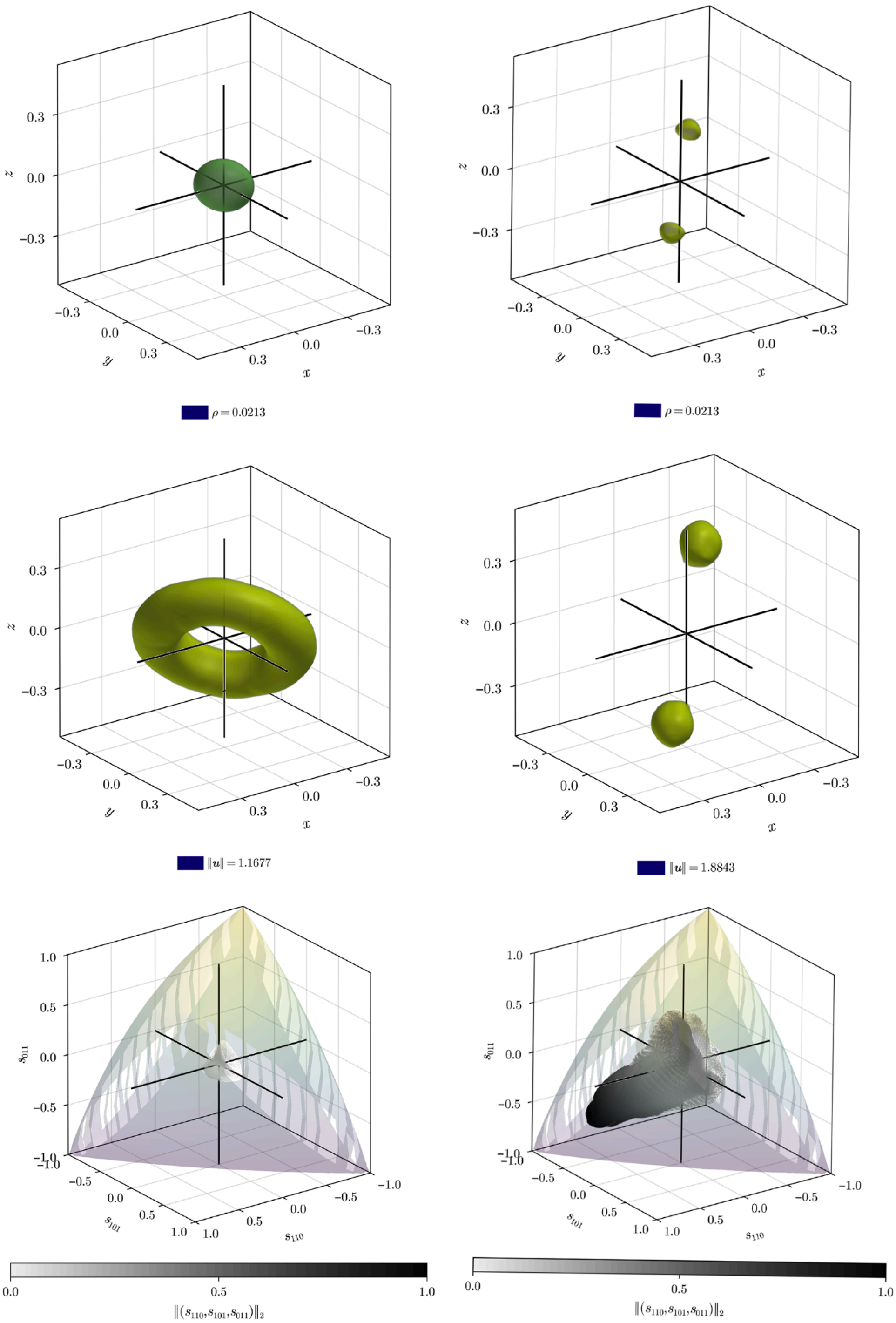


**Fig. 13.** 3D jets with $\mathrm{Ma} = 3$ at $t = 0.015$. Left column: $\mathrm{Kn} = 0.001$ (impinging jets). Right column: $\mathrm{Kn} = 1$ (crossing jets). Top row: density $m_{000}$. Center row: velocity magnitude. Bottom row: scatter plot for second-order moments showing the realizability surface.

the realizability region, as shown in Fig. 9. For large Ma, the 3D crossing jet has $(s_{110}, s_{101}, s_{011}) = (1, -1, -1)$ and thus for smaller Ma we expect to observe second-order moments skewed towards this point. As in 2D, the symmetry properties of the initial conditions will be retained at later times, which is useful for verifying the numerical algorithm. Indeed, any asymmetry in the algorithm for the spatial fluxes quickly leads to a loss of spatial symmetry.

As found in 2D, the 3D simulations for larger Ma, non-realizability of the second-order moments was not observed in our test cases. For example, for $\mathrm{Ma} = 3$ shown in Fig. 13 for $\mathrm{Kn} = 0.001$ and $\mathrm{Kn} = 1$, the scatter plots for the second-order moments stay well within the realizability surface. As expected, for small Kn the second-order moments are near zero, while for larger Kn they are pulled towards the 3D crossing-jet values. Note that the density and velocity-magnitude plots in Fig. 13 exhibit the expected Kn dependence (i.e., impinging vs. crossing jets). Interestingly, the impinging jets create a high-pressure region near the origin, which accelerates the fluid perpendicularly from the collision axis, resulting in a torus-like distribution of the velocity magnitude. Results for other values of Ma are included in the Supplementary Material. Generally speaking, the projection method in Appendix B is more robust and faster for large-Ma cases with only negligible differences in the lower-order moments as compared to checking the leading principal minors.

## 6. Conclusions

In this work, a multivariate, fourth-order moment closure based on 1D HyQMOM has been proposed for the free-transport term in the multivariate kinetic equation. As in the 1D case, the multivariate closures for the odd-order moments $\mathbf{M}_{2n+1}$ given the even-order moments $\mathbf{M}_{2n}$ are found from the orthogonal polynomials $Q_n(x)$ of degree $n$, which depend on the standardized univariate moments in a given direction. Using orthogonality, i.e., $\langle \mathcal{U}_i \mathcal{V}_j \mathcal{W}_k \rangle = 0$ with $i + j + k = 2n + 1$, provides a closure for $s_{ijk}$ with order $2n + 1$. By construction, the closures for the univariate moments are the same as for 1D HyQMOM, while the cross moments of orders up to $2n$ appear linearly. In principle, this procedure can be applied for larger $n$; however, in 3D, the number of moments in $\mathbf{M}_{2n}$ increases rapidly with $n$. Thus, here we have used $n = 2$ and focused on two important aspects of any moment closure: moment realizability and the hyperbolicity of the moment system when applied to the free-transport term of the kinetic equation. These properties are found to depend on whether the flow is low or high speed, as defined by the Mach number, but are independent of the Knudsen number.

*Moment realizability for low-speed flows.* For low-speed flows where the shock and/or jet Mach numbers are much smaller than unity, the moments after free transport remain realizable for arbitrary Knudsen numbers. The same behavior was found for 1D HyQMOM [12]. Thus, for low-speed flows, the moment-correction algorithm need not be implemented, which greatly facilitates the extension to larger $n$. As shown using 1D HyQMOM [12] for high-speed flows, the accuracy of the closure for large Kn increases with increasing $n$. We would thus expect to observe similar behavior for low-speed flows. On the other hand, the approximation for the collision term is likely to be of greater importance for such flows [24]. For this purpose, the Grad-HyQMOM approximation of the multivariate VDF [21] using tensor-product 1D quadrature (see Appendix C) may prove useful (e.g., for treating hard-sphere collisions in lieu of BGK). Likewise, low-speed flows in micro/nanopores will require boundary conditions at the walls that are consistent with the underlying VDF [11,52].

*Global hyperbolicity for low-speed flows.* For low-speed flows, the eigenvalues associated with free transport remain close to the roots of the 1D orthogonal polynomial $R_3$. Thus, if the initial VDF has realizable moments inside the boundary of moment space, then the moment system remains globally hyperbolic for all Kn. For small Mach numbers, it is not necessary to find the eigenvalues of the flux Jacobian at each time step and location, as they can be estimated from the initial conditions. In any case, as in 1D HyQMOM, knowing the roots of $R_{n+1}$ suffices to calculate the HLL fluxes for any $n$.

*Moment realizability for high-speed flows.* If the shock or jet Mach number is sufficiently large, the free-transport term with the multivariate HyQMOM closures will produce locally non-realizable moments. To simulate such flows, the 2D or 3D moment-correction algorithms must be applied after the free-transport step. For supersonic flows with moderate Mach numbers, non-realizable moments occur near the edges of shocks and typically involve fourth-order moments. Theoretically, for hypersonic flows, such as high-Mach crossing jets, the second-order moments can also become non-realizable. Fortunately, for the fourth-order moment system, at least, enforcing moment realizability is achievable by using the leading principal minors of the moment matrices (i.e., Sylvester's criterion), or moment projection (see Appendix B). However, for larger $n$, the sizes of the moment matrices may make using the leading principal minors computationally intractable. In any case, the value of the Knudsen number at fixed Mach numbers is not an important factor. Indeed, collisionless flows typically have fewer non-realizable moments compared to $\mathrm{Kn} = 1$.

*Global hyperbolicity for high-speed flows.* For high-speed flows, the eigenvalues can vary widely over the computational domain. However, only the $6 \times 6$ block involving 2D moments can have complex eigenvalues. Moreover, even when they are real-valued, the magnitude of some of these eigenvalues can be larger than the three roots of $R_3$. Thus, it is necessary to compute the six eigenvalues at each location to define the HLL fluxes at each time step. When complex eigenvalues for the $6 \times 6$ block are detected, the moments are corrected according to (42). From the high-jet Ma cases, complex eigenvalues typically occur locally at the edges of shock waves as they expand into undisturbed regions with very low density. In this manner, the moment system can be made globally hyperbolic with minimal moment corrections. Interestingly, for the fourth-order moment system, the hyperbolicity correction in 3D is identical to that in 2D. Nevertheless, the results for 3D systems are generally different than those for 2D because the spatial fluxes generate correlations in the third- and fourth-order cross moments that are not present in the 2D moment system.

In summary, the fourth-order HyQMOM closure developed in this work provides robust closures for the fifth-order spatial fluxes in the moment system for $\mathbf{M}_4$ found from multivariate kinetic equations. In principle, the method can be easily extended to higher-order moments; however, realizability constraints and boundary conditions will become more challenging to implement for larger moment sets. In its current form, the fourth-order HyQMOM closure provides a robust simulation tool for arbitrary Knudsen and Mach numbers. Future work is needed to validate the accuracy of the predictions by comparing them with, for example, direct simulation Monte Carlo

(DSMC) [10,11,22,53] or even direct simulation of the Boltzmann kinetic equation [54,55]. Another topic worthy of investigation is the use of the exact multivariate orthogonal polynomials [30,31], in place of the tensor-product form used in this work, to define multivariate HyQMOM (see Appendix A). In theory, such closures could eliminate the need for the moment-correction algorithm for high-speed flows. From a numerical perspective, it would be useful to implement high-order spatial reconstruction schemes to reduce numerical diffusion in the HLL solver [51], and to develop more accurate hyperbolic solvers for the 35-moment system. Finally, boundary conditions for the moments can be developed as in Bünger et al. [52] using the Grad-HyQMOM approximation of the VDF in Appendix C.

## CRediT authorship contribution statement

**Spencer H. Bryngelson:** Writing – review & editing, Writing – original draft, Visualization, Software, Resources, Methodology; **Rodney O. Fox:** Writing – review & editing, Writing – original draft, Supervision, Software, Methodology, Formal analysis, Conceptualization; **Frédérique Laurent:** Writing – review & editing, Software, Methodology, Conceptualization.

## Declaration of competing interest

The authors declare that they have no known competing financial interests or personal relationships that could have appeared to influence the work reported in this paper.


## Acknowledgments

This work used computing resource Delta at the National Center for Supercomputing Applications through allocation PHY210084 and PHY240200 (PI Bryngelson) from the Advanced Cyberinfrastructure Coordination Ecosystem: Services & Support (ACCESS) program, which is supported by National Science Foundation grants #2138259, #2138286, #2138307, #2137603, and #2138296.


## Data availability

No data was used for the research described in the article.

## Supplementary material

Supplementary material associated with this article can be found in the online version at 10.1016/j.jcp.2026.115242.

## Appendix A. 2D orthogonal polynomials and moment closures

The moment closures used in the main text are based on 1D orthogonal polynomials. Here, we briefly introduce the 2D orthogonal polynomials [31] and propose a possible pathway for using them for moment closure.

### A.1. 2D orthogonal polynomials

Theorem 2.7 in Krall and Sheffer [31] provides a formula for the 2D orthogonal polynomials of degree $i + j = n$, denoted by $P_{i,j}(u, v)$, in terms of the standardized moment matrices in (12). Up to degree $n = 2$, we have $P_{0,0} = 1$, $P_{1,0} = u$, $P_{0,1} = v$, and

$$\begin{aligned}
P_{2,0} &= |\Delta_1|(u^2 - 1) && + \ (s_{11}s_{21} - s_{30})u + (s_{11}s_{30} - s_{21})v, \\
P_{1,1} &= |\Delta_1|(uv - s_{11}) && + \ (s_{11}s_{12} - s_{21})u + (s_{11}s_{21} - s_{12})v, \\
P_{0,2} &= |\Delta_1|(v^2 - 1) && + \ (s_{11}s_{03} - s_{12})u + (s_{11}s_{12} - s_{03})v,
\end{aligned} \tag{A.1}$$

where $|\Delta_1| = 1 - s_{11}^2 > 0$. Two polynomials with different degrees are orthogonal, e.g., $\langle P_{0,1}P_{1,1}\rangle = 0$. In contrast, for the same degree, the polynomials form a non-orthogonal basis [31] for a vector space:

$$\mathbf{p}_0 := [P_{0,0}], \quad \mathbf{p}_1 := \begin{bmatrix} P_{1,0} \\ P_{0,1} \end{bmatrix}, \quad \mathbf{p}_2 := \begin{bmatrix} P_{2,0} \\ P_{1,1} \\ P_{0,2} \end{bmatrix} = |\Delta_1| \begin{bmatrix} u^2 - 1 \\ uv - s_{11} \\ v^2 - 1 \end{bmatrix} + \mathbf{R}_2 \begin{bmatrix} u \\ v \end{bmatrix} \ \text{with} \ \mathbf{R}_2 = \begin{bmatrix} s_{11}s_{21} - s_{30} & s_{11}s_{30} - s_{21} \\ s_{11}s_{12} - s_{21} & s_{11}s_{21} - s_{12} \\ s_{11}s_{03} - s_{12} & s_{11}s_{12} - s_{03} \end{bmatrix} \tag{A.2}$$

where $\mathbf{R}_2$ depends on moments up to third order. The vector of monic polynomials is $\hat{\mathbf{p}}_n = \mathbf{p}_n/|\Delta_1|$. Here, we mainly work with $\mathbf{p}_n$ whose coefficients are multivariate polynomials of the standardized moments.

### A.1.1. Moment matrices

In general, $\langle \mathbf{p}_k \mathbf{p}_k^t \rangle$ is a $(k+1)\times(k+1)$ positive, symmetric, moment matrix that depends on the standardized moments up to order $2k$. Moreover, the components of $\langle \mathbf{p}_k \mathbf{p}_k^t \rangle$ are multivariate polynomials of these moments. In particular, we have

$$\langle \mathbf{p}_0 \mathbf{p}_0^t \rangle = 1, \quad \langle \mathbf{p}_1 \mathbf{p}_1^t \rangle = \begin{bmatrix} 1 & s_{11} \\ s_{11} & 1 \end{bmatrix}, \quad \langle \mathbf{p}_2 \mathbf{p}_2^t \rangle = |\Delta_1|^2 \Delta_2^* = |\Delta_1|^2 \mathbf{R}_4 + |\Delta_1| \mathbf{R}_3 + \mathbf{R}_2 \langle \mathbf{p}_1 \mathbf{p}_1^t \rangle \mathbf{R}_2^t \tag{A.3}$$

where the positive matrix $\Delta_2^*$ is defined in (13). The other matrices are defined by

$$\mathbf{R}_3 = \begin{bmatrix} s_{30} & s_{21} \\ s_{21} & s_{12} \\ s_{12} & s_{03} \end{bmatrix} \mathbf{R}_2^t + \mathbf{R}_2 \begin{bmatrix} s_{30} & s_{21} & s_{12} \\ s_{21} & s_{12} & s_{03} \end{bmatrix}, \quad \mathbf{R}_4 = \mathbf{S}_4 - \mathbf{R}_1 \text{ with } \mathbf{S}_4 = \begin{bmatrix} s_{40} & s_{31} & s_{22} \\ s_{31} & s_{22} & s_{13} \\ s_{22} & s_{13} & s_{04} \end{bmatrix}, \ \mathbf{R}_1 = \begin{bmatrix} 1 & s_{11} & 1 \\ s_{11} & s_{11}^2 & s_{11} \\ 1 & s_{11} & 1 \end{bmatrix}$$

where $\mathbf{R}_3$ depends on moments up to third order and $\mathbf{S}_4$ is the fourth-order moment matrix.

It is worth noting that (A.3) provides a closure for $\mathbf{S}_4$. For example, let $\langle \mathbf{p}_2 \mathbf{p}_2^t \rangle_G$ correspond to the anisotropic Gaussian VDF (i.e., $\mathbf{R}_2$ and $\mathbf{R}_3$ are zero, $s_{40} = s_{04} = 3$, etc.). Then, a closure for the fourth-order moments can be found from

$$\langle \mathbf{p}_2 \mathbf{p}_2^t \rangle = \langle \mathbf{p}_2 \mathbf{p}_2^t \rangle_G. \tag{A.4}$$

By construction, this closure is realizable for the limits $s_{11} = 0$ and $s_{11}^2 = 1$. Moreover, since $|\langle \mathbf{p}_2 \mathbf{p}_2^t \rangle|$ is rotationally invariant, then so should be $\mathbf{S}_4$. It thus remains to determine whether the closure is globally hyperbolic. Because $|\langle \mathbf{p}_2 \mathbf{p}_2^t \rangle_G| > 0$, a shortcoming of this closure is its inability to capture correctly jet crossing where $|\langle \mathbf{p}_2 \mathbf{p}_2^t \rangle| = 0$.

### A.1.2. Limiting behavior for $n = 2$

Recall that $|\langle \hat{\mathbf{p}}_2 \hat{\mathbf{p}}_2^t \rangle| = |\Delta_2^*|$ is positive and is a multivariate polynomial in the moments up to fourth order. Thus, unlike the approximation of the multivariate orthogonal polynomials used in the main text,[36] the realizability constraints are contained in the definition (A.1). This implies that the 2D orthogonal polynomials are well defined at the edge of moment space where $|\Delta_2^*| \to 0$. Indeed, for the crossing jets where $|\Delta_1| \to 0$, the coefficients of the linear terms in (A.1) degenerate to the 1D orthogonal polynomial with $v = s_{11} u$. We refer to this limit as *perfectly correlated* where the various matrices become

$$\mathbf{R}_2 \to -|\Delta_1| s_{30} \begin{bmatrix} 1 & 0 \\ \sigma & 0 \\ 1 & 0 \end{bmatrix}, \ \mathbf{R}_2 \langle \mathbf{p}_1 \mathbf{p}_1^t \rangle \mathbf{R}_2^t \to |\Delta_1|^2 s_{30}^2 \mathbf{R}_1, \ \mathbf{R}_3 \to -|\Delta_1| 2 s_{30}^2 \mathbf{R}_1, \ \mathbf{R}_4 \to (s_{40} - 1)\mathbf{R}_1, \ \mathbf{R}_1 \to \begin{bmatrix} 1 & \sigma & 1 \\ \sigma & 1 & \sigma \\ 1 & \sigma & 1 \end{bmatrix}$$

such that $\langle \hat{\mathbf{p}}_2 \hat{\mathbf{p}}_2^t \rangle \to H_{20} \mathbf{R}_1$ where $H_{20} = s_{40} - s_{30}^2 - 1 > 0$ and $\sigma$ is the sign of $s_{11}$. Likewise, in the limit of *independent variables*, we have $|\Delta_1| = 1$ and

$$\langle \mathbf{p}_2 \mathbf{p}_2^t \rangle \to |\Delta_1|^2 \begin{bmatrix} H_{20} & 0 & 0 \\ 0 & 1 & 0 \\ 0 & 0 & H_{02} \end{bmatrix}$$

where $H_{02} = s_{04} - s_{03}^2 - 1 > 0$. It is worth noting that the scaled matrix $\langle \hat{\mathbf{p}}_2 \hat{\mathbf{p}}_2^t \rangle$ is non-negative and finite in both limits.

## A.2. Moment closures

In analogy with 1D HyQMOM, we seek closures for the standardized moments of order $2n+1$ for $n > 0$ of the form

$$\alpha_n^u := \langle u \mathbf{p}_n \mathbf{p}_n^t \rangle = \hat{\alpha}_n^u \langle \mathbf{p}_n \mathbf{p}_n^t \rangle, \quad \alpha_n^v := \langle v \mathbf{p}_n \mathbf{p}_n^t \rangle = \hat{\alpha}_n^v \langle \mathbf{p}_n \mathbf{p}_n^t \rangle \tag{A.5}$$

where the matrices $\alpha_n^u$ and $\alpha_n^v$ are symmetric. Here, $\hat{\alpha}_n^u$ and $\hat{\alpha}_n^v$ are matrices of size $(n+1)\times(n+1)$ whose components are multivariate polynomials in the moments up to fourth order. Let $a_n^u$ and $a_n^v$ be the 1D HyQMOM closures [28], e.g., for $n = 2$, $(a_2^u, a_1^u, a_0^u) = (s_{30}/2, s_{30}, 0)$ and $(a_0^v, a_1^v, a_2^v) = (0, s_{03}, s_{03}/2)$. For arbitrary $n > 0$, and for independent variables with $|\Delta_1| = 1$, the coefficient matrices will have the following values:

$$\hat{\alpha}_n^u = \mathrm{diag}(0, \ a_{n-1}^u - a_n^u, \ \cdots \ a_0^u - a_n^u), \quad \hat{\alpha}_n^v = \mathrm{diag}(a_0^u - a_n^v, \ \cdots \ a_{n-1}^v - a_n^v, \ 0). \tag{A.6}$$

In the perfectly correlated limit, we will have $(\hat{\alpha}_n^u, \hat{\alpha}_n^v) = \mathbf{0}$. Note that these matrices are invariant under a change of variables (e.g., reflections and rotations).

Evaluating $\langle u \mathbf{p}_2 \mathbf{p}_2^t \rangle$ and $\langle v \mathbf{p}_2 \mathbf{p}_2^t \rangle$, starting from the definition of $\mathbf{p}_2$ in (A.3), we find

$$\mathbf{S}_5^u = \hat{\alpha}_2^u \langle \hat{\mathbf{p}}_2 \hat{\mathbf{p}}_2^t \rangle + \mathbf{R}_5^u, \quad \mathbf{S}_5^v = \hat{\alpha}_2^v \langle \hat{\mathbf{p}}_2 \hat{\mathbf{p}}_2^t \rangle + \mathbf{R}_5^v \tag{A.7}$$

where the fifth-order moment matrices are

$$\mathbf{S}_5^u = \begin{bmatrix} s_{50} & s_{41} & s_{32} \\ s_{41} & s_{32} & s_{23} \\ s_{32} & s_{23} & s_{14} \end{bmatrix}, \quad \mathbf{S}_5^v = \begin{bmatrix} s_{41} & s_{32} & s_{23} \\ s_{32} & s_{23} & s_{14} \\ s_{23} & s_{14} & s_{05} \end{bmatrix}.$$

[36] In the main text, the 2D polynomials correspond to (A.1) with $(s_{11}, s_{21}, s_{12}) = 0$.

The components of the symmetric matrices $\mathbf{R}_5^u$ and $\mathbf{R}_5^v$ are multivariate polynomials depending on the moments up to fourth order. For example,

$$\mathbf{R}_5^u = a_2^u\langle\hat{\mathbf{p}}_2\hat{\mathbf{p}}_2^t\rangle + \mathbf{R}_3^u - \frac{1}{|\Delta_1|}(\mathbf{R}_2^u\mathbf{R}_2^t + \mathbf{R}_2\mathbf{R}_2^{ut}) - \frac{1}{|\Delta_1|^2}\mathbf{R}_2\mathbf{R}_1^u\mathbf{R}_2^t \tag{A.8}$$

where $a_2^u = \frac{1}{2}s_{30}$ is the 1D HyQMOM closure,

$$\mathbf{R}_3^u = \begin{bmatrix} 2s_{30} & s_{11}s_{30}+s_{21} & s_{30}+s_{12} \\ s_{11}s_{30}+s_{21} & 2s_{11}s_{21} & s_{11}s_{12}+s_{21} \\ s_{30}+s_{12} & s_{11}s_{12}+s_{21} & 2s_{12} \end{bmatrix}, \quad \mathbf{R}_2^u = \begin{bmatrix} s_{40}-1 & s_{31}-s_{11} \\ s_{31}-s_{11} & s_{22}-s_{11}^2 \\ s_{22}-1 & s_{13}-s_{11} \end{bmatrix}, \text{ and } \mathbf{R}_1^u = \begin{bmatrix} s_{30} & s_{21} \\ s_{21} & s_{12} \end{bmatrix}.$$

The expression for $\mathbf{R}_5^v$ can be found by permuting the indices. It is worth noting that $|\Delta_1|^2\mathbf{R}_5^u$ is a multivariate polynomial in the standardized moments up to fourth order. As shown below, the inclusion of the term involving $a_2^u$ in (A.8) ensures that in the perfectly correlated limit, we have $(\hat{\alpha}_2^u, \hat{\alpha}_2^v) \to \mathbf{0}$.

### A.2.1. *Limiting behavior of moment matrices for $n = 2$*

In the independent-variables limit, the fifth-order moment matrices approach

$$\mathbf{S}_5^u \to \begin{bmatrix} s_{50} & 0 & s_{30} \\ 0 & s_{30} & s_{03} \\ s_{30} & s_{03} & 0 \end{bmatrix}, \quad \mathbf{S}_5^v = \begin{bmatrix} 0 & s_{30} & s_{03} \\ s_{30} & s_{03} & 0 \\ s_{03} & 0 & s_{05} \end{bmatrix};$$

In this limit, the other matrices become

$$\mathbf{R}_3^u = \begin{bmatrix} 2s_{30} & 0 & s_{30} \\ 0 & 0 & 0 \\ s_{30} & 0 & 0 \end{bmatrix}, \quad \mathbf{R}_2^u = \begin{bmatrix} s_{40}-1 & 0 \\ 0 & 1 \\ 0 & 0 \end{bmatrix}, \quad \mathbf{R}_1^u = \begin{bmatrix} s_{30} & 0 \\ 0 & 0 \end{bmatrix}.$$

Thus, the matrices $\mathbf{R}_5^u$ and $\mathbf{R}_5^v$ approach the following limits:

$$\lim_{|\Delta_1|\to 1}\mathbf{R}_5^u \to \frac{1}{2}s_{30}\begin{bmatrix} H_{20} & 0 & 0 \\ 0 & 1 & 0 \\ 0 & 0 & H_{02} \end{bmatrix} + \begin{bmatrix} s_{30}(2s_{40}-s_{30}^2) & 0 & s_{30} \\ 0 & 0 & s_{03} \\ s_{30} & s_{03} & 0 \end{bmatrix} = \frac{1}{2}\begin{bmatrix} 2s_{50} & 0 & 2s_{30} \\ 0 & s_{30} & 2s_{03} \\ 2s_{30} & 2s_{03} & s_{30}H_{02} \end{bmatrix},$$

$$\lim_{|\Delta_1|\to 1}\mathbf{R}_5^v \to \frac{1}{2}s_{03}\begin{bmatrix} H_{20} & 0 & 0 \\ 0 & 1 & 0 \\ 0 & 0 & H_{02} \end{bmatrix} + \begin{bmatrix} 0 & s_{30} & s_{03} \\ s_{30} & 0 & 0 \\ s_{03} & 0 & s_{03}(2s_{04}-s_{03}^2) \end{bmatrix} = \frac{1}{2}\begin{bmatrix} s_{03}H_{20} & 2s_{30} & 2s_{03} \\ 2s_{30} & s_{03} & 0 \\ 2s_{03} & 0 & 2s_{05} \end{bmatrix}.$$

Hence, for this limit, the closures for $\hat{\alpha}_2^u$ and $\hat{\alpha}_2^v$ are given in (A.6).

Recall that in the limit $|\Delta_1| \to 0$, the ratio $\mathbf{R}_2/|\Delta_1|$ is finite. The other matrices in the perfectly correlated limit are

$$a_2^u\langle\hat{\mathbf{p}}_2\hat{\mathbf{p}}_2^t\rangle \to \frac{1}{2}s_{30}H_{20}\mathbf{R}_1, \quad \mathbf{R}_3^u \to 2s_{30}\mathbf{R}_1, \quad \mathbf{R}_2^u = (s_{40}-1)\begin{bmatrix} 1 & \sigma \\ \sigma & 1 \\ 1 & \sigma \end{bmatrix}, \quad \mathbf{R}_1^u = s_{30}\begin{bmatrix} 1 & \sigma \\ \sigma & 1 \end{bmatrix};$$

so that $\mathbf{R}_5^u \to s_{50}\mathbf{R}_1$ and $\mathbf{R}_5^v \to s_{05}\mathbf{R}_1$. Thus, the moment matrices go to $\mathbf{S}_5^u \to s_{50}\mathbf{R}_1$ and $\mathbf{S}_5^v \to s_{05}\mathbf{R}_1$ with $s_{05} = \sigma s_{50}$ where $(s_{50}, s_{05})$ are found from 1D HyQMOM. As shown above, $\langle\hat{\mathbf{p}}_2\hat{\mathbf{p}}_2^t\rangle$ is non-negative and finite in the perfectly correlated and independent variable limits. Thus, by construction, in the perfectly correlated limit both $\hat{\alpha}_2^u$ and $\hat{\alpha}_2^v$ are zero.

### A.2.2. *Symmetry and commutativity conditions*

From (A.5), we observe that the components of $\hat{\alpha}_n^u$ and $\hat{\alpha}_n^v$ must satisfy a *symmetry condition*:

$$\hat{\alpha}_n^u\langle\mathbf{p}_n\mathbf{p}_n^t\rangle = \langle\mathbf{p}_n\mathbf{p}_n^t\rangle\hat{\alpha}_n^{ut}, \quad \hat{\alpha}_n^v\langle\mathbf{p}_n\mathbf{p}_n^t\rangle = \langle\mathbf{p}_n\mathbf{p}_n^t\rangle\hat{\alpha}_n^{vt}. \tag{A.9}$$

For $n = 2$, each matrix has six elements for which each symmetry condition provides three constraints. Six other constraints on the unknown components are found from the following *commutativity condition* [30]:

$$\beta_{n-1}^u\langle\mathbf{p}_n\mathbf{p}_n^t\rangle^{-1}\alpha_n^v + \alpha_{n-1}^u\langle\mathbf{p}_{n-1}\mathbf{p}_{n-1}^t\rangle^{-1}\beta_{n-1}^v = \beta_{n-1}^v\langle\mathbf{p}_n\mathbf{p}_n^t\rangle^{-1}\alpha_n^u + \alpha_{n-1}^v\langle\mathbf{p}_{n-1}\mathbf{p}_{n-1}^t\rangle^{-1}\beta_{n-1}^u \tag{A.10}$$

where the positive, $n \times (n+1)$ matrices $\beta_{n-1}^u$ and $\beta_{n-1}^v$ are defined for $n > 0$ by

$$\beta_{n-1}^u := \langle u\mathbf{p}_{n-1}\mathbf{p}_n^t\rangle = \hat{\beta}_{n-1}^u\langle\mathbf{p}_n\mathbf{p}_n^t\rangle, \quad \beta_{n-1}^v := \langle v\mathbf{p}_{n-1}\mathbf{p}_n^t\rangle = \hat{\beta}_{n-1}^v\langle\mathbf{p}_n\mathbf{p}_n^t\rangle. \tag{A.11}$$

Thus, these coefficients are multivariable polynomials in the standardized moments up to order $2n$.

For example, we have $\hat{\beta}_1^u = [\mathbf{I}_2 \ \ \mathbf{0}]$ and $\hat{\beta}_1^v = [\mathbf{0} \ \ \mathbf{I}_2]$ and hence the commutativity condition relating $\hat{\alpha}_2^u$ and $\hat{\alpha}_2^v$ is

$$[\mathbf{I}_2 \ \ \mathbf{0}]\hat{\alpha}_2^v - [\mathbf{0} \ \ \mathbf{I}_2]\hat{\alpha}_2^u = |\langle\mathbf{p}_1\mathbf{p}_1^t\rangle|\hat{\alpha}_1^v[\mathbf{I}_2 \ \ \mathbf{0}] - |\langle\mathbf{p}_1\mathbf{p}_1^t\rangle|\hat{\alpha}_1^u[\mathbf{0} \ \ \mathbf{I}_2] = \mathbf{C} \tag{A.12}$$

where

$$|\langle\mathbf{p}_1\mathbf{p}_1^t\rangle|\hat{\alpha}_1^u = \begin{bmatrix} s_{30}-s_{11}s_{21} & s_{21}-s_{11}s_{30} \\ s_{21}-s_{11}s_{12} & s_{12}-s_{11}s_{21} \end{bmatrix}, \quad |\langle\mathbf{p}_1\mathbf{p}_1^t\rangle|\hat{\alpha}_1^v = \begin{bmatrix} s_{21}-s_{11}s_{12} & s_{12}-s_{11}s_{03} \\ s_{12}-s_{11}s_{21} & s_{03}-s_{11}s_{12} \end{bmatrix},$$

and

$$\mathbf{C} = \begin{bmatrix} s_{21} - s_{11}s_{12} & s_{12} - s_{30} & s_{11}s_{30} - s_{21} \\ s_{12} - s_{11}s_{03} & s_{03} - s_{21} & s_{11}s_{21} - s_{03} \end{bmatrix}.$$

This condition provides six constraints on the elements of $\hat{\alpha}_2^u$ and $\hat{\alpha}_2^v$. The commutativity condition ensures that the fifth-order moments found from the two expressions in (A.7) are the same. Thus, only six elements remain undetermined, leaving at most three unknowns since the other three can be found by permutation of the moment indices. These unknowns must yield the correct limiting behaviors for the fifth-order moment matrices. For the following, it is worth noting that $\mathbf{C}$ depends only on moments up to third order.

### *A.3. Fifth-order moment closures*

From (A.7), it is clear that the closures for $\mathbf{S}_5^u$ and $\hat{\alpha}_2^u$ cannot be chosen independently. For the moment system found from the kinetic equation, we would like $\mathbf{S}_5^u$ to have certain properties, for example, a flux Jacobian with real eigenvalues. Moreover, we would like $\hat{\alpha}_2^u$ to be invariant under rotation of the 2D standardized velocity vector. Here, we will define closures for $\hat{\alpha}_2^u$ starting from (A.7). First, however, we will demonstrate that only the diagonal components of $\hat{\alpha}_2^u$ must be closed.

#### *A.3.1. Application of symmetry and commutativity*

Let $\hat{\alpha}_2^u = [u_{ij}]$, $\hat{\alpha}_2^v = [v_{ij}]$, and $\mathbf{C} = [c_{ij}]$ be the right-hand side of (A.12). Applying the commutativity condition yields the following six relations between the off-diagonal components of $\hat{\alpha}_2^u$ and $\hat{\alpha}_2^v$:

$$u_{21} = v_{11} - c_{11},\ u_{31} = v_{21} - c_{21},\ u_{32} = v_{22} - c_{22},\ v_{12} = u_{22} + c_{12},\ v_{13} = u_{23} + c_{13},\ v_{23} = u_{33} + c_{23}. \tag{A.13}$$

Then, by applying the symmetry condition, we find a well-posed linear system for $(u_{12}, u_{13}, u_{23}, v_{21}, v_{31}, v_{32})$, which depends only on $(u_{11}, u_{22}, u_{33}, v_{11}, v_{22}, v_{33})$. Thus, only the diagonal elements of $\hat{\alpha}_2^u$ and $\hat{\alpha}_2^v$ are free variables. It is significant to note that the symmetry condition causes the components of $\hat{\alpha}_2^u$ and $\hat{\alpha}_2^v$ to depend on the fourth-order moments.

#### *A.3.2. A simple closure for the diagonal elements*

A simple closure for the diagonal elements that satisfies the limiting conditions is

$$u_{11} = u_1,\ u_{22} = \hat{\alpha}_{1,11}^u - a_2^u + u_2,\ u_{33} = \hat{\alpha}_{1,22}^u - a_2^u + u_3,\quad v_{11} = \hat{\alpha}_{1,22}^v - a_2^v + v_1,\ v_{22} = \hat{\alpha}_{1,11}^v - a_2^v + v_2,\ v_{33} = v_3 \tag{A.14}$$

with $a_2^u = \frac{1}{2}s_{30}$ and $a_2^v = \frac{1}{2}s_{03}$. The other coefficients are components from the known matrices $\hat{\alpha}_1^u$ and $\hat{\alpha}_1^v$:

$$\hat{\alpha}_{1,11}^u = \frac{1}{|\Delta_1|}(s_{30} - s_{11}s_{21}),\quad \hat{\alpha}_{1,22}^u = \frac{1}{|\Delta_1|}(s_{12} - s_{11}s_{21}),\quad \hat{\alpha}_{1,11}^v = \frac{1}{|\Delta_1|}(s_{21} - s_{11}s_{12}),\quad \hat{\alpha}_{1,22}^v = \frac{1}{|\Delta_1|}(s_{03} - s_{11}s_{12}).$$

Combined with (A.13), the components $(u_{21}, u_{31}, u_{32}, v_{12}, v_{13}, v_{23})$ depend only on third-order moments. The remaining components $(u_{12}, u_{13}, u_{23}, v_{21}, v_{31}, v_{32})$ depend on the fourth-order moments due to the symmetry condition. Thus, unlike for 1D HyQMOM, $\hat{\alpha}_2^u$ and $\hat{\alpha}_2^v$ depend on the fourth-order moments. It is worth noting that it is straightforward to extend (A.14) to larger $n$.

With $(u_1, u_2, u_3) = (v_1, v_2, v_3) = 0$ in (A.14), the simplest closure is analogous to (A.6), and it can be computed symbolically to find formulas for the fifth-order moments. Otherwise, these variables must be zero in both limits. For example, we can (1) set them to zero, (2) choose $u_1$ and $v_3$ to make $s_{50}$ and $s_{05}$ the same as for 1D HyQMOM, (3) try to use them to make the moment system hyperbolic, or (4) try to eliminate some fourth-order moments in $\hat{\alpha}_2^u$ and $\hat{\alpha}_2^v$. Implementation of (2) is straightforward and has negligible effect on the computational cost. The resulting flux Jacobian has a $5 \times 5$ HyQMOM block with known eigenvalues. In principle, $(u_2, u_3)$ and $(v_1, v_2)$ can then be used to control the eigenvalues of the remaining $10 \times 10$ block. However, in all cases, care must be taken to ensure that they are chosen consistently and respect rotational invariance.

#### *A.3.3. A symmetric closure with simple diagonal elements*

The definitions in (A.5) were made to avoid using square-root matrices. One symmetric alternative is

$$\alpha_n^u := \langle u\mathbf{p}_n\mathbf{p}_n^t\rangle = \langle \mathbf{p}_n\mathbf{p}_n^t\rangle^{1/2}\tilde{\alpha}_n^u\langle \mathbf{p}_n\mathbf{p}_n^t\rangle^{1/2},\quad \alpha_n^v := \langle v\mathbf{p}_n\mathbf{p}_n^t\rangle = \langle \mathbf{p}_n\mathbf{p}_n^t\rangle^{1/2}\tilde{\alpha}_n^v\langle \mathbf{p}_n\mathbf{p}_n^t\rangle^{1/2} \tag{A.15}$$

where $\tilde{\alpha}_n^u$ and $\tilde{\alpha}_n^v$ automatically satisfy the symmetry condition. Note that $\hat{\alpha}_n^u = \langle \mathbf{p}_n\mathbf{p}_n^t\rangle^{1/2}\tilde{\alpha}_n^u\langle \mathbf{p}_n\mathbf{p}_n^t\rangle^{-1/2}$,[37] such that the commutativity condition depends on the square-root matrix $\langle \mathbf{p}_n\mathbf{p}_n^t\rangle^{1/2}$; however, it provides constraints on the off-diagonal elements of $\tilde{\alpha}_n^u$ and $\tilde{\alpha}_n^v$ given the diagonal elements. The latter can then be closed as done above in (A.14) for $n = 2$. The simplest symmetric closure uses $(u_1, u_2, \ldots, u_n) = (v_1, v_2, \ldots v_n) = 0$. For $n = 2$, the fifth-order moment closures are

$$\mathbf{S}_5^u = \langle \hat{\mathbf{p}}_2\hat{\mathbf{p}}_2^t\rangle^{1/2}\tilde{\alpha}_2^u\langle \hat{\mathbf{p}}_2\hat{\mathbf{p}}_2^t\rangle^{1/2} + \mathbf{R}_5^u,\quad \mathbf{S}_5^v = \langle \hat{\mathbf{p}}_2\hat{\mathbf{p}}_2^t\rangle^{1/2}\tilde{\alpha}_2^v\langle \hat{\mathbf{p}}_2\hat{\mathbf{p}}_2^t\rangle^{1/2} + \mathbf{R}_5^v. \tag{A.16}$$

From a computational perspective, finding the square-root matrix is an added expense, even though we avoid the cost of computing the symmetry condition. Simulations run with both methods clearly show that (A.15) is significantly more expense (and less reliable[38]) than the asymmetric closure in (A.14). In either case, the simplest closure is straightforward to extend to larger $n$. Finally, from a theoretical perspective, the vector $\mathbf{q}_n = \langle \mathbf{p}_n\mathbf{p}_n^t\rangle^{-1/2}\mathbf{p}_n$ is orthonormal (i.e., polynomials with the same degree are orthogonal) and, hence, more convenient for investigating the properties of 2D orthogonal polynomials [29,30].

---

[37] This equality implies that the diagonal elements of $\hat{\alpha}_n^u$ are related to those of $\tilde{\alpha}_n^u$. Thus, fixing the latter to the simplest possible form provides the former, and vice versa. In other words, $(u_1, u_2, \ldots, u_n)$ and $(v_1, v_2, \ldots v_n)$ will differ between the two closures.

[38] When the code produces a set of moments with negative $\langle \mathbf{p}_2\mathbf{p}_2^t\rangle$ due to numerical errors or otherwise, the square-root matrix is complex and corrupts the moments. This is not an issue with the asymmetric closure.

 

### A.4. Numerical implementation

Compared to the closures used in the main text, the expressions for the fifth-order moments found from 2D orthogonal polynomials are more complex, e.g., they are nonlinear in the cross-moments. In the simulation code, the 15 flux eigenvalues are computed numerically for the HLL solver. However, at least for low-speed flows, the $s_{50}$ block may provide them as in the 1D case. Numerical tests with the simplest closures in a 2D domain provide some evidence that this closure is hyperbolic for low Mach numbers, but future work is needed to validate this point. More importantly, the principal advantage of using 2D orthogonal polynomials is to eliminate the realizability-correction algorithm, and our numerical results confirm this behavior for low-speed flows. However, for high-speed flows, $|\langle \mathbf{p}_2 \mathbf{p}_2^t \rangle|$ moves closer to zero with increasing Mach number and complex eigenvalues are observed. For such flows, the linear closures with the projection algorithm in Appendix B perform better.

## Appendix B. A realizable hyperbolic closure based on projection

In the main text, we developed a hyperbolic closure starting from the 1D orthogonal polynomials. With a small modification to $s_{32}$,[39] this provides the following closure for the fifth-order moments that is linear in the cross-moments:

$$
\begin{aligned}
s_{50} &= \frac{1}{2} s_{30}(5s_{40} - 3s_{30}^2 - 1), \\
s_{41} &= -\frac{1}{4} s_{30}(8s_{40} - 9s_{30}^2 - 4)s_{11} + \frac{1}{4}(10s_{40} - 15s_{30}^2 - 6)s_{21} + 2s_{30}s_{31}, \\
s_{32} &= \frac{1}{2}(2s_{40} - 3s_{30}^2)s_{12} + \frac{1}{2}s_{30}(3s_{22} - 1),
\end{aligned}
\tag{B.1}
$$

with $s_{05}$, $s_{14}$ and $s_{23}$ found by permuting the indices. The flux Jacobian for the $x_1$ direction is then block diagonal with characteristic polynomial $P_{15} = R_3 Q_2 Q_4 Q_3 P_3$ where only $P_3$ depends on the cross-moments through the block:

$$
J_3 = \begin{bmatrix} 0 & 1 & 0 \\ \frac{\partial s_{23}}{\partial s_{03}} & \frac{\partial s_{23}}{\partial s_{13}} & \frac{\partial s_{23}}{\partial s_{04}} \\ \frac{\partial s_{14}}{\partial s_{03}} & \frac{\partial s_{14}}{\partial s_{13}} & \frac{\partial s_{14}}{\partial s_{04}} \end{bmatrix} = \begin{bmatrix} 0 & 1 & 0 \\ -3s_{03}s_{21} + \frac{1}{2}(3s_{22} - 1) & 0 & s_{21} \\ -\frac{1}{4}(8s_{04} - 27s_{03}^2 - 4)s_{11} - \frac{15}{2}s_{03}s_{12} + 2s_{13} & 2s_{03} & -2s_{03}s_{11} + \frac{5}{2}s_{12} \end{bmatrix}.
$$

Note that when $s_{21} = 0$ and $s_{22} \geq 1/3$, the eigenvalues are real-valued. Otherwise, for large enough $|s_{11}|$, two eigenvalues can be locally complex. Thus, when complex eigenvalues are encountered, we set $s_{21} = 0$ and check that $s_{22} \geq 1/3$. With this correction, the system is globally hyperbolic. Note that the HLL eigenvalues will come from either $R_3$, $Q_4$ or $P_3$; and hence the numerical Jacobian is not required. The eigenvalues is the $y$ direction are controlled in the same manner using $s_{12}$.

### B.1. 2D moment projection

In general, it is possible to choose $(u_1, u_2, u_3, v_1, v_2, v_3)$ in (A.14) such that the fifth-order moments are given by (B.1). However, as seen in the main text, for crossing jets with large Mach number, the matrix $\langle \mathbf{p}_2 \mathbf{p}_2^t \rangle$ becomes negative locally. Thus, it will be necessary to check for and correct the moments when this occurs. The algorithm in the main text checks and corrects individual moments. Here, instead, we propose a moment-projection method with the following steps at each grid cell:

1. After the spatial flux is applied, find the smallest eigenvalue $\lambda_1$ of $\langle \mathbf{p}_2 \mathbf{p}_2^t \rangle$.
2. If $\lambda_1 < \lambda_{\min}$, then reset $s_{ij}$ for $i + j > 2$ to the moments of a target distribution $S_{ij}$ with non-negative $\langle \mathbf{p}_2 \mathbf{p}_2^t \rangle$.
3. For the target distribution, verify that the moment system is hyperbolic.

Here, the cut-off value $\lambda_{\min} \geq 0$ controls how far the moment system is from its boundary. In our simulations, we set $\lambda_{\min} = 0$. Ideally, the target distribution would not change the univariate moments. However, since a negative eigenvalue is often associated with a crossing jet where $s_{03} = s_{11}s_{30}$ and $s_{04} = s_{40}$, the univariate moments are not independent.

### B.2. Target distributions

A suitable target distribution must have realizable moments at the boundary of moment space. Ideally, the projection step will change only a few moments, but at the same time be simple enough to minimize computations. Two 2D possibilities are as follows.

#### B.2.1. 2D extended AG distribution

We can extend the anisotropic Gaussian to allow for univariate fourth-order moments larger than 3. For example, the target moments are

$$
S_{11} = s_{11},\ S_{30} = S_{21} = S_{12} = S_{03} = 0,\ S_{40} = S_4,\ S_{31} = s_{11}S_4,\ S_{13} = s_{11}S_4,\ S_{04} = S_4
$$

[39] i.e., we remove the dependence on $s_{03}$ (see Section 3.8). Removing this dependence, the $6 \times 6$ block becomes two $3 \times 3$ blocks.

and, fixing $S_{22}$ on the lower boundary of moment space (i.e., $|\langle \mathbf{p}_2 \mathbf{p}_2^t \rangle| = 0$),[40]

$$S_{22} = \frac{1}{2}\left[\left(4s_{11}^2 S_4(2S_4-1) + (S_4-1)^2\right)^{1/2} - (S_4-1)\right]$$

with $S_4$ fixed as $(s_{40}+s_{04})/2$.[41] In order to ensure hyperbolicity, we then check that $S_{22} \ge 1/3$ and, if not, use $S_{22} = 1/3$. Note that this target distribution has zero skewness and is realizable when $s_{11} = \pm 1$, even when $S_4 = 1$. However, for high jet Mach numbers, lack of skewness gives poor results for crossing jets. The main benefit of using the extended AG distribution is that it is simple to ensure non-negative $\langle \mathbf{p}_2 \mathbf{p}_2^t \rangle$. The 3D extended AG distribution is found analogously.

*B.2.2. 2D skewed-central distribution*

It is possible to allow for non-zero third-order central moments, while still accounting for realizability and hyperbolicity at the edge of moment space.[42] One way to achieve this is to use the following target moments:

$$\begin{aligned} &S_2 = 1 - s_{11}^2, \quad S_3 = \frac{1}{2}(s_{30} + sign(s_{11}) s_{03}), \quad S_4 = 1 + S_3^2 + \frac{1}{2}(H_{20} + H_{02}) S_2, \\ &S_{11} = s_{11}, \quad S_{30} = S_{12} = S_3, \quad S_{03} = S_{21} = S_{11} S_3, \quad S_{31} = S_{13} = S_{11} S_4, \quad S_{40} = S_{04} = S_4, \quad S_{22} = S_4 \end{aligned} \tag{B.2}$$

where $S_{22}$ is fixed on the boundary of moment space where $|\langle \mathbf{p}_2 \mathbf{p}_2^t \rangle| = 0$ for arbitrary $S_3$. These target moments are not unique, but are exact for $S_2 = 0$ (i.e., 2D crossing jet). Other realizable choices for $(S_2, S_3, S_4)$ can be used (e.g., $S_4 = 1 + S_3^2 + 2S_2$, which is Gaussian for $S_2 = 1$ and $S_3 = 0$), but may increase the HLL eigenvalues. Also, the sign of $S_3$ must respect the directional symmetry between $S_{30}$ and $S_{03}$ determined by $sign(s_{11})$. For high-speed jet-crossing problems where $S_2 \to 0$, the ultimate target distribution is the double-delta function in (D.1) with target moments in (D.2), $S_{11} = sign(s_{11})$ and $S_4 = 1 + S_3^2$. We use the same when the univariate moments are close to their boundary, i.e., $s_{40} - s_{30}^2 - 1 \approxeq 0$. In practice, the 2D projection method is computationally faster then checking and correcting individual moments using the leading principal minors.

*B.3. Extension to 3D target moments*

The extension of the projection step to a 3D moment system for high-speed flows is relatively straightforward. The main challenge is to find suitable target moments $S_{ijk}$ on the boundary of moment space. Extending the 2D target moments in (B.2), a simple form for the 3D target moments is as follows:

$$\begin{aligned} &S_2 = 1 + 2s_{110}s_{101}s_{011} - s_{110}^2 - s_{101}^2 - s_{011}^2, \\ &S_3 = \frac{1}{3}(s_{300} + sign(s_{110})s_{030} + sign(s_{101})s_{003}), \quad S_4 = 1 + S_3^2 + \frac{1}{3}(H_{200} + H_{020} + H_{002})S_2, \\ &S_{110} = s_{110}, \quad S_{101} = s_{101}, \quad S_{011} = s_{011}, \quad S_{300} = S_3, \quad S_{030} = S_{110}S_3, \quad S_{003} = S_{101}S_3, \quad S_{111} = S_{011}S_3, \\ &S_{120} = S_{102} = S_{300}, \quad S_{210} = S_{012} = S_{030}, \quad S_{201} = S_{021} = S_{003}, \\ &S_{310} = S_{130} = S_{112} = S_{110}S_4, \quad S_{301} = S_{103} = S_{121} = S_{101}S_4, \quad S_{031} = S_{013} = S_{211} = S_{011}S_4, \\ &S_{400} = S_{040} = S_{004} = S_4, \quad S_{220} = S_{202} = S_{022} = S_4. \end{aligned} \tag{B.3}$$

If these moments are non-realizable, then the smallest magnitude correlation coefficient is reset to the product of the two others (e.g., if $|s_{011}|$ is the smallest, then $S_{011} = s_{110}s_{101}$). The target moments are then guaranteed to be on the boundary of moment space for any realizable choice of $(S_2, S_3, S_4)$. Note that although the target moments reduce to the correct values of the cross moments for 3D crossing jets (e.g., the four corners of second-order moment space), they are not unique elsewhere. For example, a different target distribution may be preferred when $s_{110}^2 + s_{101}^2 + s_{011}^2 \le 3/4$, i.e., far from the corners of second-order moment space. In any case, further work is needed to identify potential 3D target moment sets and to investigate their properties.

Generally speaking, the 3D projection method is much faster and more robust than checking the leading principal minors. The speedup is mainly due to $S_{220} = S_{202} = S_{022} = S_4$, which removes the need to compute the roots of the third-order polynomials discussed in Section 5.1.7. In fact, the three largest leading principal minors are zero for the 3D target moments in (B.3).

## Appendix C. Grad-HyQMOM approximation of the VDF

The Grad approximation of the VDF uses a tensor-product Hermite-polynomial expansion about a Maxwellian VDF [1]. Analogously, an expansion using a tensor-product of the 1D orthogonal polynomials from 1D HyQMOM whose coefficients depend on the cross moments can be defined [21]. In terms of the standardized moments, the Grad-HyQMOM approximation of the 3D VDF for fixed $n \ge 1$ is

$$g(u,v,w) = f_1(u) f_2(v) f_3(w) \sum_{i+j+k=0}^{2n} \kappa_{ijk} \mathcal{U}_i(u) \mathcal{V}_j(v) \mathcal{W}_k(w) \tag{C.1}$$

[40] The other positive root is $S_{22} = S_4 \ge 1$ and yields the upper boundary. Note that $s_{11} = 0$ gives $S_{22} = 0$ and $s_{11} = \pm 1$ yields $S_{22} = S_4$. For hyperbolicity, with $S_{21} = 0$ or $S_{12} = 0$ we must have $S_{22} \ge 1/3$.

[41] This choice is exact for a rotation-invariant distribution with $s_{22} = 0$ and $\rho^2 = u^2 + v^2$.

[42] In the perfectly correlated limit, two eigenvalues are zero and $s_{11} = \pm 1$. In simulations, usually only one eigenvalue becomes negative. However, for crossing jets, all eigenvalues are near zero.

where the summation is over all $i, j, k \geq 0$ such that $i + j + k \leq 2n$. Using orthogonality, the coefficients $\kappa_{ijk}$ are defined by

$$\kappa_{ijk} = \frac{\langle \mathcal{U}_i \mathcal{V}_j \mathcal{W}_k \rangle}{\langle \mathcal{U}_i^2 \rangle \langle \mathcal{V}_j^2 \rangle \langle \mathcal{W}_k^2 \rangle}, \tag{C.2}$$

which forces the 3D cross moments to be equal to those in $\mathbf{S}_{2n}$. Note that $\kappa_{000} = 1$, and for $i + j + k > 2n$, we have $\langle \mathcal{U}_i \mathcal{V}_j \mathcal{W}_k \rangle = 0$, which is the closure for the free-transport flux developed in the main text. Phase-space integrals with respect to $g(u, v, w)$ are evaluated numerically using 1D Gaussian quadrature formulas found from the univariate moments in each direction [21,40], and depend linearly on the cross moments through $\kappa_{ijk}$.

## Appendix D. High-Mach-number crossing jets

In terms of moment realizability, the most difficult case to simulate with classical moment methods occurs when both Ma and Kn are large [18,48,56]. For the fourth-order moment system, the 2D VDF for the standardized variables approaches[43]

$$f(\tilde{u}, \tilde{v}) = p_1 \delta(\tilde{u} - \tilde{u}_1)\delta(\tilde{v} - \tilde{v}_1) + p_2 \delta(\tilde{u} - \tilde{u}_2)\delta(\tilde{v} - \tilde{v}_2), \tag{D.1}$$

with $p_2 = 1 - p_1$. For this VDF, $\tilde{v} = s_{11}\tilde{u}$ with $s_{11} = \pm 1$, so that the standardized moments are

$$\begin{aligned} &s_{00} = 1,\ s_{10} = s_{01} = 0,\ s_{20} = s_{02} = 1,\ s_{03} = s_{11}s_{30},\ s_{21} = s_{11}s_{30},\ s_{12} = s_{30}, \\ &s_{40} = s_{04} = 1 + s_{30}^2,\ s_{31} = s_{11}s_{40},\ s_{13} = s_{11}s_{40},\ s_{22} = s_{40}, \end{aligned} \tag{D.2}$$

and thus depend on a single moment $s_{30}$. The positive weight $0 < p_1 < 1$ and the velocity abscissae are

$$p_1 = \frac{1}{2}\left(1 + \frac{s_{30}}{\sqrt{s_{30}^2 + 4}}\right),\ \tilde{u}_1 = \left(\frac{1 - p_1}{p_1}\right)^{1/2},\ \tilde{u}_2 = -\left(\frac{p_1}{1 - p_1}\right)^{1/2}, \quad \tilde{v}_1 = \pm\tilde{u}_1,\ \tilde{v}_2 = \pm\tilde{u}_2. \tag{D.3}$$

Thus, if $\tilde{v}_1 = \tilde{u}_1$ then $s_{11} = 1$, or if $\tilde{v}_1 = -\tilde{u}_1$ then $s_{11} = -1$. In terms of moment realizability, for large Ma, the 1D Hankel determinants $H_{20}, H_{02} \to 0$, as do $|\Delta_1|$ and $|\Delta_2|$. Thus, the VDF is close to the boundary of 2D moment space, and the fifth-order standardized moments depend only on $(s_{11} = \pm 1, s_{30})$. Note that the crossing angle of the jets depends on the central moments $(c_{20}, c_{02})$, but this information is not needed for the flux closure written in terms of the standardized moments.

Close to, but inside the boundary of moment space, the delta functions in (D.1) will be replaced with a 2D VDF with small variances such that $H_{20}$, $H_{02}$, $|\Delta_1|$ and $|\Delta_2|$ are small but positive. The fourth-order moments will then be close to, but different than those given in (D.2). A consideration for the robustness of the moment system is that the closures for the fifth-order moments should not cause the spatial fluxes to generate non-realizable moments for moment sets near the boundary of moment space. For 1D moment systems, 1D HyQMOM is robust in this sense. However, in 2D, the following additional realizability and hyperbolicity constraints must also be satisfied:

*Correction algorithm.* In the case where $s_{11}^2 > 1$, we reset $s_{11}^2 = 1$ keeping the same sign for $s_{11}$. The third- and fourth-order standardized moments keep the same sign, but are reset such that $s_{30}^2 = s_{03}^2 = s_3^2$ with $s_3 = \max_{|.|}(s_{03}, s_{30})$ and $s_{40} = s_{04} = s_4$ with $s_4 = 1 + s_3^2 + \min(H_{20}, H_{02})$. The cross moments are reset using (D.2). Simulations of a 2D crossing jet with large Ma run successfully with these corrections.

*Limit on skewness.* Another issue observed for high-Ma crossing jets is that in front of the jets, the standardized moments $s_{30}$ and $s_{03}$ can have very large magnitudes. (The same phenomenon was seen in Fox et al. [20].) The eigenvalues for the 1D HyQMOM closure are then large compared to the jet velocity, and the time step must be decreased to capture the highest wave speed. To lower the maximum wave speed, we can place an upper bound on $|s_{30}|$ and $|s_{03}|$, and decrease $s_{40}$ and $s_{04}$, keeping $H_{20}$ and $H_{02}$ constant. As seen above in (D.3), for a crossing jet, the value of $s_{30}$ fixes the weight $p_1$. For example, the limit $|s_{30}| \leq 4 + \mathrm{Ma}/2$ gives a reasonable value for the maximum node velocity (i.e., for $\max(|u_1|, |u_2|)$) for any value of Ma. (See the results for Ma = 4 and 100 in the main text.) Note that for small Kn, the maximum of $|s_{30}|$ and $|s_{03}|$ will usually be controlled by collisions.

*3D crossing jet.* The extension to 3D crossing jets multiplies each term in (D.1) by $\delta(\tilde{w} - \tilde{w}_i)$ with $i \in \{1, 2\}$ where $\tilde{w}$ is the standardized velocity in direction $x_3$. Using a fourth-order moment system, only two weights can be represented exactly (i.e., two crossing jets). For this VDF, $\tilde{v} = s_{110}\tilde{u}$ and $\tilde{w} = s_{101}\tilde{u}$ with $s_{110}, s_{101} = \pm 1$ and $s_{011} = s_{110}s_{101}$, which are the four corners in Fig. 9. The standardized moments for $i + j + k > 2$ are $s_{ijk} = s_{110}^j s_{101}^k s_{i+j+k\,00}$ such that

$$\begin{aligned} &s_{030} = s_{110}s_{300},\ s_{003} = s_{101}s_{300}, \\ &s_{210} = s_{110}s_{300},\ s_{201} = s_{101}s_{300},\ s_{120} = s_{300},\ s_{102} = s_{300},\ s_{021} = s_{101}s_{300},\ s_{012} = s_{110}s_{300}, \\ &s_{111} = s_{011}s_{300},\ s_{400} = s_{040} = s_{004} = 1 + s_{300}^2,\ s_{220} = s_{202} = s_{022} = s_{400}, \end{aligned}$$

[43] Using a fourth-order moment system, only two weights can be represented exactly (i.e., two crossing jets). In general, to exactly represent $N$ crossing jets, the order of the moment system must be $2N$.

$$s_{310} = s_{110}s_{400},\ s_{301} = s_{101}s_{400},\ s_{130} = s_{110}s_{400},\ s_{103} = s_{101}s_{400},\ s_{031} = s_{011}s_{400},\ s_{013} = s_{011}s_{400},$$
$$s_{211} = s_{011}s_{400},\ s_{121} = s_{101}s_{400},\ s_{112} = s_{110}s_{400}, \tag{D.4}$$

and thus again depend on a single moment $s_{300}$. As done for 2D crossing jets, whenever the second-order cross moments are rescaled to ensure $S_2(s_{110}, s_{101}, s_{011}) \geq 0$, the moments are corrected using (D.4) with $s_3 = \max_{|.|}(s_{300}, s_{030}, s_{003})$ and $s_4 = 1 + s_3^2 + S_2$.

## Appendix E. Realizability constraints for $(s_{310}, s_{111})$ given $s_{220}$

The second leading principal minor yields the constraint

$$\begin{vmatrix} s_{400} - d_{11} & s_{310} - d_{12} \\ s_{310} - d_{12} & s_{220} - d_{22} \end{vmatrix} = (s_{400} - d_{11})(s_{220} - d_{22}) - (s_{310} - d_{12})^2 > 0$$

where $d_{12}$ is linear and $d_{22}$ is quadratic in $s_{111}$:

$$d_{12} = |\Delta_1|^{-1}(a s_{111} + b), \quad d_{22} = |\Delta_1|^{-1}(c s_{111}^2 - 2\, d s_{111} + e) > 0$$

with coefficients $(a, b, c, d, e)$ that depend on second- and third-order moments:

$$\begin{aligned}
a &= (1 - s_{110}^2)s_{201} + (s_{101}s_{110} - s_{011})s_{210} + (s_{011}s_{110} - s_{101})s_{300} \\
b &= |\Delta_1| s_{110} + (s_{011}s_{101} - s_{110})s_{210}^2 + (1 - s_{101}^2)s_{210}s_{120} + (s_{011}s_{110} - s_{101})s_{210}s_{201} \\
&\quad + (1 - s_{011}^2)s_{210}s_{300} + (s_{101}s_{110} - s_{011})s_{120}s_{201} + (s_{011}s_{101} - s_{110})s_{120}s_{300} \\
c &= 1 - s_{110}^2 \\
d &= (s_{101} - s_{011}s_{110})s_{210} + (s_{011} - s_{101}s_{110})s_{120} \\
e &= |\Delta_1| s_{110}^2 + \begin{bmatrix} s_{210} \\ s_{120} \end{bmatrix}^t \begin{bmatrix} 1 - s_{011}^2 & s_{011}s_{101} - s_{110} \\ s_{011}s_{101} - s_{110} & 1 - s_{101}^2 \end{bmatrix} \begin{bmatrix} s_{210} \\ s_{120} \end{bmatrix}
\end{aligned}$$

where $c, e > 0$ and $d^2 < c\, e$ (i.e., $d_{22} > 0$). Note that for the 26-moment system, $s_{310}$ is known so that the second leading principal minor yields a quadratic constraint for $s_{111}$.

Separating the terms depending on $(s_{310}, s_{111})$ from those depending on $s_{220}$ gives

$$\begin{bmatrix} s_{310} - \frac{ad+bc}{c|\Delta_1|} \\ s_{111} - \frac{d}{c} \end{bmatrix}^t \begin{bmatrix} |\Delta_1| & -a \\ -a & \frac{a^2 + (s_{400} - d_{11})c|\Delta_1|}{|\Delta_1|} \end{bmatrix} \begin{bmatrix} s_{310} - \frac{ad+bc}{c|\Delta_1|} \\ s_{111} - \frac{d}{c} \end{bmatrix} < (s_{400} - d_{11})(|\Delta_1| s_{220} - (c\, e - d^2)/c) \tag{E.1}$$

where the coefficient matrix on the left-hand side is positive. For this constraint to hold, the right-hand side must be non-negative, which puts a lower bound on $s_{220}$:

$$0 \leq |\Delta_1|^{-1}(c\, e - d^2)/c \leq s_{220}. \tag{E.2}$$

As expected, (E.1) reduces to the 2D case when the third direction is independent. Moreover, by permuting the indices $s_{111}$ is unchanged so that the coefficients $(c, d, e)$ are the same for the pair $(s_{310}, s_{220}, s_{111})$ and $(s_{130}, s_{220}, s_{111})$. Likewise, they are the same for the pair $(s_{301}, s_{202}, s_{111})$ and $(s_{103}, s_{202}, s_{111})$, and for the pair $(s_{013}, s_{022}, s_{111})$ and $(s_{031}, s_{022}, s_{111})$.

The boundary of $(s_{310} - (ad + bc)/(c|\Delta_1|), s_{111} - d/c)$-moment space found from (E.1) is a rotated ellipse. As noted above, the center of the ellipse will be different for each permutation. If (E.1) is not satisfied, we can use a scaling factor to reduce the magnitude of the vector $\mathbf{V} = \mathbf{R}[s_{310} - (ad + bc)/(c|\Delta_1|), s_{111} - d/c]^t$ as done for the third-order moments in Section 5.1.3. However, since $d/c$ depends on which permutation is used, unless $\mathbf{V}$ is the same for all permutations, we may have six different values for the bounds on $s_{111}$. The moment projection method in Appendix B removes this ambiguity.

## References

[1] H. Grad, On the kinetic theory of rarefied gases, Commun. Pure Appl. Math. 2 (1949) 331–407.
[2] C.D. Levermore, Moment closure hierarchies for kinetic theories, J. Stat. Phys. 83 (1996) 1021–1065.
[3] M. Junk, A. Unterreiter, Maximum entropy moment systems and Galilean invariance, Contin. Mech. Thermodyn. 14 (2002) 563–576.
[4] H. Struchtrup, Macroscopic transport equations for rarefied gas flows, Interaction of Mechanics and Mathematics, Springer, Berlin, Germany, 2005. Approximation methods in kinetic theory.
[5] J.G. McDonald, M. Torrilhon, Affordable robust moment closures for CFD based on the maximum-entropy hierarchy, J. Comput. Phys. 251 (2013) 500–523.
[6] C. Kuehn, Control of Self-Organizing Nonlinear Systems, Springer International Publishing, Cham, 2016, pp. 252–271.
[7] M. Torrilhon, Modeling nonequilibrium gas flow based on moment equations, Annu. Rev. Fluid Mech. 48 (2016) 429–458.
[8] K. Schmüdgen, The Moment Problem, vol. 277 of Graduate Texts in Mathematics, Springer, Cham, 2017.
[9] Z. Cai, Moment method as a numerical solver: challenge from shock structure problems, J. Comput. Phys. 444 (2021) 110593.
[10] E. Rice, E. Plante-Sabourin, J.G. McDonald, Robustly hyperbolic high-order moment-closures for multidimensional gases, J. Comput. Phys. (2026). https://doi.org/10.1016/j.jcp.2026.115026
[11] E. Rice, Affordable Extended Hyperbolic Moment Closures for Rarefied Gas-Flow Predictions, Ph.D. thesis, University of Ottawa, Ottawa, Canada, 2026..
[12] R.O. Fox, F. Laurent, Hyperbolic quadrature method of moments for the one-dimensional kinetic equation, SIAM J. Appl. Math. 82 (2022) 750–771.
[13] F. Laurent, R.O. Fox, Evaluation of the 1-D hyperbolic quadrature method of moments for non-equilibrium flows, ESAIM: Proc. Surv. 76 (2024) 52–67.
[14] E. Yilmaz, G. Oblapenko, M. Torrilhon, On nonlinear closures for moment equations based on orthogonal polynomials, SIAM J. Appl. Math. 86 (2026) 839–869.
[15] J.O. Habscheid, Modeling and Analysis of Nonlinear Closures in Hierarchical Moment Equations Using Discontinuous Galerkin Methods, Master's thesis, RWTH Aachen University, 2026.

[16] W. Morin, J.G. McDonald, Development of globally hyperbolic one-dimensional moment closures based on orthogonal polynomials, J. Comput. Phys. 523 (2025) 113659.

[17] R. Zhang, Y. Chen, Q. Huang, W.-A. Yong, Dissipativeness of the hyperbolic quadrature method of moments for kinetic equations (2024). arXiv preprint arXiv:2406.13931.

[18] O. Desjardins, R.O. Fox, P. Villedieu, A quadrature-based moment method for dilute fluid–particle flows, J. Comput. Phys. 227 (2008) 2514–2539.

[19] R.O. Fox, Higher-order quadrature-based moment methods for kinetic equations, J. Comput. Phys. 228 (2009) 7771–7791.

[20] R.O. Fox, F. Laurent, A. Vié, Conditional hyperbolic quadrature method of moments for kinetic equations, J. Comput. Phys. 365 (2018) 269–293.

[21] R.O. Fox, F. Laurent, A Grad-like expansion of the hyperbolic quadrature method of moments for multidimensional kinetic equations, in: 9th European Congress on Computational Methods in Applied Sciences and Engineering, CIMNE, Lisboa, Portugal, 2024.

[22] S. Boccelli, W. Kaufmann, T.E. Magin, J.G. McDonald, Numerical simulation of rarefied supersonic flows using a fourth-order maximum-entropy moment method with interpolative closure, J. Comput. Phys. 497 (2024) 112631.

[23] P.-Y.C.R. Taunay, M.E. Mueller, Quadrature-based moment methods for kinetic plasma simulations, J. Comput. Phys. 473 (2023) 111700.

[24] A. Berger, N. Lequette, T. Magin, A. Bourdon, A. Alvarrez Laguna, Comparison of high-order moment models for the ion dynamics in bounded low-temperature plasma, Phys. Plasma. 32 (2025) 103503.

[25] S.H. Bryngelson, R.O. Fox, T. Colonius, Conditional moment methods for polydisperse cavitating flows, J. Comput. Phys. 477 (2023) 111917.

[26] A. Charalampopoulos, S.H. Bryngelson, T. Colonius, T.P. Sapsis, Hybrid quadrature moment method for accurate and stable representation of non-Gaussian processes and their dynamics, Philos. Trans. R. Soc. A 380 (2022).

[27] Q. Huang, S. Li, W.-A. Yong, Stability analysis of quadrature-based moment methods for kinetic equations, SIAM J. Appl. Math. 80 (2020) 206–231.

[28] Z. Liu, A. Narayan, A Stieltjes algorithm for generating multivariate orthogonal polynomials, SIAM J. Sci. Comput. 45 (2023) A1125–A1147.

[29] Y. Xu, On multivariate orthogonal polynomials, SIAM J. Math. Anal. 24 (1993) 783–794.

[30] Y. Xu, Multivariable Special Functions, vol. II of Encyclopedia of Special Functions, Cambridge University Press, 2021, p. 19–78.

[31] H.L. Krall, I.M. Sheffer, Orthogonal polynomials in two variables, Ann. Mat. Pura Appl. 76 (1967) 325–376.

[32] C.D. Levermore, W.J. Marokoff, B.T. Nadiga, Moment realizability and the validity of the Navier-Stokes equations for rarefied gas dynamics, Phys. Fluid. 10 (1998) 3214–3226.

[33] L. Fialkow, S. Petrovic, A moment matrix approach to multivariate cubature, Integral Equ. Oper. Theory 52 (2005) 85–124.

[34] H.L. Hamburger, Hermitian transformations of deficiency-index (1,1), Jacobian matrices, and undetermined moment problems, Am. J. Math. 66 (1944) 489–552.

[35] H. Dette, W.J. Studden, The theory of canonical moments with applications in statistics, probability, and analysis, Wiley Series in Probability and Statistics: Applied Probability and Statistics, John Wiley & Sons Inc., New York, 1997.

[36] G.T. Gilbert, Positive definite matrices and Sylvester's criterion, Am. Math. Mon. 98 (1991) 44–46.

[37] C. Groth, P. Roe, T. Gombosi, S. Brown, On the nonstationary wave structure of a 35-moment closure for rarefied gas dynamics, in: AIAA, 1995. https://arc.aiaa.org/doi/abs/10.2514/6.1995-2312

[38] R.P. Schaerer, M. Torrilhon, The 35-moment system with the maximum-entropy closure for rarefied gas flows, Eur. J. Mech. - B/Fluid. 64 (2017) 30–40. Special Issue on Non-equilibrium Gas Flows.

[39] M.H.L. Reddy, S. Ganesan, Thirty-five moment theory for dilute smooth hard sphere gases, AIP Conference Proceedings, 2132, 2019, p. 120002.

[40] R.O. Fox, F. Laurent, A. Passalacqua, The generalized quadrature method of moments, J. Aerosol Sci. 167 (2023) 106096.

[41] W. Gautschi, Orthogonal Polynomials: Computation and Approximation, Oxford University Press, Oxford, UK, 2004.

[42] J.C. Wheeler, Modified moments and Gaussian quadratures, Rocky Mt. J. Math. 4 (1974) 287–296.

[43] C.D. Levermore, W.J. Morokoff, The Gaussian moment closure for gas dynamics, SIAM J. Appl. Math. 59 (1998) 72–96.

[44] D.L. Marchisio, R.O. Fox, Computational Models for Polydisperse Particulate and Multiphase Systems, Cambridge University Press, Cambridge, UK, 2013.

[45] P.L. Bhatnagar, E.P. Gross, M. Krook, A model for collision processes in gases. I. Small amplitude processes in charged and neutral one-component systems, Phys. Rev. 94 (1954) 511.

[46] A. Vié, F. Doisneau, M. Massot, On the anisotropic Gaussian velocity closure for inertial-particle laden flows, Commun. Comput. Phys. 17 (2015) 1–46.

[47] E.F. Toro, Riemann Solvers and Numerical Methods for Fluid Dynamics: A Practical Introduction, Springer, New York, 1999.

[48] H.-S. Tsien, Superaerodynamics, mechanics of rarefied gases, J. Aeronaut. Sci. 13 (1946) 653–664.

[49] H. Grad, Note on N-dimensional Hermite polynomials, Commun. Pure Appl. Math. 2 (1949) 325–330.

[50] A. Harten, P.D. Lax, B. Van Leer, On upstream differencing and Godunov-type schemes for hyperbolic conservation laws, SIAM Rev. 25 (1983) 35–61.

[51] C. Fan, Q. Huang, K. Wu, Provably realizability-preserving finite volume method for quadrature-based moment models of kinetic equations (2025). arXiv preprint arXiv:2510.18380.

[52] J. Bünger, E. Christhuraj, A. Hanke, M. Torrilhon, Structured derivation of moment equations and stable boundary conditions with an introduction to symmetric, trace-free tensors, Kinet. Relat. Models 16 (2023) 458–494.

[53] G.A. Bird, Molecular Gas Dynamics and the Direct Simulation of Gas Flows, Oxford University Press, Oxford, UK, 1994.

[54] V.V. Aristov, I.V. Voronich, S.A. Zabelok, Direct methods for solving the Boltzmann equations: comparisons with direct simulation Monte Carlo and possibilities, Phys. Fluid. 31 (2019) 097106.

[55] Z. Zhu, C. Xiao, K. Tang, J. Huang, C. Yang, APTT: Accuracy-preserved tensor-train method for the Boltzmann-BGK equation, SIAM J. Sci. Comput. 47 (2025) A2672–A2698.

[56] R.O. Fox, A quadrature-based third-order moment method for dilute gas–particle flow, J. Comput. Phys. 227 (2008) 6313–6350.